CLASSIFYING NEURAL SIGNALS RELATED TO THE PERCEPTION OF ACTION

by

M.A. Palazzolo

B.S. in Biomedical Engineering, Tulane University, 2003

Submitted to the Graduate Faculty of

the Swanson School of Engineering in partial fulfillment

of the requirements for the degree of

Doctor of Philosophy

University of Pittsburgh

2014

UNIVERSITY OF PITTSBURGH

SWANSON SCHOOL OF ENGINEERING

This dissertation was presented

by

M.A. Palazzolo

It was defended on

November 11, 2014

and approved by

Andrew Schwartz, Ph.D., Professor, Department of Neurobiology

Peter Strick, Ph.D., Professor, Department of Neurobiology

Aaron Batista, Ph.D., Assistant Professor, Department of Bioengineering

Douglas Weber, Ph.D., Assistant Professor, Department of Bioengineering

Dissertation Director: Andrew Schwartz, Ph.D., Professor, Department of Neurobiology

CLASSIFYING NEURAL SIGNALS RELATED TO THE PERCEPTION OF ACTION

M.A. Palazzolo, PhD

University of Pittsburgh, 2014

Activity from individual neurons in primary motor cortex (M1) and ventral premotor cortex (PMv) can be modeled as a linear function of the direction of arm movement. If this signal is generated, it represents an extrinsic construct built upon various coordinate transformations from the areas of the brain associated with vision. Previous work suggests that the PMv is a unique area in which to investigate how these visual signals are transformed into motor commands. We evaluated evidence of this visuospatial transformation in PMv and M1. In the first set of experiments, we recorded neuronal activity in M1 and PMv while each monkey reached to 14 targets represented in a 3D virtual environment. The monkey's hand was hidden from view and was represented on the display by a cursor. Goal position was represented with a spherical target. Across experiments, identical hand movements were performed with varying views of the task. Each view dissociated one of three putative coordinate frames: hand-centered velocity, cursor-centered target location, and displayed motion. In the second set of experiments, each monkey passively observed visually congruent replays of the trials from the first set of experiments. This paradigm was used to evaluate neuronal response in an action-related context without the monkey having the intention to move. In the third set of experiments, each monkey passively observed object motion on the display. This paradigm was used to evaluate neuronal response to a dynamic visual stimulus without action context. Results were as follows: 1) During active reaching, neural activity corresponded to the three coordinate systems in distinct anatomical locations, each with different latencies. This suggests a systematic substrate for visuospatial transformation. 2) Activity from a subpopulation of units located in M1 and PMv corresponded to hand velocity during active movement only. This implies the presence of a motor command-related signal. 3) Activity from a subpopulation of units located in anterior M1

and PMv corresponded to cursor-centered target location during action context, with or without the intention to move. This suggests the presence of a signal related to the visualized goal of a learned action.

TABLE OF CONTENTS

LIST OF TABLES

LIST OF FIGURES

PREFACE

This dissertation represents my proudest achievement to date. I could have never finished without the contributions from the following people.

First and foremost, Andrew Schwartz, who has always set the standard for my writing and research at a high level, even when I did not. Teaching me to think and write like a scientist was not an easy endeavor, and I am grateful for the time and energy he has spent with me over the years. Meel Velliste, who helped me with MRI analysis, CNC, coding, RTMA, and was generally awesome in all situations. George Fraser, who taught me quite a few lessons in coding while we worked together to develop the virtual display and also shared some golf tips. Peter Strick, who offered financial support when my project lost funding. Aaron Batista, who gave me second opinions on the big picture. Chance Spalding, who showed me a new and better definition of work ethic. Sagi Perel, for countless discussions on coding, quantitative issues, and single-unit recording. Steve Chase, for discussions on statistics and logical thinking. Andrew Whitford, my office mate and pep talker who also helped with statistics. Scott Kennedy and Sam Clanton, for second opinions that helped me further define the purpose of my research. Doug Weber, for helpful discussions about the experimental paradigm. Rob Rasmussen, and Rex Tien, for various related discussions. Laurel Sinko and Heather Dipetro, for making electrodes and preparing for surgeries. Kathy Prigg, for administrative support.

My friends and family were instrumental in helping me through this arduous process. Jamie Shuller, who trudged through some of the darkest hours with me. David Leonard, for being a role model who inspired me to pursue higher education. Erika Laing and Xander Hendrickson, who helped me recover from a house fire that consumed most of my belongings. Lisa Kennedy, who gave me a place to stay when I had no other options in the aftermath of the fire. Peter and Shelly Sandrian, for awesome home-cooked meals when I didn't have time to cook. Meghan McCord,

for defense advice and generalized awesomeness. Ran Liu and Patrick Beukema, for beers after long days. Darcy Mandell, for helping me with writing technique. Kristina O'Neill, for the pilot illustration. To my current roommates, Stephanie, Gunther, and Matt for being supportive and understanding during the writing process. Lastly and most important, I'd like to thank my nuclear family: Dominic Palazzolo, Julie Leonard, and Lydia Palazzolo, for always believing in me over the years. There is no way I could have completed this process without their love and support.

1.0 BACKGROUND

This project is a study of how visually-guided arm movement is represented in the activity of single neurons in the motor and premotor areas of the brain. Our main goal is to determine how visuomotor transformations take place in ventral premotor cortex (PMv). This chapter contains a summary of previous studies with a focus on neurophysiological methods. Section 1.1 introduces three major psychophysical studies that strongly suggest reaching movements are guided in visually-derived kinematic space. Section 1.2 summarizes the history of anatomical studies of the premotor cortex and its interconnections with visual and motor cortices. Section 1.3 summarizes the most relevant neurophysiological results in visually guided reaching experiments.

1.1 PSYCHOPHYSICAL STUDIES OF REACHING

1.1.1 A Two-Phase Model For Vision during Reaching

Classic work by Woodworth [90] pioneered the notion that there are two distinct temporal epochs during reaching movements. First, while the eyes are fixed on the target location and the hand is unseen, the *initial impulse* phase propels the hand toward the general vicinity of the target. As the location of the hand translates into view, it is honed onto the location of the target during the *current control phase*. These conclusions were reached by evaluating the accuracy of aiming while varying the time allotted for overt movement with a metronome, thereby limiting the length of the current control phase. At short movement times, reaching error increased to a level equivalent to trials while the eyes were closed, establishing visual feedback as a requisite for accurate reaching.

1.1.2 Visually-Derived Precursors for Reaching

Reaching to a target position under natural conditions tends to be smooth and straight with a bell-shaped velocity profile, which is often considered a sign of optimality. Modeling results suggest either the minimization of jerk, in a kinematic coordinate frame mediated by vision, or the minimization of torque, in a dynamic coordinate frame mediated by proprioception [26, 85]. Two significant studies have compared these models by observing adaptation in one coordinate frame in response to perturbations in the other. Wolpert and colleagues [89] distorted the view of the hand during a reach task using a sinusoidal curve illusion that increased the perception of curvature maximally at the midpoint of movement. Results showed that true hand movement became more curved in the opposite direction to reduce the perceived curvature, suggesting that the motor system's ideal trajectory is a straight line in visual coordinates.

Shadmehr and Mussa-Ivaldi [75], applied an altered force field while learning a directional reach task using a robotic manipulandum. In early trials, the kinematics of movement reflected the changes in the force field, which became irregular and distorted. Trajectories straightened in late trials by changing muscle stiffness, which alters the relationship between force and the resultant displacement, illustrating again that the motor system prefers an optimization in kinematic space. Flanders et al. presented a model that utilized error data from a memorized pointing task to infer the coordinate system of target location [25]. In these tasks, subjects consistently undershot the distance of the more distal targets. According to the model, this error in pointing resulted from the neural implementation of transforming shoulder-centered target parameters into a set of arm orientations for capturing the target. This transformation places a visually-derived final location into a coordinate system compatible with kinesthetically derived initial coordinates of the arm. The authors conclude that the difference of these representations could be a precursor to a kinematic reach command.

Results in this section support the idea of a model system that is at least partially controlled by a high-level *difference vector*, which can be constructed by subtracting the position of the hand from the target in a visual coordinate frame. This could feed into an adaptive *inverse model*, which in turn outputs a motor command for muscle activation (see figure 1.1). One of the main goals of this dissertation is to determine if neuronal activity in PMv corresponds to the difference vector.

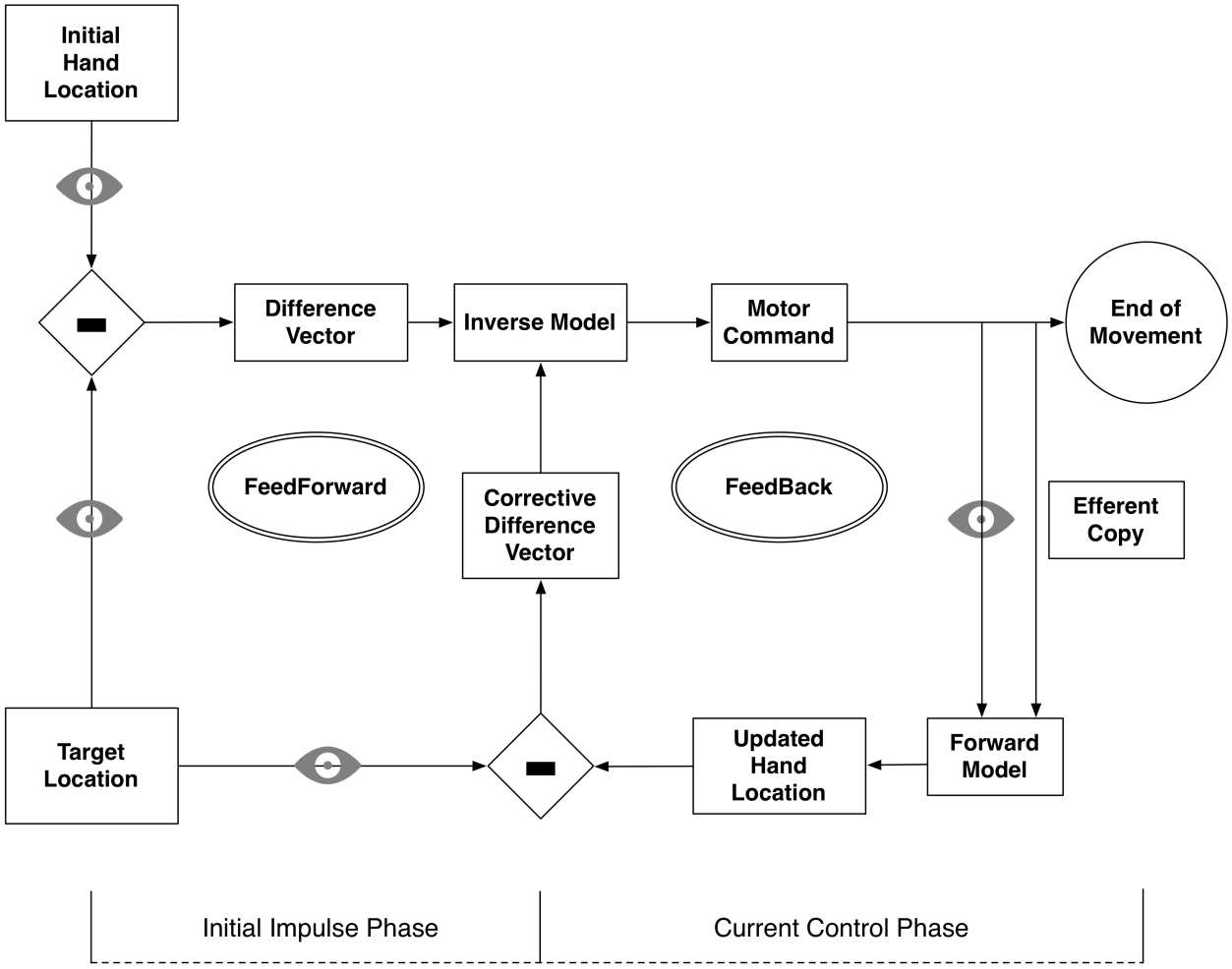

Figure 1.1: **Vision for Action** A model showing how vision may be used in a hybrid control system. Eye icons correspond to visual information. *Feedforward:* Initial hand location is subtracted from the target position, resulting in a difference vector feeding into the Inverse Model, which takes into account the stiffness properties of the arm to estimate a dynamic motor command that will produce the desired displacement. This initiation of movement may represent Woodworth's Initial Impulse Phase. *Feedback Loop:* Sensory inflow and motor command outflow feed into the Forward Model, which quickly predicts an updated end-point (hand) location based on the dynamic state of the arm. This is subtracted from the location of the target, and if there is a discrepancy, an updated motor command is generated. This homing stage of movement may represent Woodworth's Current Control Phase. Derived from [16, 52, 65, 46, 90].

1.2 ANATOMICAL CHARACTERIZATION OF THE PREMOTOR AREAS

1.2.1 Early Lesion Studies and Cytoarchitecture

In the late 19th century, physicians lacked a unified conceptual framework for diagnosing disorders of the nervous system. To address this, John Hughlings Jackson, an English neurologist, applied the principles of *The Origin of Species* to observations from focal lesion studies to develop a systematic procedure for identifying neurological disease. He posited that the motor system is composed of discrete levels that arose evolutionarily, with higher levels controlling and suppressing the action of lower levels [43]. The lowest level consisted of the ventral spinal cord and cranial motor nerves, with representations of each body part. The intermediate somatotopically organized level was composed of the motor cortex and the basal ganglia. The highest level consisted of the *premotor frontal cortex*, which was referred to as a "complex rearrangement of lower centres". In 1882, Jackson concluded that "The higher the centre the more numerous, different, and more complex, and more special movements it represents." [44]. In 1905, Cambell et al. and Brodmann et al. established cytoarchitectonic results, describing an area called the "intermediate precentral cortex" (including Brodmann areas 4 and 6) that may contain the site of Jackson's highest level [5, 10].

The term "premotor cortex" was coined by Fulton, during the first half of the 20th century [30]. Most motor system research during this time defined the boundaries of motor cortex using cytoarchtectonic methods, namely by evaluating the size of pyramidal neurons. The premotor cortex was generally determined to be the agranular region anterior to the dense population of giant pyramidal neurons in layer V of the primary motor cortex (M1) [6]. This afforded much controversy, since giant pyramidal cell diameters were hard to discretely classify, and some large cells still existed in anterior regions [88]. In addition, these boundaries rarely delimited consistent functional characteristics[18].

1.2.2 Functional Characterization

To address issues with cytoarchtectonic methods, more recent techniques investigate corticospinal projections and direct muscle connections to determine somatotopic motor representation. The dorsal premotor area (PMd) and the ventral premotor area (PMv) (see figure 1.2) have been found to project both to the spinal cord and the M1 arm region [17].

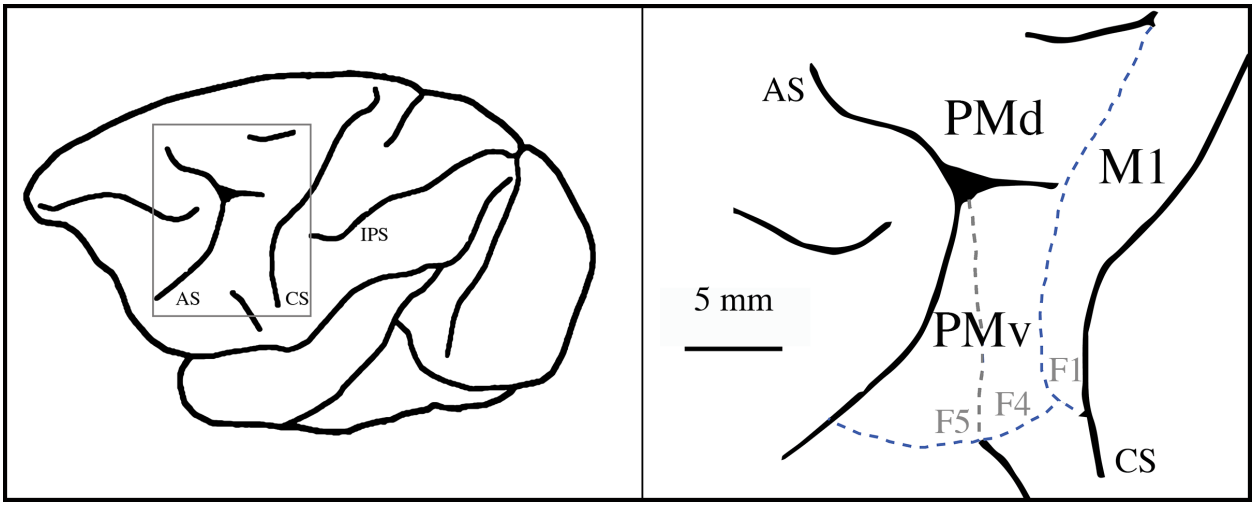

Figure 1.2: Modern subdivisions of cortex in the macaque monkey. Cortical areas include: **PMd:** Dorsal Premotor area, **PMv**: Ventral Premotor area (cytoarchitecturally divided into F4 and F5 regions), **M1:** Primary Motor cortex (F1 region). Cortical landmarks include: **CS:** Central Sulcus, **AS:** Arcuate Sulcus, **IPS:** Intraparietal Sulcus. Illustration derived from [59].

1.2.2.1 Lesions of the Ventral Premotor Cortex

Ablation of the ventral premotor area produces peripersonal hemispatial neglect in both the somatosensory and visual modalities [68] in monkeys, and may also be the case for humans [40]. An interesting study by Berti and Frassinetti [2] reported observations of a patient who exhibited peripersonal neglect following a right hemisphere stroke. The patient was proficient in line-bisection tasks with a light pen, however, when a wooden rod was used for the same task, the spatial neglect re-emerged. The experimenters suggested that the use of the rod extended the region of space contiguous with the body, concluding that far space was remapped as near space. Other lesion studies showed deficits in visual tracking [55], and remapping visual space to motor space during tasks requiring prism adaptation [56]. In the latter study, it was shown that lesions of area PMd had little to no effect on prism adaptation. These studies generally support the idea that it is the PMv that is responsible for interpreting visuospatial features near the body to serve action planning.

1.2.2.2 Projections to Premotor Cortex from the Parietal Cortex

Qualifying downstream connections from the parietal areas is one way to interpret functional differences in the premotor areas. Tanne-Gariepy and colleagues, utilizing simultaneous retrograde tracers, found a clear dichotomy between the PMd and the PMv. They concluded that neuronal circuits from superior parietal lobule project to PMd, and those of the inferior parietal lobule project to the PMv [80]. These sets of projections may correspond to segregated visuospatial information streams. A summary of inputs and their salient functional properties from multiple studies are outlined below:

Parietal areas with major or moderate inputs to the PMv:

- *Area 5d (PE):* Firing rate may encode kinematics of the arm with respect to the body [49]. They also encode proprioceptive information for more than one joint, and somatosensory skin responses (60% directionally selective) [71].
- *Area AIP:* Neurons modulate during grasping of specific objects, sometimes when only presented with a graspable shape. [72].
- *Area 7b (PF):* Neurons may encode a *polysensory* receptive field; a visual receptive field surrounding a somatosensory receptive field. This is often called *peripersonal space* encoding [61].

- *Area VIP:* Projections primarily to medial PMv (F4). Neurons encode gaze-independent receptive fields for peripersonal space with preferred directions for stimulus direction [15, 35].

Parietal Areas with major or moderate inputs to the PMd:

- *Area MIP:* Neurons encode target location with respect to an eye-centered reference frame [1].
- *Area PEc:* Neurons modulate with limb posture, whether or not the arm is passively moved. [4].

Parietal Areas with major or moderate inputs to both the PMd and the PMv:

- *Area PEip:* Neurons modulate with arm movement, usually in a specific direction only [49], and may also encode peripersonal space [69].

The division of downstream parietal projections to the premotor areas suggests that a) pre-movement target location, and proprioceptive information is transferred to the PMd, b) somatosensory, proprioceptive, and object shape/grasp information is transferred to the PMv, and c) both receive peripersonal space information, with stronger input to the PMv.

1.2.2.3 The Function of the Ventral Premotor Cortex Two parallel networks are utilized for visuomotor processing, one for reaching, and the other for grasping [45]. The reaching pathway receives spatial information about the location of an object and the proximal muscles of the arm, and the grasping pathway receives information about the attributes of the object (e.g., size and shape) and distal muscles of the hand. Judging from functional inputs, the PMd may be included in the former, and the PMv the latter [80]. In the following section, results from neurophysiological studies that add complexity to this hypothetical construct are discussed. First, the PMv contains neurons that encode object location near the body during passive behavior [27, 37, 70]. Second, work has shown that neuronal activity in PMv corresponds to the direction of arm movement in extrinsic space during overt movement [48, 64, 70, 74] (see section 1.3.5), and during passive observation of the same movements [28] (see section 1.3.5.2). One goal of this project is to determine whether these seemingly disparate signals may be encoded by activity from the same neurons in the PMv, suggesting coordination of multiple sensorimotor channels.

1.3 RELEVANT NEUROPHYSIOLOGICAL STUDIES OF PMV

1.3.1 Early Studies

Before the 18th century, it was generally accepted that the striatum was the brain's highest motor center, and the cerebral cortex was dismissed as a "rind" of no consequence [81]. In 1870, Fritsch and Hitzig [29] controversially established its functional importance by applying electrical stimulation to the cortex to artificially generate discrete movements. They also demonstrated a topographic representation of the contralateral body by stimulating different regions. Responses from the scientific community at the time expressed skepticism based on the high amount of current that was being used, claiming that the striatum may be still activated. Consequently many of the studies that followed focused on finding somatotopic maps using progressively smaller current injections and measuring resultant muscle flicks and twitches [57, 66]. M1 became known as a collection of coordinated subregions, each activating one or two muscles. Woolsley and colleagues[91, 84] attempted the same methods in the premotor area and found stimulation did not evoke movement (in deeply anesthetized monkeys) nor did lesions reveal deficits in control of the arm. They concluded that the premotor area was not a part of the cortical motor system, however they defined the boundaries for *non-primary* motor cortex as "an area anterior to the central sulcus and not excitable using conventional means".

In the late 60's, Evarts expanded the field of motor neurophysiology by performing single neuron recording in awake behaving monkeys. In his early experiments, he found that pyramidal neurons with descending projections in M1 (identified by recording back-excitation from the medullary pyramids), changed their firing rate just prior to movement [22], and many increased their firing rate with the magnitude of force (or the magnitude of change in force over time) generated during the movement [23]. Subsequent experiments led to two concepts that have since been utilized and supported by investigators of the motor areas. First, he found changes in firing rate that were temporally correlated with the intention of an animal to carry out a trained movement before an anticipated stimulus, referred to as *set-related activity* [20]. Second, he posited that M1 pyramidal neurons may be modulated or "gated" for voluntary movement control by nearby cortical areas [21]. In summation, Evarts established that the M1 is not simply a mosaic of discrete muscle controllers, and has complex attributes that reflect planned movement coordinated by other areas of the brain.

1.3.2 Spatial Descriptions of Neuronal Modulation

Neurophysiological studies of the motor system often rely on paradigms that vary specific features of movement while recording electrical activity. Models are then built to describe the relation between recorded neural activity and those features.

1.3.2.1 Reference Frames Spatial descriptions usually depend on the perspective of an observer. For example, a marble dropping to the floor inside of moving car can be described in two different ways depending the location of the observer. A reference frame fixed to the car (the passenger) will witness a fall straight down, while a reference frame fixed to the earth (a pedestrian) will witness a curved trajectory (straight fall + velocity of the car). In neuroscience, neurons "observe" stimuli from reference frames fixed to parts of the body, such as the retina, the head, and the arm. We can examine these reference frames by recording firing rate while moving the location of stimuli with respect to potential reference frame origins. For instance, in a retinotopic reference frame, the firing rate of the neuron should remain constant as long as the location of the stimulus remains stationary with respect to the retina. The location of a point or stimulus with respect to the origin of the reference frame can be described with a vector. If parameters in a reference frame seem

to be encoded vectorially, it should be possible to choose a coordinate system that describes the neural modulation with a set of base vectors that share an origin with the reference frame. Any point observed in a reference frame can then be described by the amplitude along each base vector - serving as a coordinate axis. In motor neurophysiology, two reference frames are often used to model firing rate in an effort to determine if modulation is driven by kinetic or kinematic features of movement. An *intrinsic* reference frame can be constructed from the contraction of muscles in the arm as base vectors. *Extrinsic* reference frames can be constructed from orthogonal cartesian base vectors located in exterior space, and are used for visually-derived variables. Our experiments are primarily concerned with comparing how neuronal activity varies as a function of one of several extrinsic features, which can be described using vectors defined by the instantaneous change of position over time. For example, a vector representing the direction of hand velocity originates on the hand and points in the instantaneous direction of translation.

1.3.3 Generating Motor Action from Sensory Information

1.3.3.1 An Effector-Centered Reference Frame A component of volitional movement is driven by sensory input from visual, tactile, and proprioceptive sensors that must be integrated and transformed into a pattern of muscle activation. Visuomotor studies of parietal and premotor neuronal activity emphasize coordinate transformations and suggest that these structures encode an eye-centered representation modulated by eye-, head-, body-, or limb-position signals (see section 1.2.2.2). This reference frame may facilitate communication between various sensory areas to generate a successful reach by subtracting the end-effector position from target position to yield an effector-centered coordinate system for target location. This dissertation addresses whether or not such a signal may be represented in the PMv. Since the PMv receives information from the parietal and other premotor cortices [67], it seems likely that this vector could be constructed and may contribute to velocity-correlated activity found in other cortical areas [8, 76]. Robot arm controllers align visual input and position feedback to construct an ideal trajectory vector as a reference signal for iterative dynamic output [7, 32]. Descending command areas may utilize similar input from the PMv for the same purpose, establishing a difference vector from the hand to the target before parameters such as acceleration and muscle torque are incorporated.

1.3.3.2 Temporal Structure of Motor Processing Once a suitable coordinate system has been matched to neural activity, the latency of this modulation can be evaluated relative to movement onset (15% of peak reach speed). Conventionally, the minimum time between a visual stimulus (i.e. presentation of a target) and movement onset is 175-200 mS [14, 12]. Instructional delay periods are often incorporated into experimental paradigms to extend this epoch allowing more temporal subdivision of pre-movement activity [48, 50]. In this dissertation we will be reporting latencies without a delay period to broadly determine whether neural activity corresponds to early variables for motor planning, motor command execution during movement onset, or visual feedback after movement onset.

1.3.3.3 Cosine Tuning for Dynamic Parameters Neuronal activity associated with coordinate frames has been found to peak in a single direction of arm movement referred to as the *preferred direction*. Firing rate decreases linearly with the cosine of the angular difference with the preferred direction [34]. This behavior can be modeled using a cartesian coordinate system:

$$\Phi = b_0 + b_x m_x + b_y m_y + b_z m_z \tag{1.1}$$

$$= b_0 + k \cdot cos(\theta_{CM}) \tag{1.2}$$

$$\bar{\Phi} = cos(\theta_{CM}) \tag{1.3}$$

where $m_{x,y,z}$ is hand speed in three dimensions of cartesian space, $b_{0,x,y,z}$ are the dimensional weights, b_0 is the baseline firing rate, and Φ is the firing rate of the cell [73]. This model can be shortened to equation 1.2, where k is the range of firing rate for the neuron, also referred to as the *modulation depth*, and θ_{CM} is the angular difference between the preferred direction of the cell and the movement velocity. When b_0 and k are shifted to the left side of the equation, normalized firing rate ($\bar{\Phi}$) is equivalent to $cos(\theta_{CM})$ (equation 1.3). Predicted firing rate is the highest when θ_{CM} is zero, or when the direction of movement is in the preferred direction. This dissertation attempts to determine how directional variables associated with movement may be represented in M1 and PMv during active reaching. Multiple linear models like the one above can be evaluated as a function of various kinematic features. For example, discharge rate can be predicted as a function of cursor velocity instead of hand velocity. The relative fit of each assumed model to the data set can be evaluated after finding the dimensional weights using linear least squares. This method is discussed further in section 2.5.1.

1.3.4 Activity Corresponding to Extrinsic Features in PMv

1.3.4.1 Visually-Derived Motor Coordinate Frames Previous work has shown that motor action can be accurately decoded in a visual reference frame. One example is an elegant study done by Kakei et al. [48] in which animals were instructed to move the wrist in eight different directions while varying forearm posture, which effectively dissociated extrinsic from intrinsic coordinates. By examining directional modulation, they found that activity from the PMv primarily corresponds to an extrinsic representation of hand movement direction, independent of muscle contraction. Results from the same experiments in M1 [47] found a similar representation in a smaller number of neurons. The authors pointed out that these findings, concerning the origin on the extrinsic coordinate system, could be interpreted in at least three different ways - directional tuning could be centered on the hand, the cursor, or the target. One of the main goals of this project was to determine the origin(s) of the extrinsic coordinate system in PMv. Three tasks were designed to directionally dissociate three putative origins, where each task directionally dissociates one from the other two. By building linear models of firing rate as a function of velocity in each coordinate frame, we were able to compare firing rate modulation in each task. The origin of the reference frame was revealed when preferred directions were similar in all three tasks in one coordinate system.

Schwartz et al. employed an illusion to dissociate the displayed direction of movement (the cursor trajectory) from the physical direction of hand movement using a virtual ellipse-drawing paradigm [74]. Population activity in the PMv represented the cursor trajectory, while those in M1 matched the hand trajectory (see figure 1.3). The authors concluded that cell populations from PMv may be part of a visual processing circuit that represents perceived action. Cross correlation analysis of cortical discharge relative to movement revealed that latencies for the PMv population roughly fell into two intervals, $<$100 mS before and $>$100 mS after hand movement (see figure **??**). These findings suggest separate processing mechanisms for visual planning and visual feedback. Perhaps this is evidence of the components of visually-guided reaching found in Woodworth's two-phase model (see figure 1.1). We evaluate latencies in this dissertation to determine when putative features of movement are represented relative to movement onset.

Ochiai et al. [64] constructed a paradigm that also dissociated the display of hand movement from actual hand movement using a hand-shaped cursor. In agreement with the previous study by Schwartz et al., they found that neuronal activity in PMv was predominantly correlated with the trajectory of the cursor. In addition, half of these neurons showed a preference for which side of the cursor intercepted the target. The authors referenced the Kakei et al. study ([48]), and speculated that single cell activity was encoding the displayed movement of the cursor. Several features of this experiment left questions unanswered. First, the experimenters only sampled three directions of reach, separated 45° on a 2-D plane. No tuning functions for direction were presented. Second, the experiment was a delay task, yet they did not utilize activity during the cue period, before the go period, to control for visual responses. Third, only pre-movement activity was sampled, so as to avoid visual feedback.

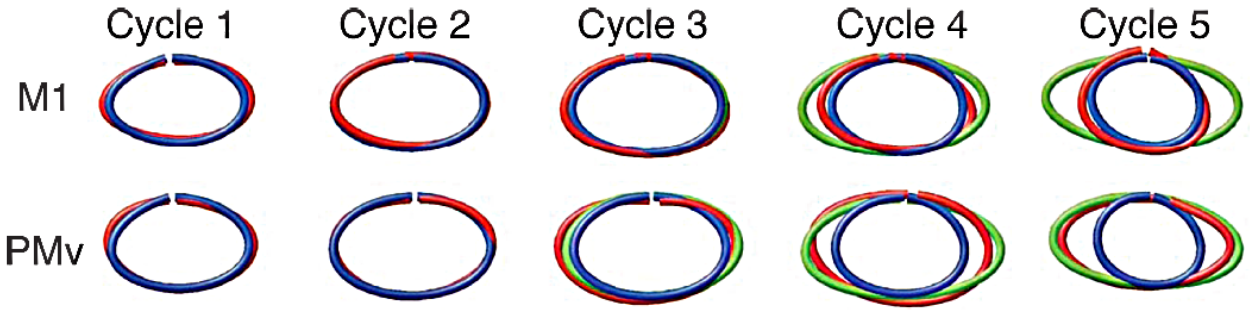

Figure 1.3: **Differential Action and Perception:** . Red = neural trajectory, blue = hand trajectory, and green = cursor trajectory. Monkeys were trained to trace ellipses in a virtual paradigm, while the hand was occluded. The figure above shows five cycles of tracing, as the gain in the horizontal direction was increased on the last three cycles. By the fifth cycle, the monkey was drawing a circle with its hand, even though the displayed figure was still an ellipse. Neural trajectories matched the displayed trajectory in PMv, and the hand trajectory in M1[74].

The body of work summarized in this section establishes that neural activity in the PMv corresponds to visually-derived movement features. This dissertation will analyze neural activity from reach tasks while changing the view so as to dissociate activity corresponding to different visual contexts. We hypothesize that neural activity may vary in correspondence depending on the reference frame used for the model.

1.3.5 Modulation during Passive Behavior in the Ventral Premotor Cortex

1.3.5.1 Polysensory Neurons Two different studies have shown that neurons in the PMv (referred to as *polsensory neurons*) encode object location near patches of the skin on the face, arm, or hand [27, 37]. These neurons respond to tactile stimuli, with gaze-independent visual *receptive fields* (RFs) extending outward (see figure 1.4). Some have intersecting auditory fields [39], suggesting that multiple modes of sensory input are incorporated. Similar neurons in the parietal cortex have been shown to transfer their RF to an image of the hand on a screen [42]. The complexity of this activity suggests that this signal is more than an evoked response, implying a perceptual construct. Graziano and colleagues illustrated this by turning off the lights as a silent stimulus, already previously observed by the subject while the lights were on, was moved out of the RF, eliminating all sensory information about the location of the object. A fraction of these cells persisted with their response until light was restored, suggesting that neural activity corresponded to a memorized location in space [38].

There are two interpretations of this work. These responses may correspond to a multipurpose sensory map for proximal interactions (i.e. to serve defensive behavior) [79, 36], or they may correspond to an *effector-centered* coordinate frame for target location [27]. Computational methods have implied the existence of a high-level signal that encodes visualized discrepancies between the effector and the target online (see section 1.1.2). Furthermore, polysensory discharge is correlated with stimulus direction, suggesting that more dynamic parameters may be encoded [27, 38]. There is also much variation in the shape and nature of these receptive fields. In some cases, neuronal activity will respond to the direction of motion >1 meter away. Since activity in PMv is also related to head and arm movement [33], the extension of this work to volitional behavior is likely to reveal new features of polysensory cells.

1.3.5.2 Mental Rehearsal and Action Recognition Another form of passive modulation in the motor areas takes place during action observation. Neurons that discharge during active arm movement also discharge while watching or preparing to watch the same movements being performed. There are two main subclassifications of this modulation, namely *mental rehearsal* and

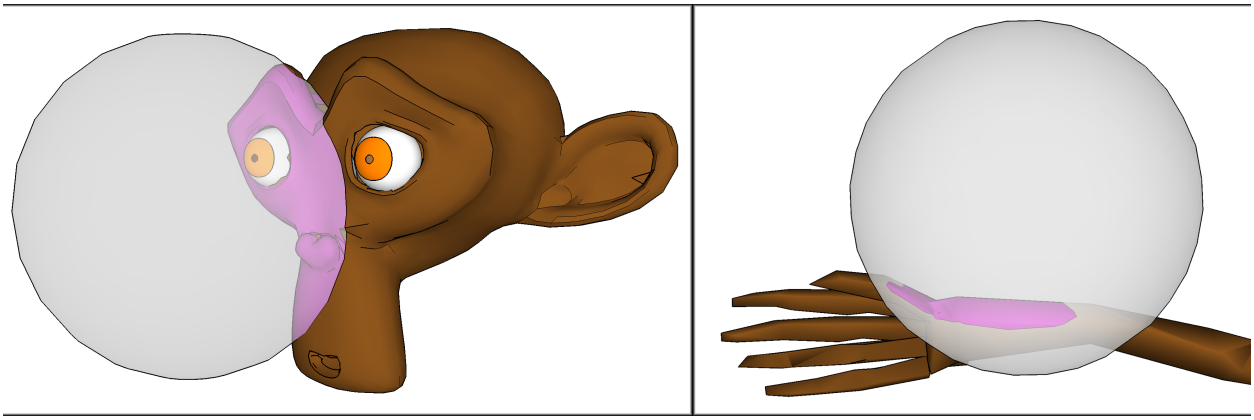

Figure 1.4: **Polysensory Neurons:** Artistic rendering of the receptive fields of two neurons found in the PMv of Monkey D. Pink overlay represents the somatosensory component, and the spherical region extending outward represents the visual component.

action recognition. Mental rehearsal has been studied in the PMd [13], and M1 [19, 82] and may represent the intended trajectory of an effector (or surrogate effector) whether or not the action is generated. This signal is most active before movement onset (in a delay period task) and is speculatively related to anticipated visualized action[13]. A recent experiment performed by Lemon and colleagues tested pyramidal tract neurons in M1 while observing grasping [87]. They found observation-like activity, but also *suppression neurons* which seemed to facilitate action during overt movement, and then reversed their response during observation, presumably to suppress descending command signals to the spinal cord. These neurons were considered closely connected to muscle control in the cortex, having a low level of visual abstraction and a coordinate system originating on the limb.

Action recognition has been studied extensively by Rizzolatti and collegues in a subgroup of cells located primarily in the F5 subregion of PMv known as *mirror neurons*. Activity from this area had previously been shown to modulate during grasping and object manipulation. Mirror properties of each neuron were evaluated while the experimenters performed a series of grasping actions in front of the monkey. The authors suggested that these neurons responded to active object interaction by either the experimenter or the monkey. Most of these responses seem to be an evoked effect after movement onset. Pieces of the whole movement, including object presentation and the

grasping motion only, did not evoke the same response. Other studies have focused on response persistence by observing discharge similarity between performance and observation while changing the availability of sensory information [28]. For example, replaying sounds of salient actions can activate some mirror neurons [53]. They proposed that these neurons are involved in generating an internal representation of a motor event [31]. Area F5 is considered a cortical homologue of Broca's area in humans, which is a speech processing area. Communication also relies on recognizing the movement of others, and must be compared internally to facilitate understanding.

Directional preference during observation has been found in a small number of cells in F5 when the experimenters performed the action originating from one side of the monkey vs. the other [31], but there has never been a study performed that evaluates firing rate models as a function of the direction of observed arm movement in the PMv. Emphasis on multiple coordinate systems during observation-related activity in PMv and M1 has been minimal. Previous work from our lab has found that these models are fit well during overt movement. We wish to extend this work by evaluating multiple directional tuning models based on various visuomotor features of observed action throughout M1 and PMv to determine what visuomotor processing stages may be taking place. We ask: *Is observation activity driven by sensory information, a visualized version of action, or a true rehearsal of limb kinematics?*

2.0 SPECIFIC AIMS & METHODS

2.1 INTRODUCTION

Voluntary movements are often a reaction to a visual stimulus and are monitored visually. The underlying cortical mechanisms can be considered serial because they originate with visual input from the retina and end with impulses to the muscles. The intermediate process incorporates a series of coordinate transformations from which reach plans are generated. Neural activity corresponding to visually-derived trajectories could be a immediate precursor to a motor command. Previous research from our laboratory suggests this visuomotor stage of processing may take place in the ventral premotor cortex. We propose that this representation may be separable when the displayed action differs from the actual movement. We will use a virtual reality paradigm to display several different viewpoints of the same arm movements in an attempt to observe and model neural activity that changes with the view. These neural events may be sensory-driven and behave similarly during active and observed movement. The PMv has been shown to respond to visual stimuli under two distinct passive conditions: reach observation, and peri-personal object motion. An analysis of the model discrepancy between active and passive conditions may reveal an underlying construct specific to the intention to generate a visually guided reach.

2.2 SPECIFIC AIM 1

Does neural activity in M1 and PMv show evidence of visuospatial transformation?

We know from everyday behavior that the brain is capable of performing visuospatial transformations that map desired visual trajectories onto motor commands for hand trajectory. For example, a pilot can fly a plane from the cockpit, or from the control tower while operating remotely (see figure 2.1). Even though the pilot has to move his hands the same way, the two viewpoints would require different transformations to produce the same flight path. We hypothesize that a component of these transformations are being generated in the ventral premotor cortex (PMv). We will test this hypothesis by recording PMv and M1 activity from primates while they perform reach tasks that require them to learn multiple visuospatial transformations. We will then determine if neural activity corresponds to reach direction in several coordinate frames. If separate representations are found, we will evaluate whether they can be mapped together using the applied experimental view transform. Finding signals in the brain that change with the required visuospatial transformation will give new insight into how the brain maps what we view to what we do.

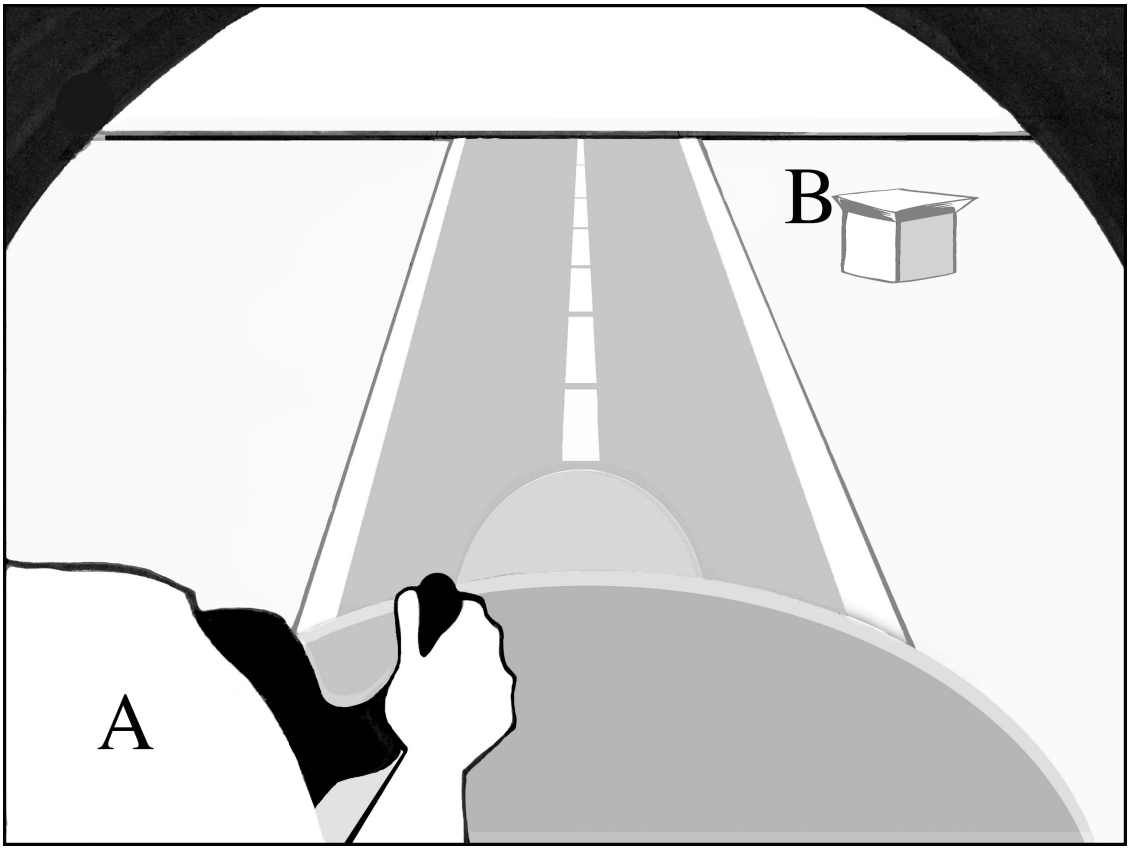

Figure 2.1: **Two visuospatial transformations:** The same flight path can be controlled by moving the hands in the same way whether viewing from the cockpit (**A**) or from the control tower (**B**).

2.2.1 Sub-Aim 1

Are there multiple discrete extrinsic coordinate systems represented in neural activity during active movement? We will search for these as the subject is required to perform different transformations to complete a task.

The motor system may plan movement as a visually-derived trajectory. Previous studies have found neuronal behavior correlated with the direction of reach, but the origin of this coordinate space has not been fully evaluated [9, 48, 51, 78]. Previous research from our laboratory suggests that PMv and M1 may be composed of subpopulations whose activity corresponds to different directional features of arm movement [74].

We will require subjects to perform three tasks with identical hand movements and different view transformations. First, subjects will perform the *standard reach task* (see task description in section 2.2.3.2) in which the motion of the hand is mapped to a cursor displayed above the shoulders in a natural framework. Second, subjects will perform the *anti-reach task*, which moves the cursor opposite to the direction of the hand. Mechanistically, this can be generated with a negative identity rotation matrix (see task description in section 2.2.3.3). Subjects will also perform the *stationary cursor task*, which changes the viewpoint of the task so that the reach target appears to moves toward the stationary cursor, in the opposite direction of the hand (see task description in section 2.2.3.4). This transformation changes only what appears to be moving in the workspace, with no required rotational transformation. After collecting data from each task, linear models of firing rate will be calculated as a function of hand direction. Neuronal modulation corresponding to the movement of the hand would have the same preferred direction across all tasks. Changes in neural activity corresponding to different views may be recognized as changes in directional tuning. Neuronal modulation related to cursor direction would be expected to change only during the anti-reach task. Neuronal modulation corresponding to displayed motion would change during the anti-reach and stationary cursor tasks. Linear models will then be calculated as a function various new hypothetical coordinate systems. Activity with similar preferred directions across tasks in the same coordinate system will be labeled.

2.2.2 Sub-Aim 2

Can these coordinate frames be differentiated in the anatomical and temporal domains, suggesting a systematic substrate for visuospatial transformation?

Coordinate systems identified with functional criteria may be related to different aspects of visuomotor control. After functional classification, we will further characterize these groups of units based on their response latency and anatomical location. To determine the latency of each neuron, we will evaluate the time, relative to movement onset, at which the tuning function is best fit. Cortical penetration locations will be examined to compare coordinate system representation in M1 and PMv.

2.2.3 Fundamental Elements of the Experimental Paradigm

2.2.3.1 Overview We designed a virtual interactive workspace that allowed us to show the subject different views of the same reaching movements. Two water-restricted monkeys were trained to perform (a) three active reaching tasks that required moving the hand to the same set of 14 different target positions chosen at random (see figure 2.2c), and (b) two passive tasks that required holding a position in the center of the workspace. Hand position was sampled in three dimensions at 60 Hz using the Optotrak system and timestamps were aligned on movement onset. We calculated the first derivative of each dimension of hand position to calculate velocity and the norm, or the length of each velocity vector, to calculate speed. In all cases, the hand location will be displayed on the screen as a green spherical cursor, target location was displayed as a blue sphere, and a checkered virtual environment was rendered in the background (see figure 2.2a,b). The subject will be required to progress through a series of states in order to be successful (see figure 2.3, passive in figure 2.8). Upon failure, the target will be shuffled with the remaining targets to be displayed again until a success results. After the subject is able to perform all of the tasks with at least a 60-70% success rate (3-6 months for a naive monkey), a chamber will be implanted to record neural activity.

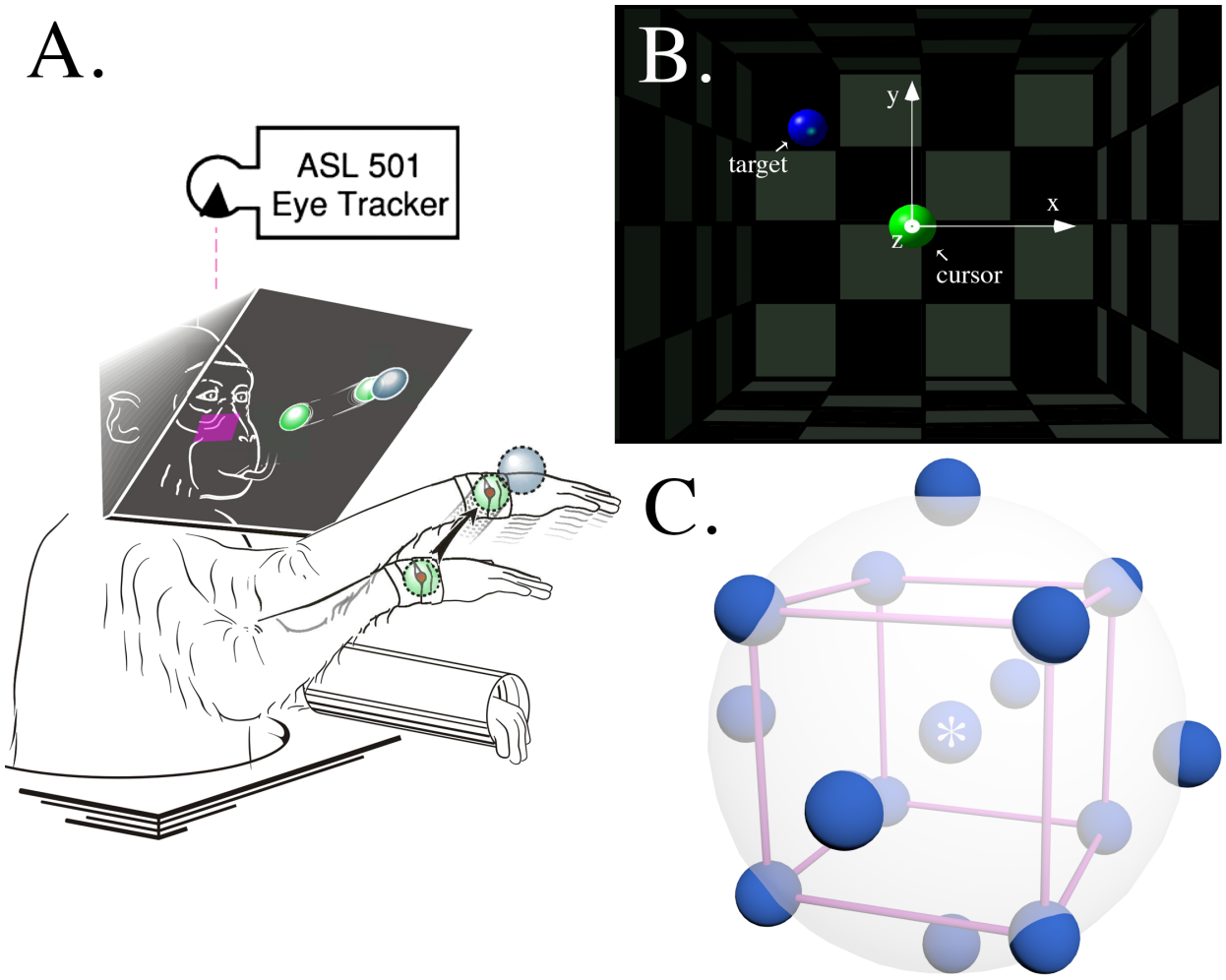

Figure 2.2: **A. Basic Paradigm:** A head-fixed monkey with its ipsilateral arm (relative to the recording site) restrained is perched in front of a mirrored stereoscopic display, which displays the virtual workspace. The hand position is recorded using an infrared tracking system (Optotrak 3020, Northern Digital, Waterloo, Ontario, Canada). Eye position is recorded with an infrared eye tracker (Model 501, Applied Science Laboratories). A "hot mirror" (pink) is positioned below the right eye to reflect the infrared image of the eye to the eye tracker, while allowing visible light to pass through. **B. Virtual Workspace:** What the monkey sees. The green cursor, a surrogate effector, moves as the hand moves. The blue target lies in one of 14 target locations. The global coordinate system is also depicted. X: left to right. Y: down to up. Z: far to near. **C. Physical Target Locations:** 14 target positions (blue spheres) were chosen to sample the Cartesian workspace. 6 targets (pointing outward from the faces of the pink cube) defined the coordinate axis while 8 more targets were positioned on the corners of the cube. A target was placed in the center of the workspace (white asterisk) to begin each trial. All reach targets lie on a sphere with a .06 meter radius. The cursor and target size had an 8mm radius each, with a zone for success upon intersection $\approx 1.6cm$ from the center of the target.

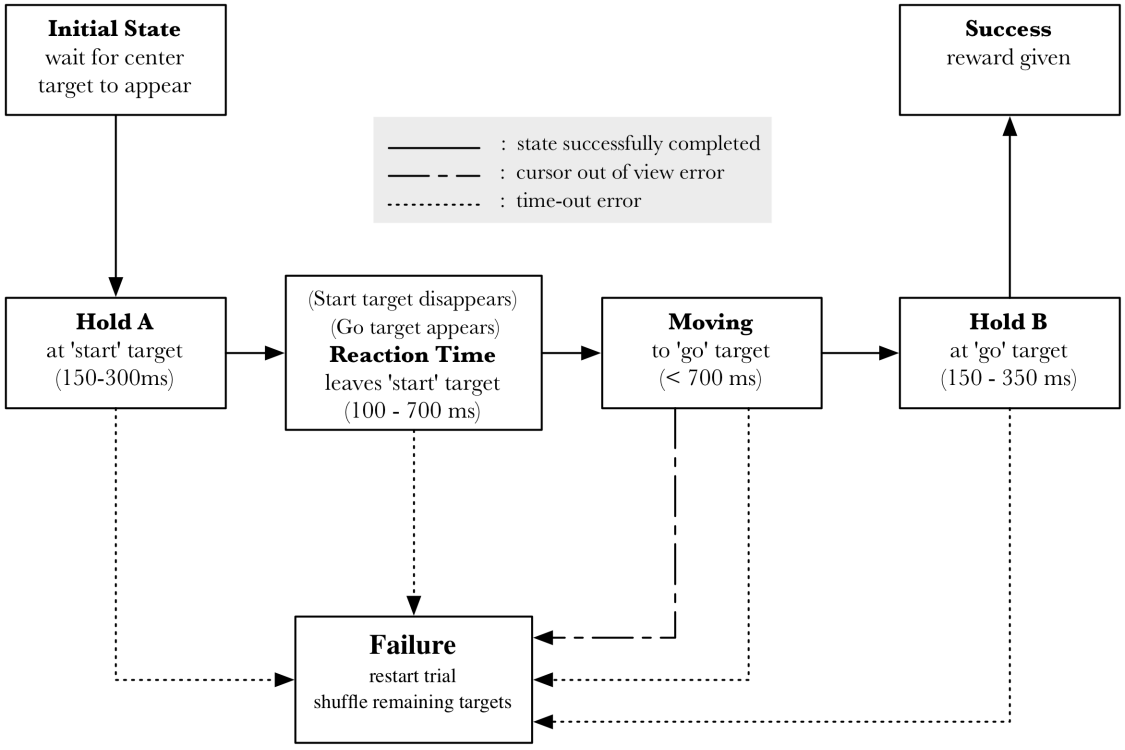

Figure 2.3: **State Progression through One Trial** A trial begins when the center target appears and the monkey holds the cursor over its location for a period of 150–300ms (Hold A) which is randomly predetermined for each trial. The center target then disappears and one of the fourteen peripheral targets appears. The monkey has 100ms–700 ms to begin to move away from the center (Reaction Time), and move the cursor to the peripheral target (Moving). When the cursor reaches the target, it must be held in that position for 150–350ms for a reward to be given (Hold B, Success). Failure results and the trial restarts if: a) a hold position is not held for the Hold A or Hold B epoch, b) the cursor leaves the visible workspace during the moving state, or c) the cursor does not leave the center position during the Reaction Time epoch.

2.2.3.2 The Standard Reach Task Hand velocity is mapped directly into the virtual workspace. For example, a physical hand velocity [1,1,1] would be displayed as cursor velocity [1,1,1] (see figure 2.4).

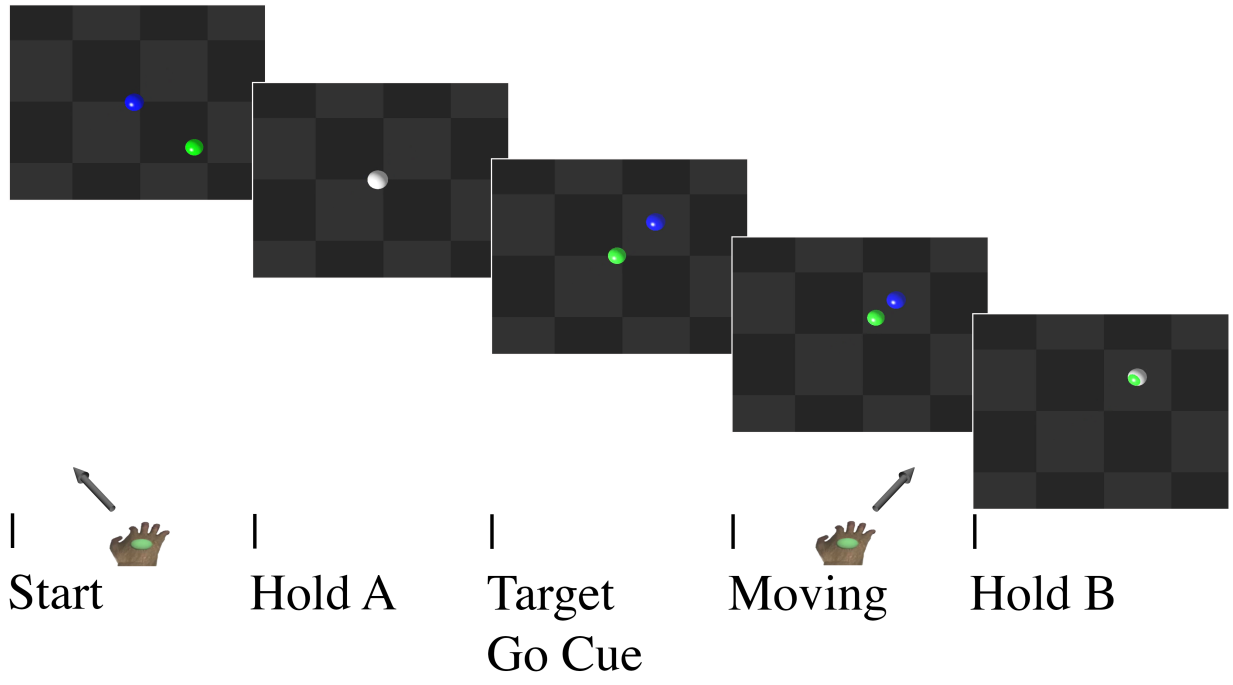

Figure 2.4: **Standard Reach Task Display:** This figure shows the display as the subject reaches up, away, and to the right. The cursor (green) represents the position of the hand without any view transformations. The virtual target (blue) is in the same location as the physical target, relative to the center of the workspace. The target changes to white upon collision with the cursor (in Hold A & B task states).

2.2.3.3 The Anti-Reach Task In this task, the cursor moves in the opposite direction than that of the hand. For example, a physical hand velocity [1,1,1] would be displayed as cursor velocity [-1,-1,-1] (see figure 2.5). This view transform is applied during the first trial of the set and removed after all 14 targets are successfully reached.

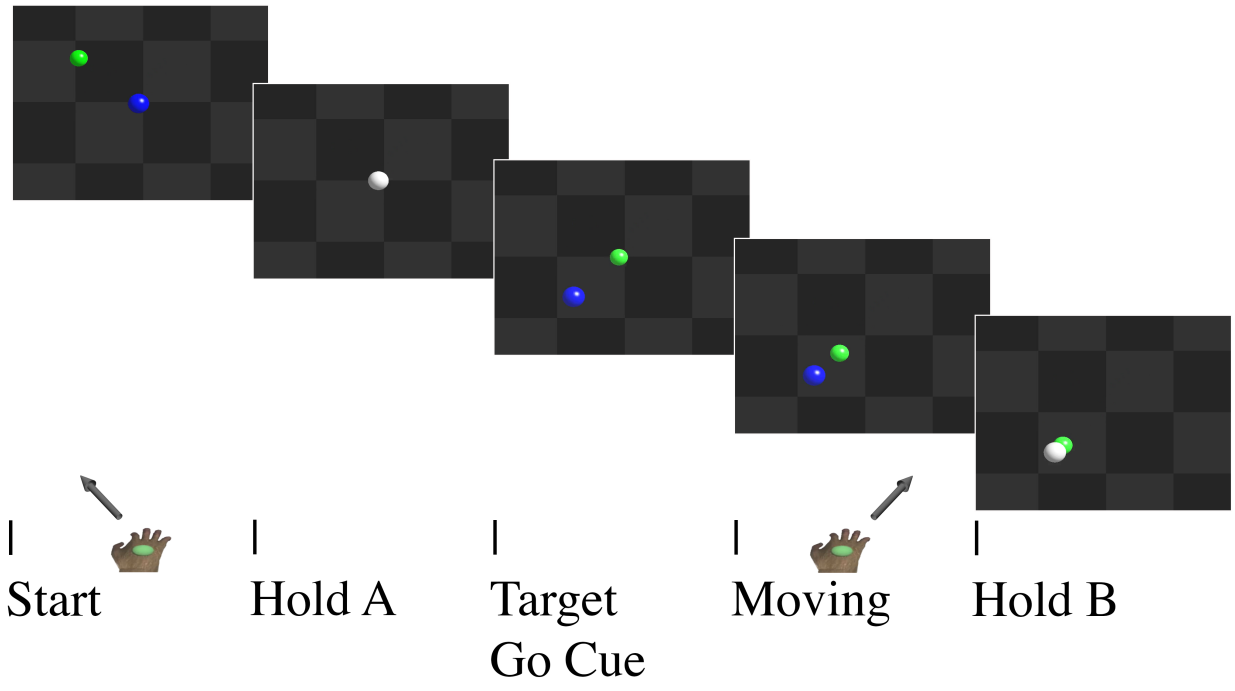

Figure 2.5: **Anti-Reach Task Display:** This figure shows the display as the subject reaches up, away, and rightward. The cursor (green) represents the position of the hand with negative identity view transformation. The virtual target (blue) is also in the opposite location as the physical target, relative to the center of the workspace. The target changes to white upon collision with the cursor (in Hold A & B task states). The view transform is applied on the first trial at the beginning of the Hold A period, and removed after the last successful trial of the task set.

2.2.3.4 The Stationary Cursor Reach Task This task changes the position of the view so that the target appears to be in motion while the cursor is stationary. To implement this, we translate the virtual camera with a fixed z offset from the cursor (see figure 2.6B). This is contrary to the standard and anti-reach tasks, in which the camera is stationary. Hand velocity is identical to the cursor's velocity, however since the viewpoint is moving with the cursor, the target will appear to move while the cursor image remains constant (see figure 2.6A).

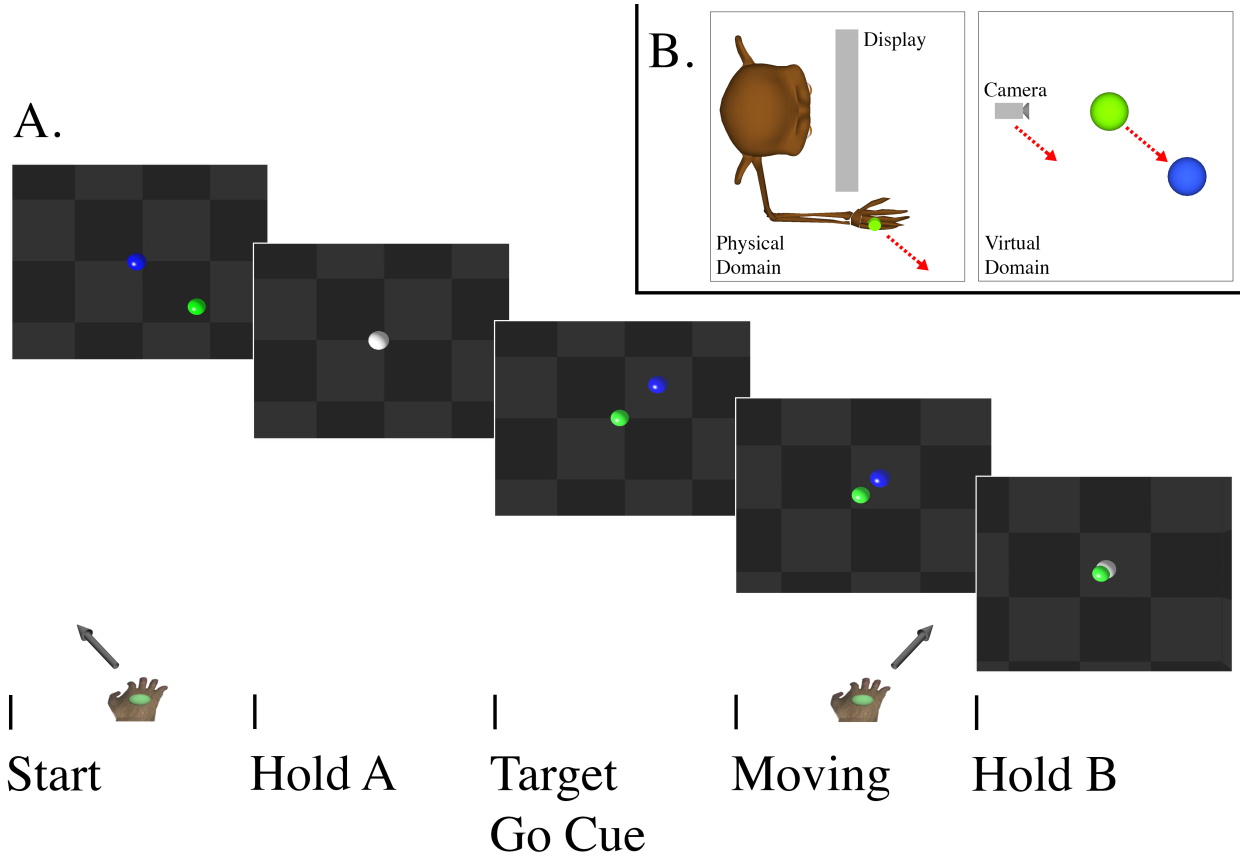

Figure 2.6: **Stationary Cursor Reach Task Display: A.** Depiction of the display as the subject reaches up, away, and rightward. The cursor (green) represents the position of the hand without a view rotation. The virtual target (blue) is in an identical location, relative to the center of the workspace. The target turns white upon collision with the cursor (in Hold A & B task states). **B.** A top view of the task in the physical and virtual domains. The camera, a virtual object, translates with a set offset from the cursor. This view change begins at the beginning of the Hold A period and reverts to the standard view upon success or failure.

2.2.4 Hypothetical Coordinate Systems

The coordinate systems in this dissertation describe dynamic variables / changes in position. All basis sets are cartesian and parallel to each other (the 'y' axis points against gravity in all basis sets). The origin of each coordinate system is different, defining unique vectors that describe the direction of individual features of movement. The same velocity vectors with different origins are parallel. The tasks discussed above dissociate the origins of visually-derived coordinate frames by altering the view across tasks while the same hand movements are performed. Four coordinate systems will be evaluated in this dissertation (listed below), and figure 2.7 summarizes how they are dissociated experimentally.

Coordinate Frame Descriptions and Icons for Future Reference:

1. **Hand-Centered Velocity:** A vector that originates on the hand and points in the direction of translation. The direction of this vector cannot be changed by the view transform.

2. **Cursor-Centered Velocity:** A vector that originates on the cursor and points in the direction of translation. The anti-reach task dissociates this coordinate frame from hand-centered velocity. This vector is only applicable during the first two tasks. The cursor does not translate during the stationary cursor task.

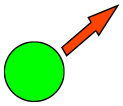

3. **The Difference Vector:** A vector that originates on the cursor and points in the direction of the target. The anti-reach task dissociates this coordinate frame from hand-centered velocity. The stationary cursor task dissociates this coordinate frame from cursor-centered velocity. The difference vector and the cursor velocity vector are not always truly parallel during the ballistic phase of movement, but the angular difference between them is negligible compared to angular differences with other vectors. For example, hand-centered velocity is always 180 degrees away from the difference vector in the anti-reach task.

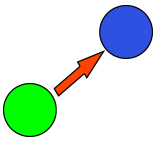

4. **Displayed Motion:** A vector that originates on the object that appears to be moving on the display and points in the direction of translation. The anti-reach task dissociates this coordinate frame from hand-centered velocity. The stationary cursor task dissociates this coordinate frame from cursor-centered velocity and the difference vector.

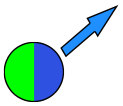

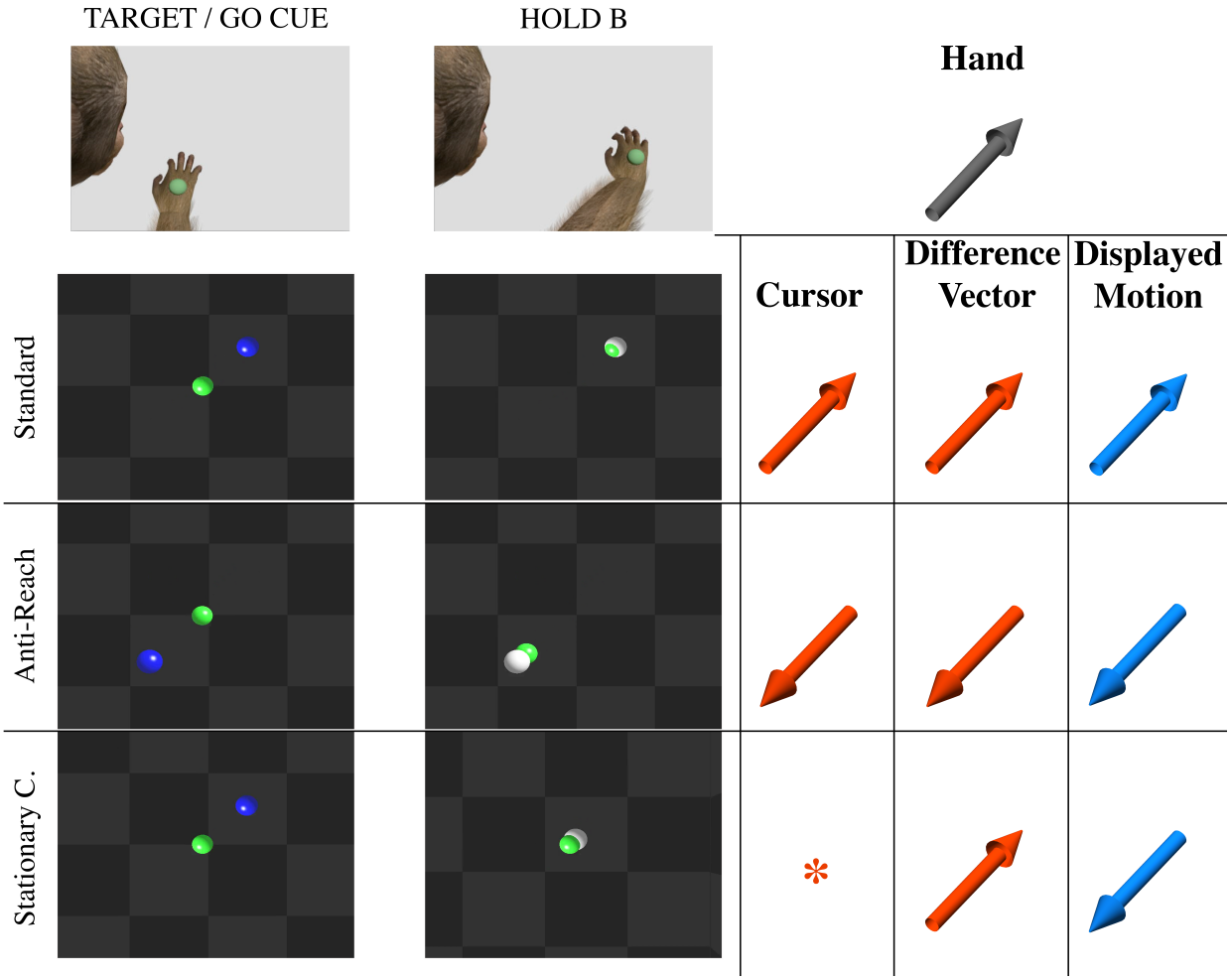

Figure 2.7: **One Reaching Movement, Three Different Views:** This figure shows how changing the view of a reach task can dissociate visually-derived coordinate frames. **Top row** shows the position of the hand before (GO CUE) and after the movement (HOLD B). The direction of the hand vector (black) is shown to the right. **Bottom three rows** show the corresponding display for each task (labeled on the left) in the first two columns. The corresponding direction of the cursor (orange) and motion vectors (blue) are in the three right-most columns. Orange arrows represent the cursor-centered velocity and difference vector. Only the difference vector is represented in the stationary cursor task (asterisk = no change).

2.3 SPECIFIC AIM 2

We hypothesize in Aim 1 that cortical neurons in motor regions have discharge rates that are sensitive to different visuomotor transformations. If this is true, is there an inherent component of this process driven by visual input in the absence of movement?

The PMv may be a processing node for visual information related to action execution. Even in the absence of movement, PMv may be processing action-related information. Experimental results have shown that neural activity during passive behavior falls into two main categories, each located in one of two subregions of the PMv. In the first sub-aim we analyze activity while observing replays of reaching in M1 and PMv, and in the second sub-aim we evaluate polysensory-like responses.

2.3.1 Sub-Aim 1

Which coordinate systems (found in the first aim) are neurally represented while watching replays of reaching? For each neuron, we will compare the most likely corresponding coordinate frame from active movement to that from visually congruent passive replays.

Previous work suggests that observing a learned action elicits a response from the neural substrate that is also active while performing the action, and could possibly reflect processing related to learning, understanding, or mental rehearsal of that action. True mental rehearsal may include the motor underpinnings of the observed action. For example, when an experienced pilot observes another pilot flying a plane upwards, does his visuomotor system respond to the nose of the plane ascending, or the limb of the other pilot pulling with his arms? We will attempt to answer this question by replaying the three active reach tasks from specific aim 1 to segregate neural activity that corresponds to the hand-centered, cursor-centered, and displayed motion coordinate frames.

2.3.1.1 The Reach Replay Task

Kinematic data from the end of the Hold A period to the end of the Hold B period (see figure 2.3) will be buffered and replayed for the monkey after each successful reach trial throughout the active reaching portion of the experiment. Once the monkey reaches the center of the workspace, the buffered replay will begin. The target will again be displayed and the cursor will move exactly as it had in the previous active trial without movement from the subject. The subject will be required to hold its hand in the center of the workspace until the end of the replayed Hold-B period. Failure to hold this position will restart the replay trial until it is successfully completed.

2.3.2 Sub-Aim 2

> Neuronal activity is modulated during passive behavior as objects move around the cursor in the virtual environment. Can this modulation be modeled as a function of cursor-centered or displayed motion coordinates? If so, do these sensory representations persist during active reaching?

The polysensory neurons lie in the posterior-medial regions of PMv, and have joint tactile-visual receptive fields for objects near the body. Activity corresponding to visually-derived object position could be used as a precursor to trajectories originating from the effector to the object. Our above hypotheses suggest that a visually-derived *difference vector*, originating from a surrogate effector (the cursor) may be neurally represented during active reaching. This vector may be constructed from position information. Using a new task, we will evaluate neural activity corresponding to virtual object position during passive behavior. Polysensory neurons also seem to correlate with dynamic variables, (e.g. object velocity in the receptive field) suggesting that changes in target location may be a salient directional feature.

We suggest two hypothetical coordinate systems. First, a vector that corresponds to target location originating on the cursor, which could be a precursor for the difference vector representation. Second, a vector that represents target velocity, which originates on the target and points in the direction of translation. Neural activity may correspond to one or a combination of both.

2.3.2.1 The Object Motion Task The object motion task requires the monkey to hold a central cursor position while the virtual target translates at a naturalistic speed (0.18 m/S) from the cursor to one of the 14 target locations (from the active reach tasks) and then back to center (see figure 2.8) so that opposite directions to each position are sampled. One goal of this paradigm is to dissociate modulation that corresponds to either static position, dynamic velocity, or both during object movement. We then will compare these results to those during active movement.

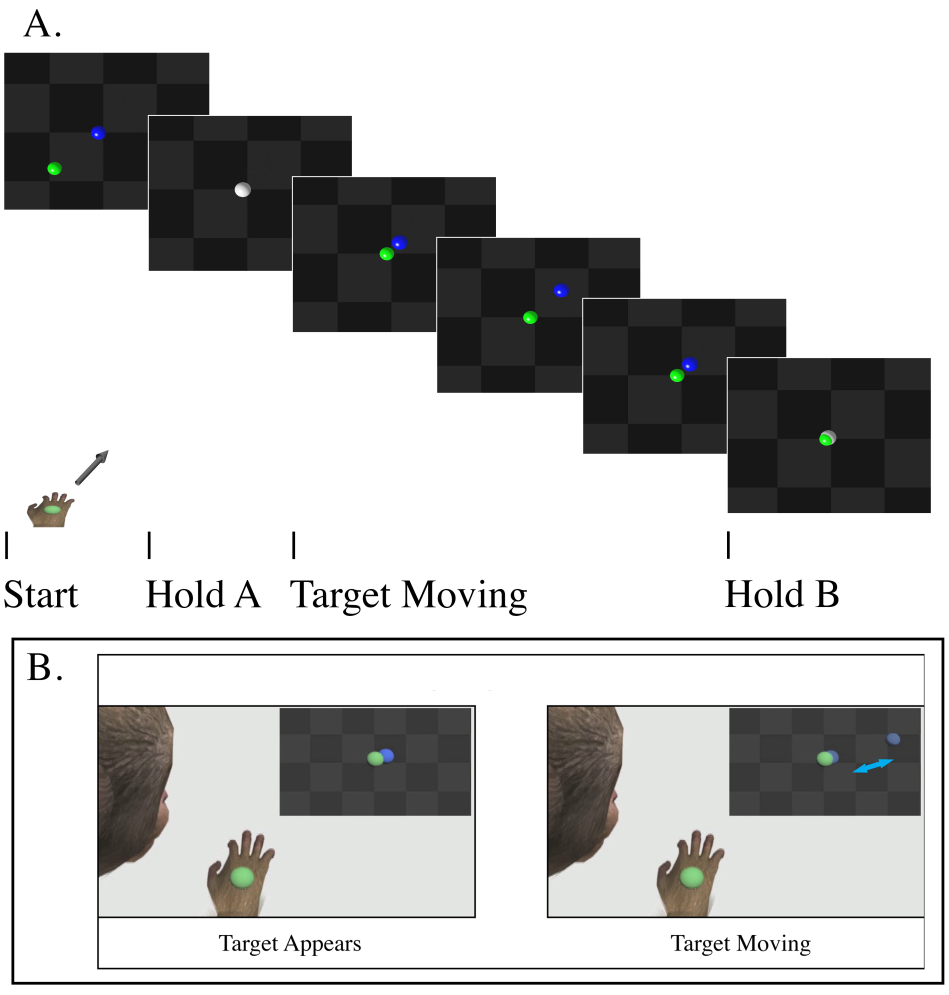

Figure 2.8: **The Object Motion Task: A.** The virtual target moves while the subject holds a central cursor position.

The origin of the virtual workspace was 52 cm away from the face and shoulders of the monkey, and the closest target would appear at 46 cm, using the biocular depth illusion inherent in the 3D

paradigm (see figure 2.8). Assuming that objects in virtual space are as salient to polysensory neurons as in physical space [42], our analysis is limited to two types of previously documented receptive fields [37]. The first type is typically centered on a section of skin on the hand or the arm, extending 25cm before modulation falls into baseline noise. Since the subjects were extensively trained in virtual interaction, we assume that the subject perceives the cursor as an extension of its own body and subsequently a candidate for the origin of a receptive field. The second type is centered on a section of skin on the face or shoulders, extending $>$1m outward, and shows directional preference for object translation. Our first priority was to classify neurons as position or velocity modulated in the virtual workspace, but also to record receptive fields in physical space whenever possible. This was performed on monkey D by physically raising the display and moving a ping-pong ball with an infrared marker mounted on the end of a rod around the body of the monkey. We recorded the position of the ball, position of the hand and head, and neural activity during this task. At first, the animals reacted to this as a threat, but were trained over time to sit quietly with minimal restraints on the contralateral arm. We found that raising the hood shifted the position of the micro electrodes for monkey J, so we evaluated receptive fields in physical space without moving the display.

2.4 METHODS

2.4.1 Eye Tracking

An infrared video eye tracker (Model 501, Applied Science Laboratories, Bedford, MA) was used to monitor the 2D position of the right eye. A *hot mirror* was placed slightly below the right eye, which reflected infrared light to the camera above while allowing visible light to pass through from the computer display. Software provided by ASL projected eye movement angles onto screen coordinates using data from daily calibration. During each calibration trial, a fixation target was displayed in one of nine positions formed by a 3 X 3 square grid (4 sides, 4 corners, and center) in the x-y plane. The target in the center of the display provided a global calibration offset. The monkey

was then required to move the cursor to the target and hold for a random interval of 150-300ms. The monkey usually fixated on the target immediately before movement onset. We manually saved each position after the first initial saccade. After all 9 positions were saved, the ASL software reliably emulated fixation position in screen coordinates. **Preprocessing:** The ASL system generates two analog voltage channels after calibration, one for horizontal and one for vertical eye direction. We sampled this at 60 Hz throughout the experiment and recorded the voltage change between fixation targets, after calibration, to calculate a scaling factor from the eye tracker voltages to the positions on the screen. Eye velocity was calculated as the first derivative of the eye position. Timestamps for each sample were aligned to movement onset and averaged across trials within the same task conditions.

2.4.2 Methods for Recording Neural Activity

2.4.2.1 Anatomical Localization Each monkey was scanned using MRI (T1, 0.5mm spacing) to attain coordinates for surgery and subsequent electrode penetration. One problem with this method was that the MRI stereotaxic frame was not in the same configuration as the surgical stereotaxic frame. Their respective planes containing the ear and eye bar contact points differed in pitch and roll. We developed a graphical software program in Matlab to transform MRI coordinates into stereotaxic coordinates. It queried the user to visually identify the locations of the eye and ear contact points, generated a coordinate transformation matrix to align them on the horizontal plane, and re-sliced the images. This method was verified first by using a rectangular bottle filled with water with a small vitamin E marker taped to a predetermined location in stereotaxic coordinates. We placed the bottle in the scanner at a random orientation and used the software to level the corners of the bottle and confirm the stereotaxic location of the marker. A second verification was performed by drilling shallow 1mm radius holes into predetermined surgical stereotaxic locations of the skull of monkey J on the same day of the scan. These were filled with a sterile mixture of vitamin E and bone wax to serve as fiducial markers.

Slice images from the MRI scan were skull-stripped using a combination of automated threshold-based removal and manual extraction. This was performed for each monkey with different available software (monkey D: *Strip District*, Kwan-Jin Jung, Pittsburgh, PA and monkey J: *MRIcro*, Chris

Rorden, Columbia, SC). The disparity in quality of the skull removal is apparent in the 3D reconstructions (see figures 2.9a & 2.10a). The skull-stripped slices were then loaded as a 3D matrix of intensity values. The appropriate pitch and roll were calculated and the intensity matrices were re-sliced. The 3D cortical surface reconstructions were referenced to locate the relevant sulci. After the craniotomy, cortical landmarks appeared to be in the estimated locations. After an elliptical chamber was implanted, with the major axis parallel to the midline of the skull, we used the chamber's angle of rotation around the poster-anterior axis to rotate our stereotaxic landmark estimates onto the plane of the chamber. Multiple observations were made the day following implantation, and during dural dissection when thin dura sometimes revealed locations of the relevant sulci. We also utilized the electrode tip to compare the posterior-anterior location of the center of the sulci to our predicted locations. We were never greater than 0.5 mm away from our estimates. No consistent offsets between predicted and actual coordinates were found. Penetrations and cortical landmarks are shown in chamber coordinates in figures 2.9b & 2.10b.

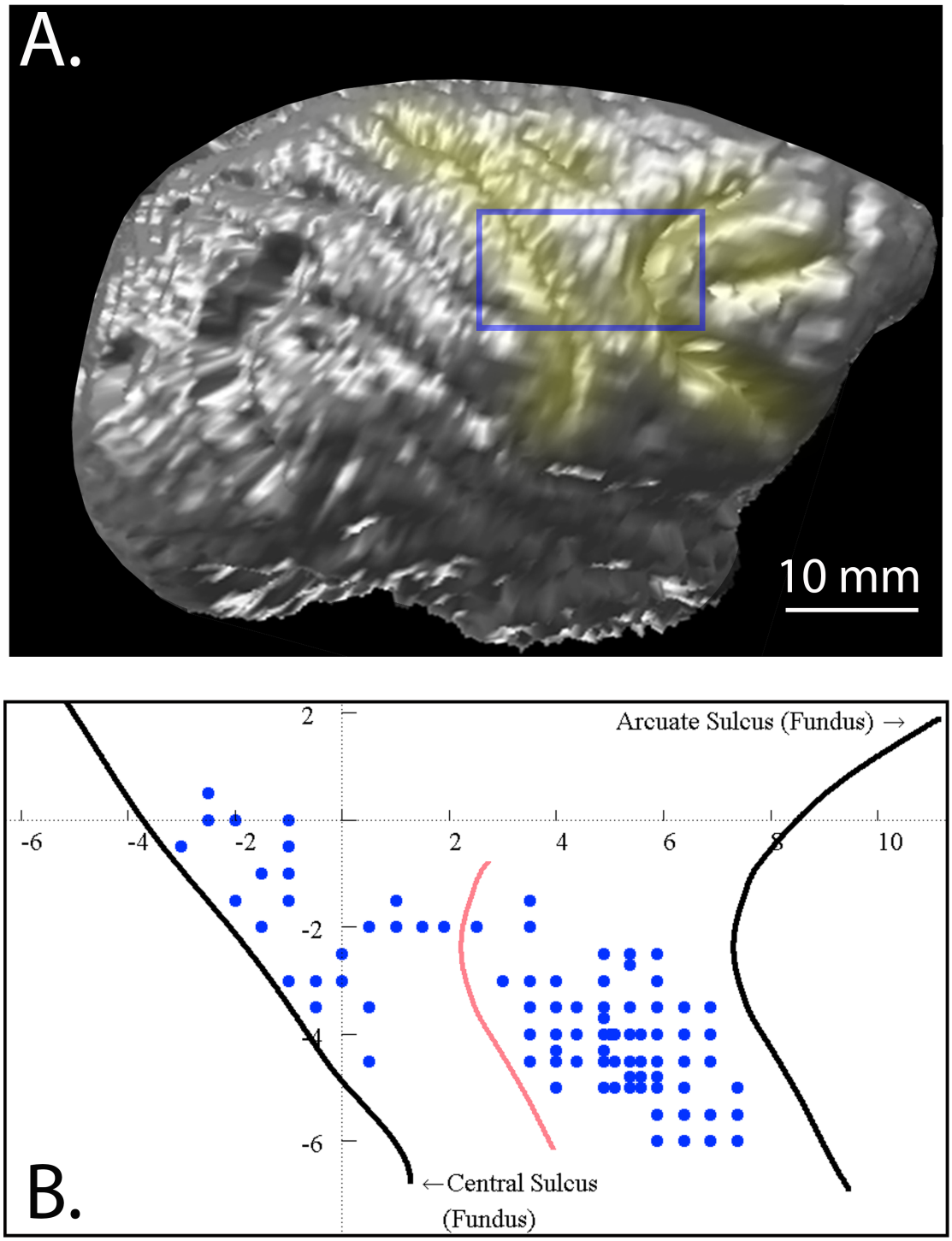

Figure 2.9: Monkey D: **A.** MRI reconstruction of the cortical surface, right hemisphere. **B.** Penetration Map with splined estimates of sulcus location. The origin of the coordinate system was the center of the chamber. Red line indicates 5mm boundary for PMv.

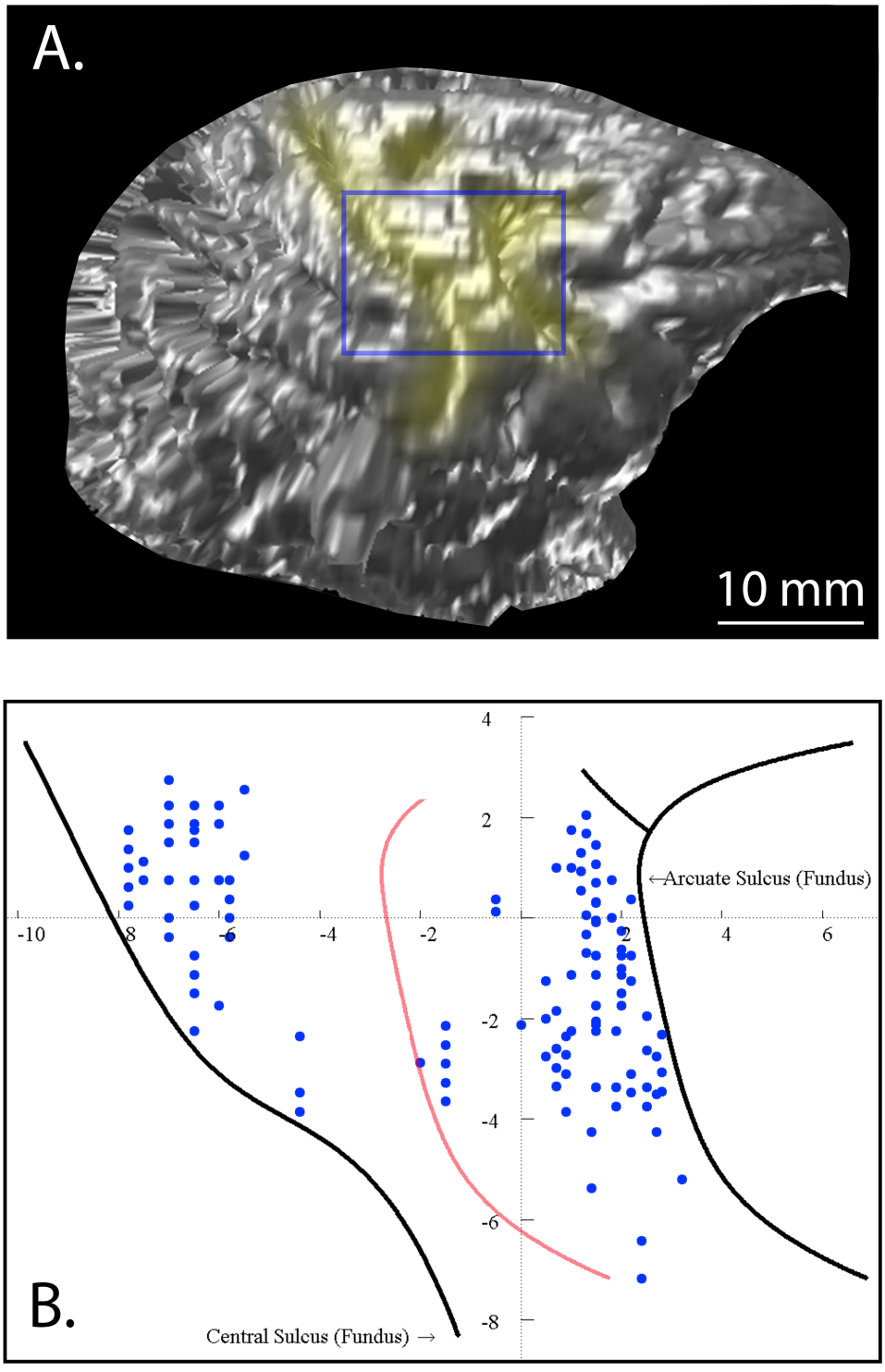

Figure 2.10: Monkey J: **A.** MRI reconstruction of the cortical surface, right hemisphere. Skull stripping methods for monkey J were less robust than for monkey D. **B.** Penetration Map with splined estimates of sulcus location. The origin of the coordinate system was the center of the chamber. Red line indicates 5mm boundary for PMv

2.4.2.2 Single-Unit Recording We used a single electrode microdrive (see figure 2.11A) while recording from Monkey D. Prefabricated platinum-iridium Electrodes were purchased with an impedance of 1-1.5 MΩ (FHC Inc, Bowdoin, ME), loaded into the drive, and positioned 2mm above the level of the dura. On every recording day, the recording chamber was opened and washed with saline. We then scraped the dura to remove soft-tissue accumulation that might have impeded electrode penetration. The drive was mounted to place the electrode into a targeted area. While driving down at a speed of approximately 10 μm/sec, the impedance of the electrode and electrical activity was monitored to determine the depth of dura contact, and penetration. The electrode was driven 3000μm past the surface of the dura and left to stabilize for at least an hour. On Monkey J, a five-channel Mini-Matrix system was used to record electrical activity (Figure 2.11 B). We fabricated recording electrodes in-house, using basic materials (Thomas Recording, Giessen, Germany). Each electrode consisted of quartz fibers filled with tungsten, beveled to a sharp point for dural penetration. Typical impedance values were of the range of 0.8-2.0 MΩ. The fibers were threaded through silicon tubing. With the recording tip extended through the tube, the other end of the wire was crushed to remove the quartz insulation, and then immobilized in a solder joint. A gold pin was connected to the solder joint, allowing an electrical connection to the pre-amplifier on the Mini Matrix.

On every recording day, the recording chamber was opened and washed with saline. A potential recording site was selected and a small patch of dura was carefully dissected with sterile surgical micro- instruments under a microscope. The Mini-Matrix drive was mounted on the recording chamber and its guide tubes lowered to make contact with the dura at a selected recording site. 5 recording electrodes, pre-loaded in the drive, were then advanced individually at a speed of 250μm/sec. Following dural penetration, the electrodes were further driven to a depth of 3000μm from the surface of the dura and left to stabilize for at least an hour.

In both monkeys, electrodes were subsequently moved at a speed of 5μm/sec until at least one neuron was isolated on each electrode. Five of 48 available channels (Multichannel Acquisition Processor or *MAP*, Plexon Inc, Dallas TX) were used to amplify, display, and record the waveforms from the electrodes. Spike waveforms were sorted on-line, and spike time stamps were stored for analysis. After the experiment, a passive exam was conducted. Activity was monitored as the animals arm was manipulated and as it reached for dried fruit in different locations. This

examination was undertaken to evaluate whether the activity was related to passive and/or active arm movement and to ensure that it was not related exclusively to finger, wrist, licking or chewing; such cells were not used for analysis. If there was sufficient stability and evidence of a polysensory response, we recorded neural activity while we placed an infrared marker attached to a ping pong ball around the body, to characterize the polysensory characteristics of the neuron.

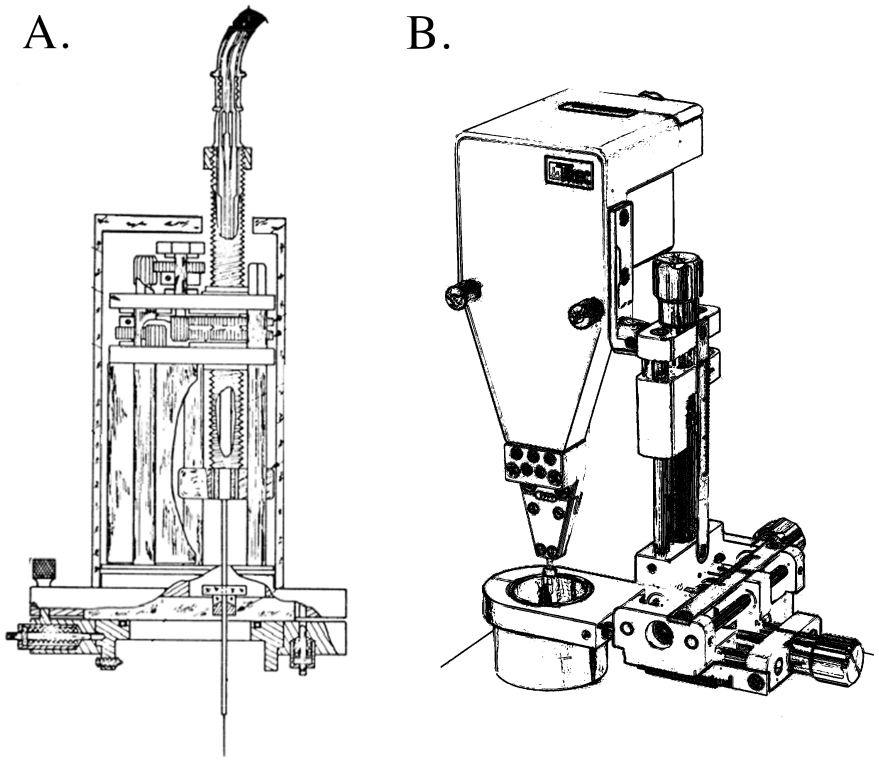

Figure 2.11: **Microdrives Used for Recording: A.** The single-channel microdrive (described in detail in [62]), mounted on Monkey D **B.** The five-channel Mini-Matrix Thomas Recording drive mounted on Monkey J

2.4.2.3 Preprocessing: For both monkeys, spikes were discriminated in real time using "box" sorting methods in RASPUTIN (Plexon, Dallas, TX), a software suite of spike sorting applications designed to work with the MAP. Spike times were buffered and saved to disk whenever a new trial began, giving us a per-trial record for each session. This was particularly useful during unpredictable computer problems or power outages. Spike times were then aligned with: a) movement onset (15% of the peak speed), in the case of an active reaching task, or b) the end of Hold A, in the case of

the passive task. Data for each trial were used from 0.15 s before the GO cue to 0.15 s after the beginning of HOLD B. In all cases, spike times were counted into 80 10 ms bins for each trial. Active reaching trials generally took approximately 0.3 ms from target presentation to movement onset, and 0.2 ms from movement onset to target contact (see figure 3.2). We allotted -0.35 to 0.45 s for active reach and replay tasks (with 0 s = movement onset), and 0-0.8 s for the passive task (0.0 s being the trail start). Individual trials that were shorter than 0.8 s were padded with NaN values. Firing rates were calculated by counting spikes within each bin and dividing by the bin size. Mean firing rate was calculated by counting spikes within the same experimental conditions, averaging, and dividing by bin size. We considered using a square-root transform to normalize the variance on firing rate data, but found that it had little to no effect on the final results.

2.4.3 Data collection using RTMA:

All data were collected from the experiment in the form of messages sent by the Real-Time Messaging Architecture (RTMA, Meel Velliste, University of Pittsburgh, PA). RTMA is a software system that forms a communication link between multiple modules running on a single computer or a set of computers on a local network. The data from the Optotrack API, Eye Tracking software, the virtual display, the spike sorting software, a reward module, and the task controller were saved on one computer at the end of each trial. A separate time base was used by the MAP for spike collection. An active high sync pulse was generated and recorded at the beginning of each trial from the data recording computer to the MAP to align the spike times with other task events.

2.5 STATISTICAL METHODS

2.5.1 Linear Models

Directional modulation was apparent after inspecting rasters of spike times. We found that a linear regression model was adequate for predicting this modulation as a function of reach direction. Given a linear regression model with n covariates:

$$y = X^T\beta \tag{2.1}$$

$$= \sum_{i=0}^{n} \beta_i x_i \tag{2.2}$$

the dependent variable y is predicted by a set, X, of n explanatory variables x_i. A column of ones was appended, x_0, to incorporate a y-intercept in the model. Expanding equation 2.2 gives us equation 1.1 in cartesian coordinates. To find the best estimate of β analytically, the *Normal Equation* was employed:

$$\hat{\beta} = (X^T X)^{-1} X^T y \tag{2.3}$$

where $\hat{\beta} = \beta_i, (i = 0 : n)$ is a least squares estimator for a linear predictor, $\hat{y}$:

$$\hat{y} = X^T \hat{\beta} \tag{2.4}$$

The *coefficient of multiple determination*, denoted R^2, measures the proportion of the variance of y explained by X:

$$R^2 = 1 - SSE/TSS \tag{2.5}$$

where SSE is the sum of squares of the residuals and TSS is the total sum of squares evaluated by:

$$SSE = \sum_{i=1}^{m} (y^{(i)} - \hat{y}^{(i)})^2 \tag{2.6}$$

$$TSS = \sum_{i=1}^{m} (y^{(i)} - \bar{y})^2 \tag{2.7}$$

where $\bar{y}$ is the mean of y and m is the number of trial examples.

For each trial, we generated an explanatory variable set X by calculating the difference between the final and the initial positions. For example, if the hand originated at the center of the workspace ([0,0,0]) and reached to the right ([1,0,0]), $[x_1^{(1)}, x_2^{(1)}, x_3^{(1)}]$ would equal [1,0,0]. After we calculated the vector β ($[\beta_1, \beta_2, \beta_3]$), we divided by its Euclidean length to calculate a directional unit vector, called the *preferred direction*, which is the reach direction for maximal predicted firing rate.

The symbol "θ" will be used throughout this dissertation to represent the angular difference between the preferred direction and the movement direction, with a subscript to indicate the data set used to calculate the preferred direction. For instance, $\theta_{S.R.T}$ refers to the angular difference between the hand velocity and the preferred direction during the Standard Reach Task (S.R.T).

2.5.1.1 Sliding Time-Window Regression Variance in discharge rate was more apparent during specific time epochs across reach trials for each unit. We used a sliding time window to find this epoch analytically; generating multiple R^2 values at 10 ms overlapping increments from the time of target presentation to that of target contact. We used the time epoch with the highest R^2 value to calculate firing rate and a preferred direction for each unit. A window size of 300 ms was found to be optimal for the best model fit. A second 100 ms sliding window was evaluated within the time boundary of the first 300 ms window to determine a latency value for each unit (see Figure 2.12).

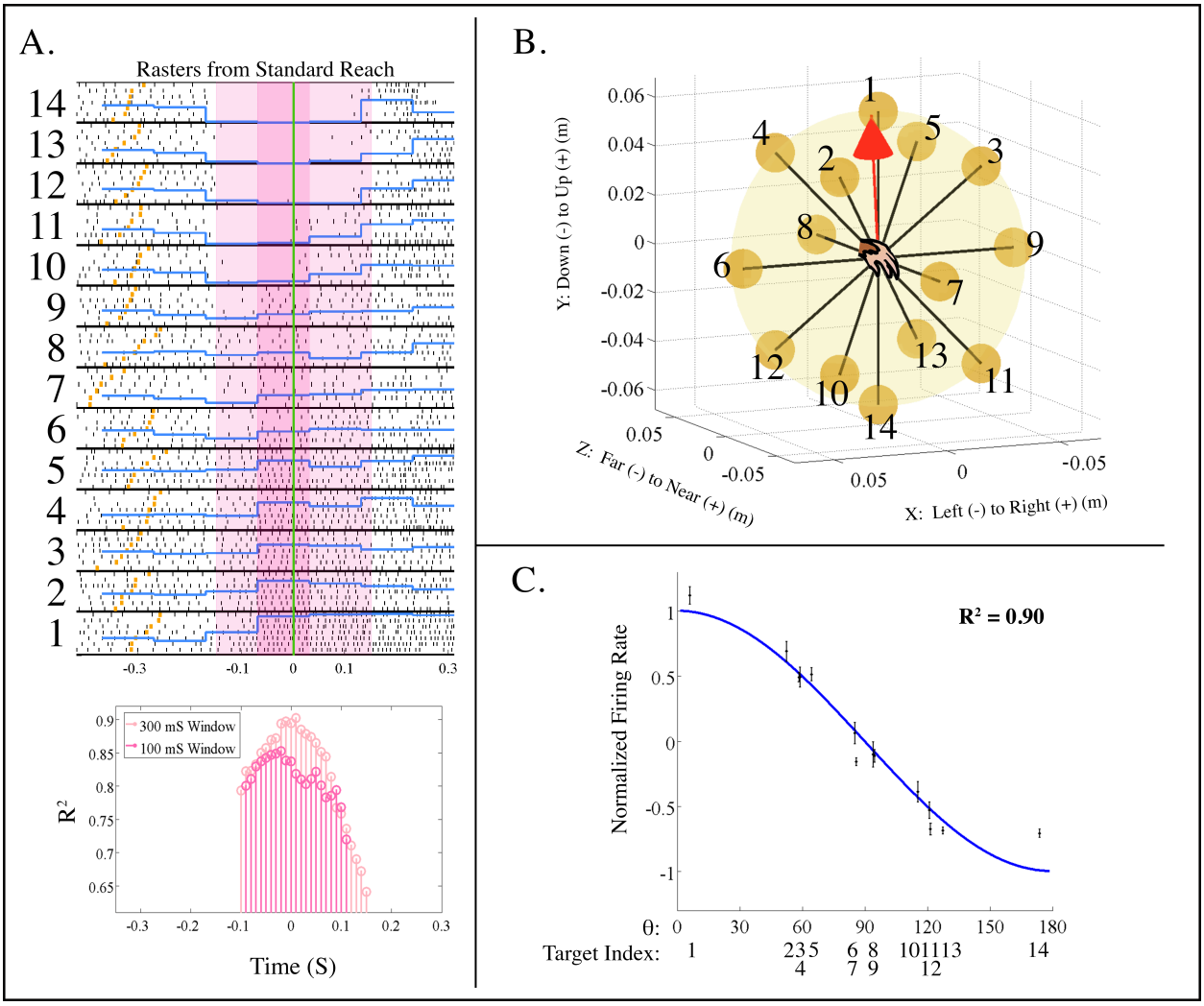

Figure 2.12: **Linear Models for Direction of Action:** A firing rate model of an example unit constructed as a function of hand velocity.

A. Each row of vertical black ticks marks shows when a unit fired over time in one trial, aligned on movement onset. Each group of rasters, between the black horizontal lines, shows neural activity from reaches to the same target (indexed). The angular distance between the hand-centered preferred direction and the hand direction, θ_{hand}, increases with each higher row.*Vertical Green Line:* Movement Onset, *Orange Ticks:* Time of Target/Go Cue, *Light Pink Transparent Column:* Best-fit regression window (300 ms), *Dark Pink Transparent Column:* Best-fit regression window (100 ms), *Blue line:* Normalized firing rate. The plot below shows R^2 values labeled at the time of the corresponding window center. Peak R^2 = 0.90, at -0.02 s (the model latency).

B. The physical workspace. Target indexes from part A are labeled. *Red arrow:* The preferred direction generated from the 300 ms sliding window.

C. The cosine tuning function. Normalized firing rates from each target (labeled on the x-axis) are plotted with error bars according to θ_{hand}. Tuning and R^2 generated from the 300 ms window in part A. See equation 1.2 for further explanation of the cosine tuning model.

2.5.2 Labeling Task-Related Activity

One-way ANOVAs ($p < 0.05$) were used to determine if the frequency of discharge varied with target direction. Firing rate was determined using the 300 ms epoch from the sliding time-window analysis (see previous section 2.5.1.1). Units with significantly varied activity across the 14 groups were labeled *task-related*. Only the activity from task-related units was included in any results. For multi-task analyses, activity had to be task-related during all individual tasks to be included.

2.5.3 Comparing Tolerance Intervals of Preferred Direction

In order to compare responses between conditions, it was necessary calculate the variance of the preferred directions with a statistical bootstrapping technique. Linear models were each evaluated multiple times, generating a re-sampled population of preferred directions from the original data set. Each sample was calculated by randomly selecting, with replacement, one trial from each set of target reaches. We tested multiple sample sizes and found the variance estimate converged for most data sets at 10,000 samples.

To determine whether or not preferred directions were similar, we developed a method to test for possible tolerance interval (TI) overlap. Since the variance was constrained to the surface area of a unit sphere, coordinates were transformed into spherical coordinates: radial distance (r), azimuth (α), and elevation (ε):

$$r = \sqrt{x^2+y^2+z^2} \tag{2.8}$$

$$\alpha = \arctan\left(\frac{z}{x}\right) \tag{2.9}$$

$$\varepsilon = \arctan\left(\frac{y}{\sqrt{x^2+z^2}}\right) \tag{2.10}$$

The r dimension was omitted in subsequent analysis, as directional vectors all had a length of 1, which reduced the dimensionality of X to two (α & ε). For observations near the poles, this coordinate system was unsuitable for bivariate normal parameterization (see figure 2.14b). The surface of the unit sphere was transformed into rectangular coordinates using an equal-area, oblique cylindrical projection. Data points were projected from the surface of the sphere onto a tangent cylinder. The tangent line was set as the great circle that intersects with the means of the two

sample populations (see figure 2.13). Setting the tangent line in this manner minimized distortion of distance, shape, and scale [77]. A *pole* ($[\alpha_p, \varepsilon_p]$) was calculated using the cross product of the population means ($pd_1 \times pd_2$). Then rectangular coordinates were generated:

$$X = \arctan\left(\frac{\tan\varepsilon\cos\varepsilon_p + \sin\varepsilon_p\sin(\alpha-\alpha_0)}{\cos(\alpha-\alpha_0)}\right) \quad (2.11)$$

$$Y = \sin\varepsilon_p\sin\varepsilon - \cos\varepsilon_p\cos\varepsilon\sin(\alpha-\alpha_0) \quad (2.12)$$

where the origin of rectangular coordinates lies at:

$$\varepsilon_0 = 0 \quad (2.13)$$

$$\alpha_0 = \alpha_p + \pi/2 \quad (2.14)$$

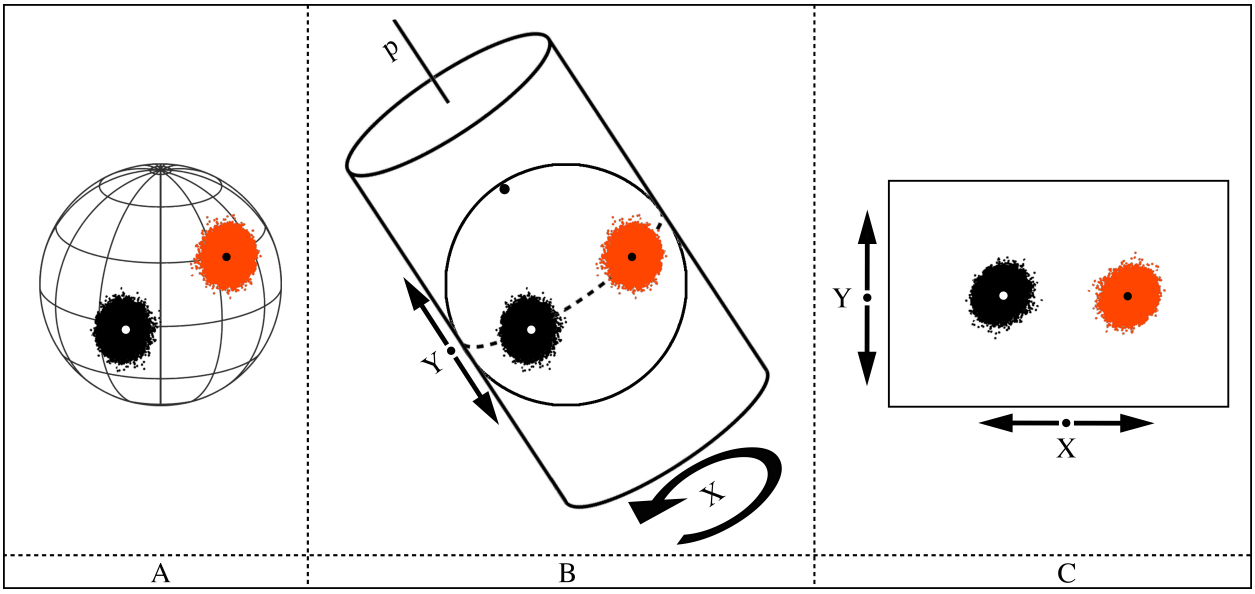

Figure 2.13: **Oblique Cylindrical Equal-Area Projection: A.** Two re-sampled preferred direction populations in spherical coordinates on the surface of a unit sphere. **B.** The cross-product of the means of the populations was used to find an ideal pole (p) for the central axis of a cylindrical projection. The intersecting great circle (dashed line) is tangent to both the cylinder and the unit sphere. This method reduces shape distortion, which increases with distance from the tangent line in the Y dimension. **C.** An equal-area projection of the two populations in rectangular coordinates. The resultant X dimension was effectively unwrapped from the surface of the cylinder.

The projected re-sampled population P, was used to calculate the covariance matrix of the preferred directions(Σ):

$$\Sigma = \frac{P^T P}{n-1} \tag{2.15}$$

which in turn was used to parameterize and consequently determine the surface area of the tolerance interval. The covariance matrix (Σ) was then decomposed into eigenvectors (V) and eigenvalues (D):

$$\Sigma = VDV^{-1} \tag{2.16}$$

The eigen-decomposition of the covariance matrix for each task provided the major and minor axes of an elliptical boundary surrounding the bivariate population. We used the Krishnamoorthy-Mondal method [54] to determine the 99.99% tolerance interval (see figure 2.14c), which was used to parameterize each sample population. We also calculated the area of each ellipse for a measure of spread (e.g. figure 3.11). Some parameterizations resulted in a bounded region larger than the surface area of a unit sphere. In these cases, we used the *PCOut* method [24] to identify and eliminate outliers in the population. Once tolerance intervals were found, the area of overlap was evaluated using the Guass-Green formula [41]. If an intersection was found, we considered the preferred direction unchanged. If no intersection was found, the preferred directions were considered different. Figure 2.14 shows an example of a neuron that changed preferred direction across tasks.

2.5.4 Partial Correlation For Eye Direction

Eye direction may have been a covariate with some of our model features, so we used partial correlation analysis to determine whether there was an interaction between these variables. If eye movement contributed to to the modeled activity of a unit, we removed that unit from our analysis. We concatenated the mean dot product (also $cos(\theta_{CM})$: see equation 1.2) of the preferred direction and reach direction (in all coordinate systems) from the entire recording session for each neuron and evaluated correlation with firing rate (see equation 2.17). We then evaluated the correlation of the dot product of eye direction vs. the preferred direction, in screen coordinates, with neural activity from the same recording session. Partial correlation coefficients (see equation 2.18) were evaluated as well, first between eye direction and firing rate removing correlation with reach direction, and then

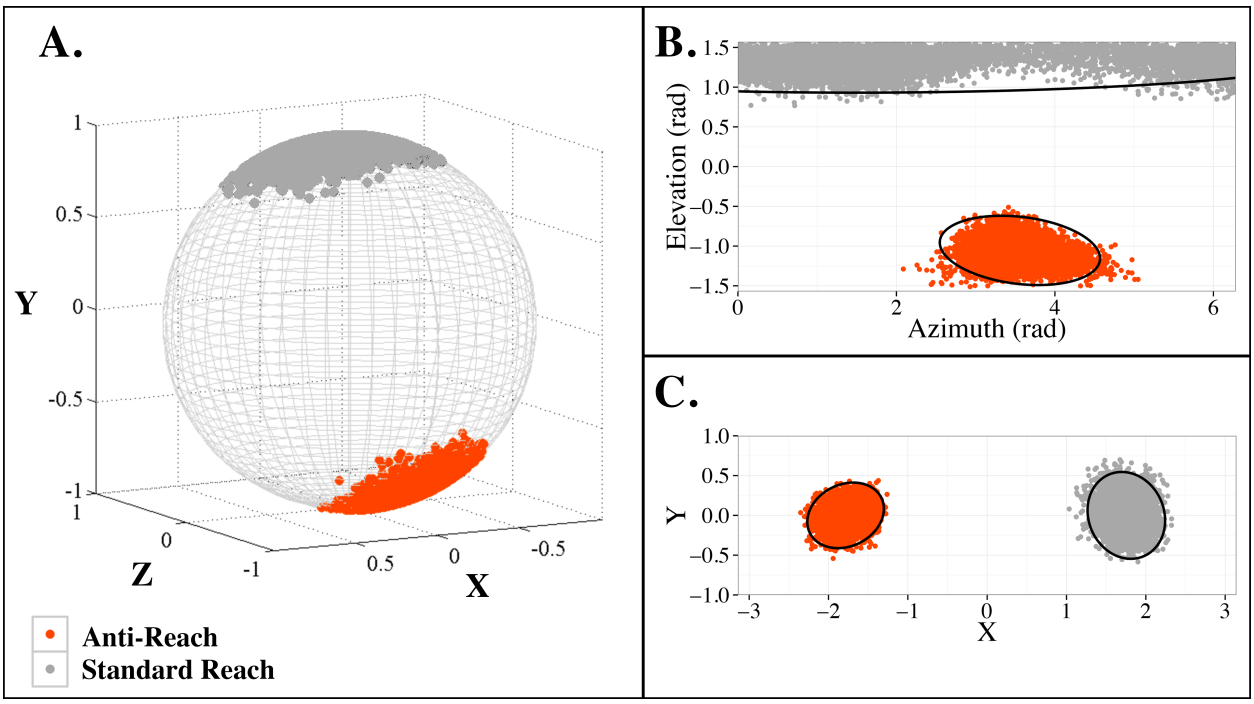

Figure 2.14: **Cartesian, Spherical, and Rectangular Coordinates: A.** 10,000 samples of preferred direction from one neuron, in cartesian coordinates, from the Standard (grey) and Anti-Reach (orange) tasks. **B.** The corresponding preferred direction sample populations in spherical coordinates. Black lines indicate the calculated tolerance interval. **C.** A cylindrical projection in rectangular coordinates of the same data with corresponding elliptical boundaries.

between the reach direction and firing rate, removing eye direction correlation. These calculations were performed multiple times over a range of time shifts for each variable. We then calculated the absolute value of the partial correlation coefficients in each time bin to determine if firing rate was more correlated with eye direction than the reach direction.

The Product-Moment Correlation Coefficient:

$$\rho_{AB} = \frac{\text{cov}(A,B)}{\sigma_A \sigma_B} \tag{2.17}$$

The Partial Correlation Coefficient:

$$\rho_{AB/C} = \frac{\rho_{AB} - \rho_{AC} * \rho_{BC}}{\sqrt{(1-\rho_{AC}^2) * (1-\rho_{BC}^2)}} \tag{2.18}$$

2.5.5 Firing Rate Models of Neural Activity during the Object Motion Task

Two firing rate models were generated that determined how well the variance in neuronal firing rate could be modeled as a function of either the velocity of *displayed motion* or the *cursor-centered* position. Since the subject was required to hold the cursor in the center of the virtual workspace, cursor-centered position coordinates were identical to the global coordinates of the targets. Regardless of whether the stimulus was moving toward or away from the center of the workspace, a unit vector from the center of the workspace to the position of the stimulus was used as the regressor. Displayed motion was defined as the direction of stimulus translation. While the stimulus was moving away from the center of the workspace, the displayed motion and cursor-centered directions were identical. While the stimulus was moving toward the center, the they pointed in opposite directions.

Linear regression (200 ms non-sliding window, mean firing rate) was used to fit models of neural activity as a function of change in one coordinate system. Each trial had two velocity directions, and were identical in distance and time length, which allowed the trials to be split in time. The last 200 ms of each trial half was sampled to a) allow visual information to reach the motor areas in the first half, and b) avoid carryover modulation in the second half (see pink shaded area in figure 5.3). Trial halves were treated as separate regressors for building the predictive models. R^2 values were compared across the two coordinate frames. A minimum R^2 value of 0.1 was deemed an acceptable value to classify activity with a coordinate system, based on minimum R^2 values from classified units during the active reaching experiment. Activity having a high R^2 value in one coordinate frame consistently had a low R^2 value in the other.

3.0 RESULTS FROM THE ACTIVE REACHING EXPERIMENT

3.1 INTRODUCTION

Single-unit recordings are evaluated in this chapter to determine whether evidence of visuospatial transformation is present in PMv and M1 during active reaching. In section 3.2, trajectories of the arm and eyes in each experimental task are compared. In section 3.3, we examine and model how neuronal discharge varies with the changes in view and segregate cells into types that behave similarly. Finally, in section 3.4, we evaluate whether these various response types fit hypothetical coordinate systems that correspond to various stages of visuomotor processing.

3.1.1 Task Summary:

The following tasks were designed for a 3D interactive display with a spherical cursor representing the position of the hand and a spherical target representing the goal position of the reach. Coordinate systems were dissociated using a different view in each task:

1. **Standard Reach Task**: Cursor direction matched the hand direction. Displayed motion was defined as the motion of the cursor. All three vector types were parallel as the subject reached to 14 different targets locations. No coordinate systems were dissociated.
2. **Anti-Reach Task**: The hand moved to the same 14 locations as in the standard reach task as the cursor moved in the opposite direction. Displayed motion was that of the cursor, so hand-centered coordinates were dissociated.
3. **Stationary Cursor Task**: The hand moved to the same 14 locations as in the anti-reach and the standard reach tasks. The target appeared to move in the opposite direction of the hand, towards the cursor, while the cursor appeared stationary in the center of the display. The cursor-centered vector pointed to the target. Displayed motion was that of the target. Displayed motion was dissociated by pointing in the opposite direction of both the hand- and cursor-centered vectors.

3.2 KINEMATIC RESULTS

3.2.1 Hand Movement

Hand kinematic analysis was necessary to evaluate: a) that the animals were making naturalistic movements and b) that they were performing similar reaches across different tasks. We calculated the mean and standard deviation of the coordinates at each time point for each reach direction in each active reaching task. For both monkeys, the kinematics were largely similar across tasks (see figure 3.1) The hand paths of monkey D differed between the standard and anti-reach tasks for some of the targets. Speed is also an indication of natural movement. All active speed profiles from both monkeys showed a natural, single-peaked, bell-shaped speed profile (see figure 3.2).

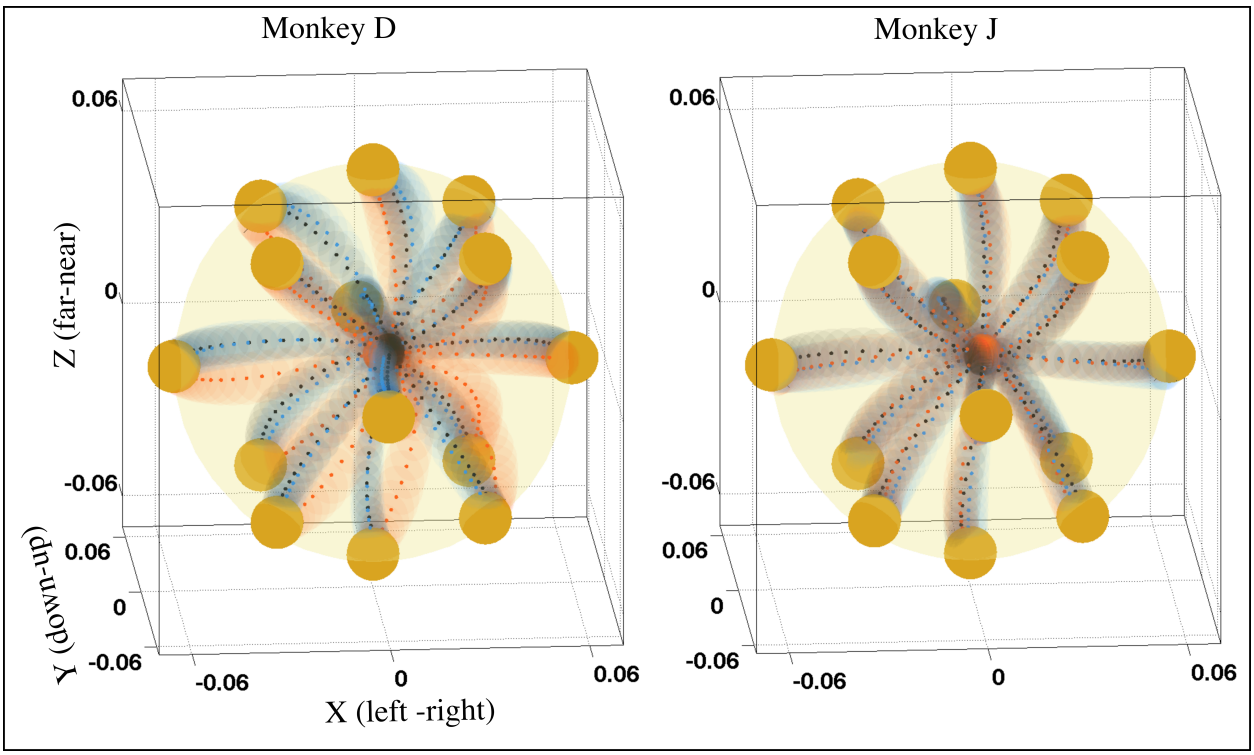

Figure 3.1: **Average Hand Position (n≈1200):** *Red:* Standard Reach Task, *Green:* Anti-Reach Task, *Cyan:* Stationary Cursor Task, *Black "X" Markers:* Hand position at the end of a successful trial. *Transparent Blue Spheres:* Three dimensional physical target positions.

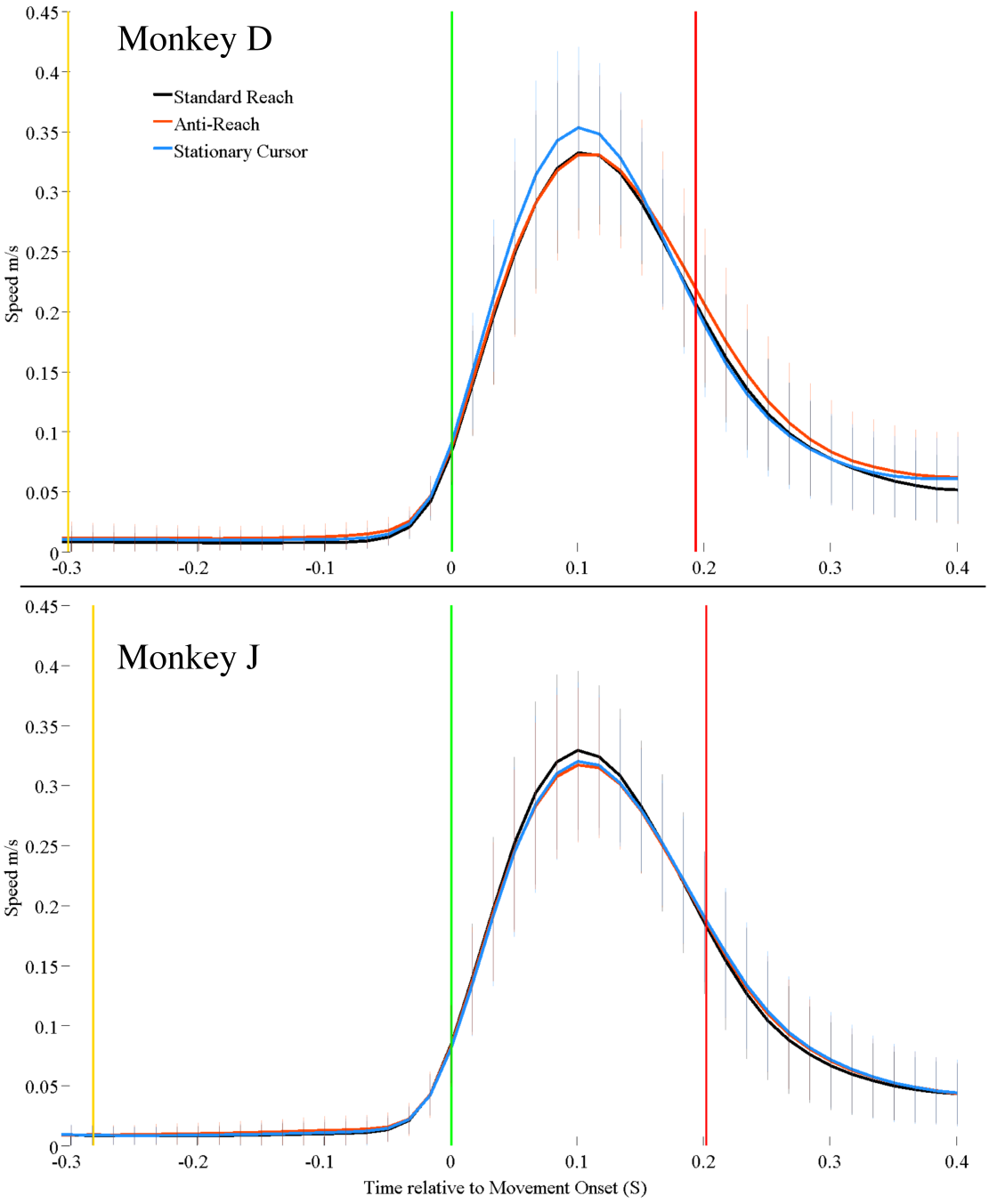

Figure 3.2: **Mean Speed Profiles from Active Reach and Replay Tasks:** Each curve is the average speed to all targets (n$\geq$15400) from the go cue to $\approx$ 200mS after target capture for either the Standard, Anti-Reach, and the Stationary Cursor reach tasks. All trials were aligned on movement onset.
Gold Vertical: Average Target/Go Cue Time, *Green Vertical:* Movement Onset Time, *Red Vertical:* Average Target Contact Time

3.2.2 Performance on New Spatial Targets

Table 1: **Success Rate for Each Monkey Reaching to New Targets.** *Trained* targets are the 14 targets that were used for training and recording. Success rates under trained targets referenced all of the trials from recording days (n $\approx$ 28000 successes/task). *New* targets had no spatial overlap with the trained targets and were not previously presented. New target success rates reference only one block of trials (n $\approx$ 56 successes/task).

Monkey	**D**		**J**	
Target Positions	Trained	New	Trained	New
Standard Reach Task	88%	87%	77%	64%
Anti-Reach Task	66%	60%	68%	32%
Stationary Cursor Task	83%	80%	68%	53%

The monkeys were highly trained to move in a direction specified by a target in a particular context. To determine whether this behavior was a memorized action triggered by a cue or target-driven reaches by processing the view transform, we presented 4 new sets of targets during a kinematic recording session. Performance on this task was used to evaluate how well each monkey understood the underlying algorithm that mapped the hand to the display. All other variables including movement time, hold times, and target/cursor size in each task were the same as during neural recording. Table 1 shows the success rate (successful trials divided by total trials) for each task. Both monkeys had little to no difficulty with the Standard Reach Task and the Stationary Cursor Task. Monkey J showed a considerable lack of adaptability with the Anti-Reach Task, performing at lower than half the success rate with familiar targets. Monkey D had considerably more training time, as it was trained on a battery of preliminary tasks similar to the anti-reach task for years during the development of the experiment. Given that several months were required to train the monkeys to perform the anti-reach task adequately, and that monkey J was still able to complete each new set of targets with an average of 3 attempts per success, it is reasonable to assume that it had learned the algorithm governing the transformation, albeit to a lesser degree than monkey D.

3.2.3 Eye Movement

We calculated the mean value of screen coordinates from ∼1200 trials for each displayed target, in each task. Results showed that the monkeys behaved similarly across tasks. In all cases, the animals fixated on the displayed target screen position (see figure 3.3), and did not track the cursor. Upon inspection of the speed profiles, Monkey J always fixated on the target before arm movement onset, while Monkey D had a slightly later saccade, fixating during or after arm movement onset. Monkey D also had a much later saccade than average for the far left bottom target.

During the stationary cursor task, fixation position initially moves to the position of the target, and subsequently follows the target position on the screen to the center. For Monkey D, since its saccade was later, the initial fixation point is closer to the center of the screen, presumably on the later moving target location. One possibility with this task was that the moving target was perceived as a cursor, since it appears to be moving with the hand. Our results here show that this is not the case, since the eye initially saccades outward and appears to track the target back toward the center.

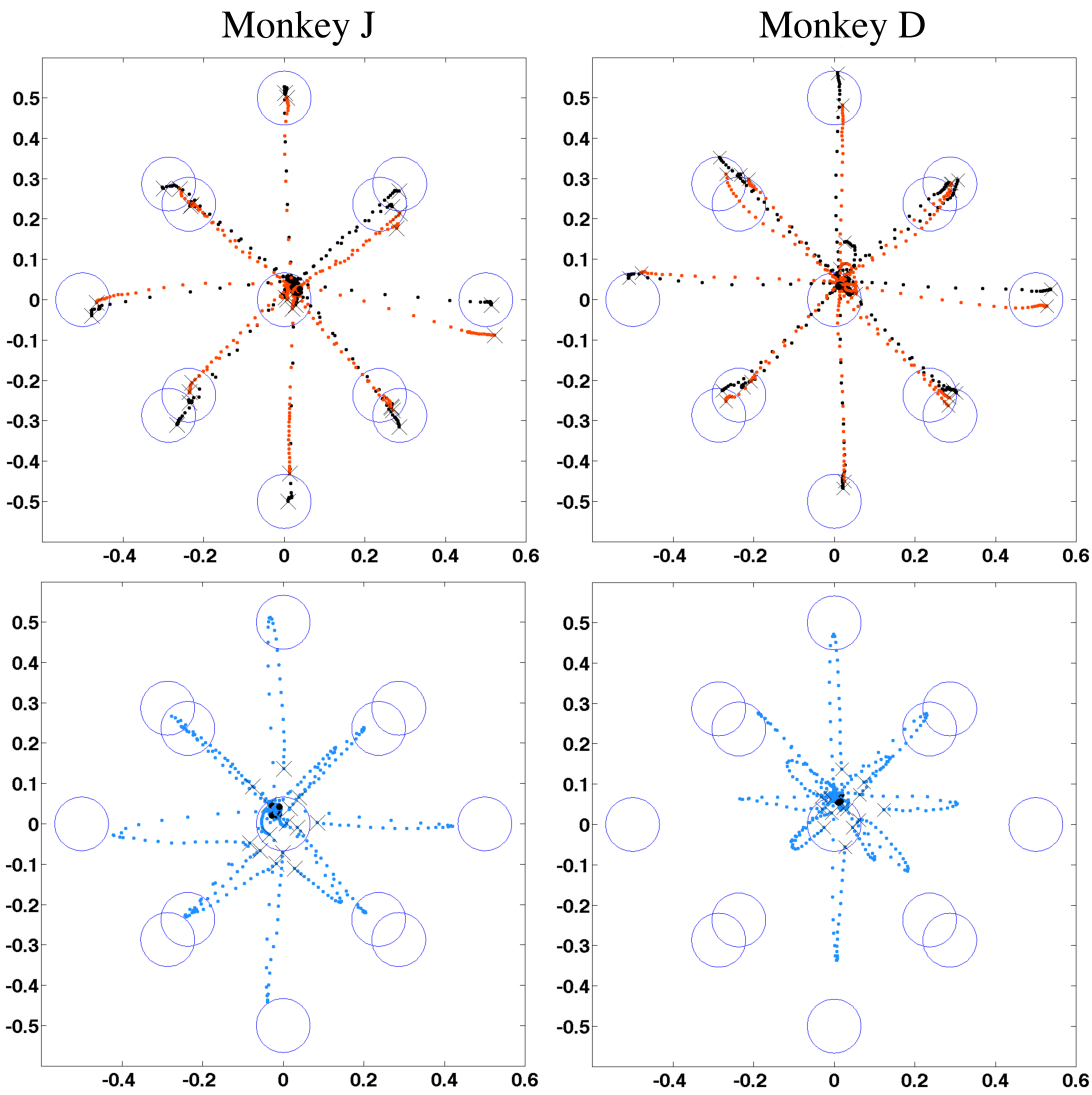

Figure 3.3: **Average Screen Coordinates of Eye Position** (n≈1200)
Screen Coordinates: Coordinates generated by the eye tracker. Center = (0,0). Right Top Corner of the screen = (1,1) *Red:* Standard Reach Task, *Green:* Anti-Reach Task, *Cyan:* Stationary Cursor Task, *Black filled circles:* Eye position during the time of the Target/Go cue, *Black "X" Markers:* Eye position at the end of a successful trial, *Dark Blue Circles:* Initial screen position of the 14 targets.

3.3 NEURAL ACTIVITY RESULTS

3.3.1 Results from the Standard Reach Task

Activity from 296 task-related units was individually modeled as a function of hand movement direction. Preferred directions appeared to be uniformly distributed and did not seem constrained to any subset of dimensions (see figure 3.4).

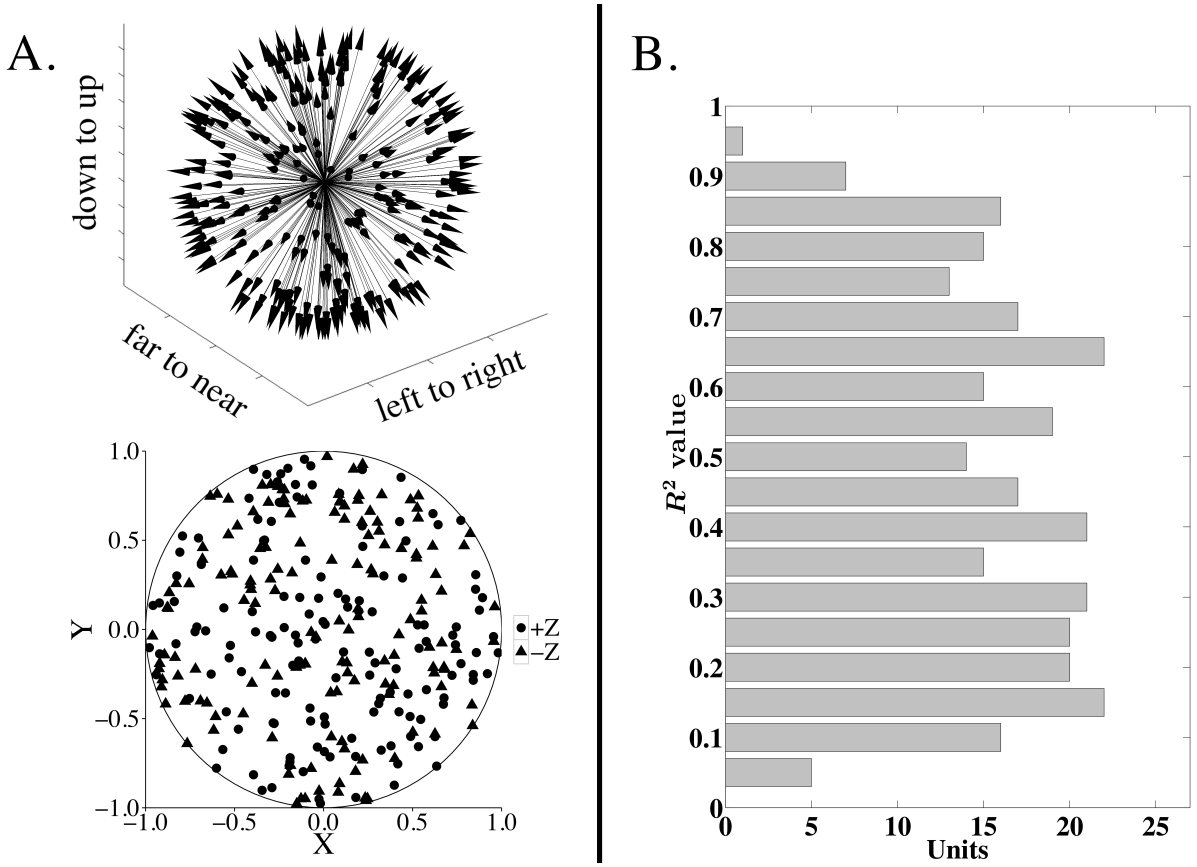

Figure 3.4: **Model Results, Standard Reach Task A.** Shows distribution of 296 preferred directions. Top shows 3D arrows representing preferred directions in cartesian coordinates. Bottom shows the surface of the unit sphere; an equal-area plot using azimuthal projection (method: [60]). **B.** Resultant R^2 values for all 296 units.

3.3.2 Results from the Anti-Reach Task

Activity from 307 task-related units was individually modeled as a function of hand direction. Preferred directions appeared to be uniformly distributed and did not seem constrained to any subset of dimensions (see figure 3.5).

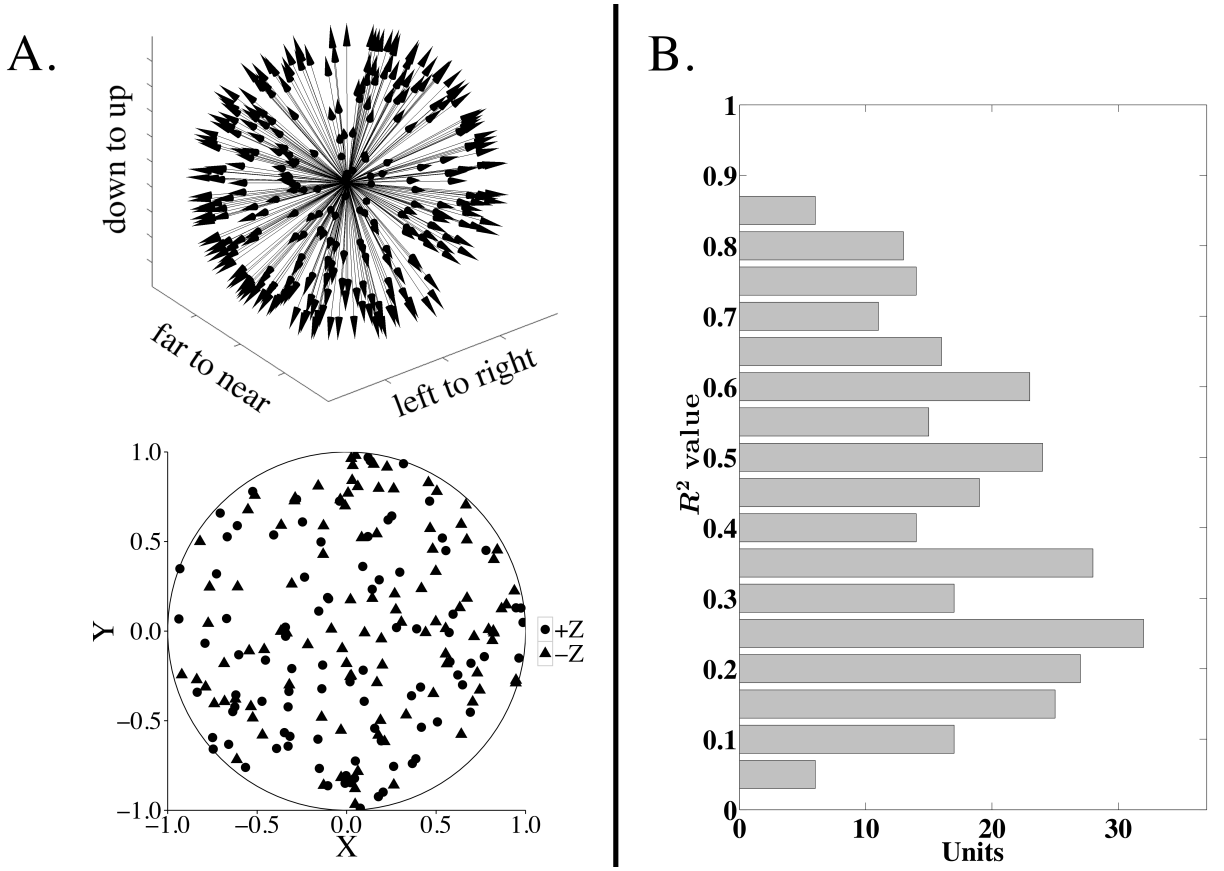

Figure 3.5: **Model Results, Anti-Reach Task: A.** Shows distribution of 307 preferred directions. Top shows 3D arrows representing preferred directions in cartesian coordinates. Bottom shows the same data on the surface of the unit sphere; an equal-area plot using azimuthal projection. **B.** Resultant R^2 values for all 307 units.

3.3.3 Changes in Neural Activity Across Tasks

Upon comparing rasters of firing rate across tasks, it was apparent that some neurons had different response-target relations. Figure 3.6 shows the response of two example units in both tasks. Neuron 1 had an opposite preferred direction in the anti-reach task (see figure 3.7).

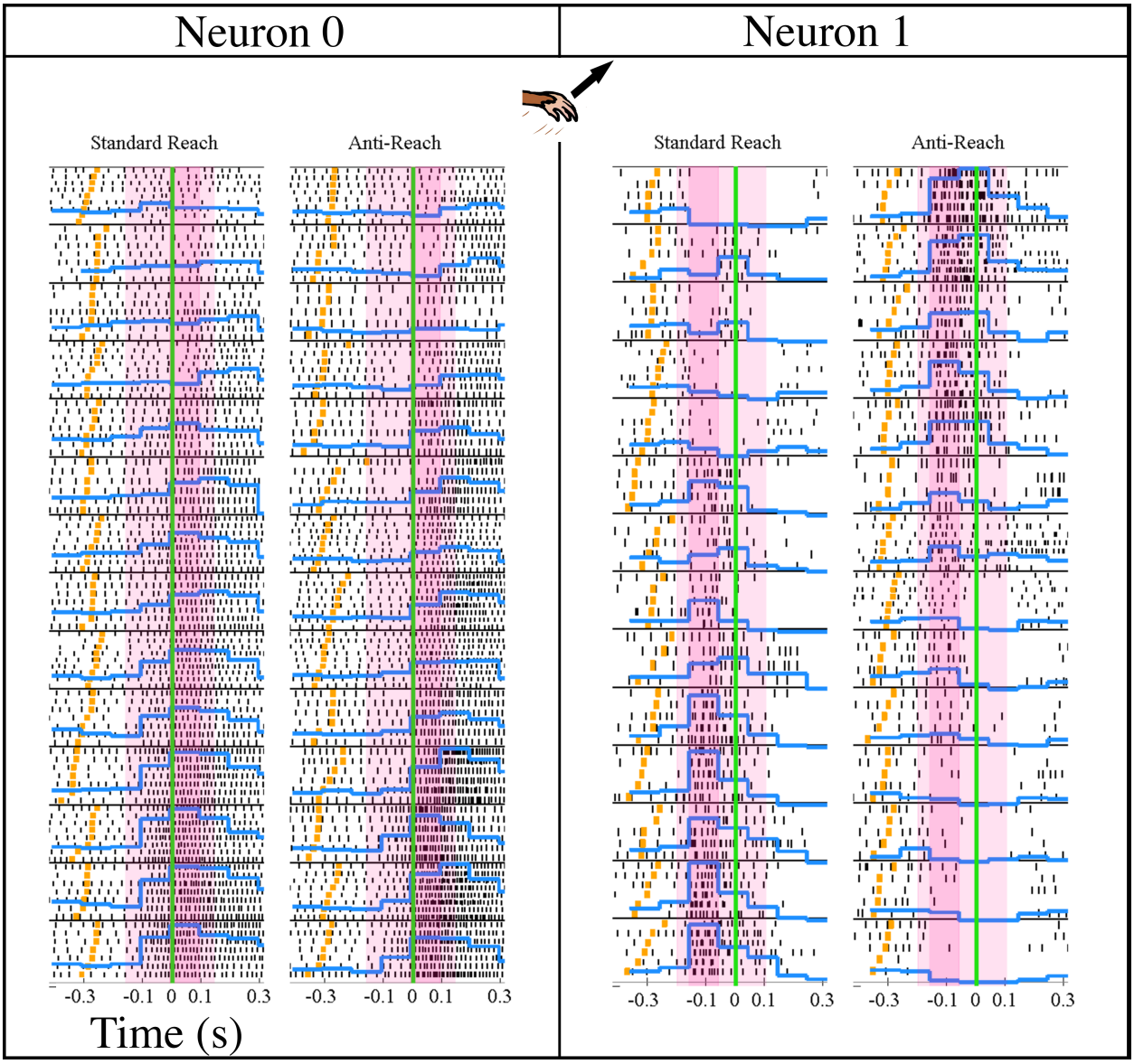

Figure 3.6: **Raster Plot, Two Response Examples:** Raster plot features previously explained in figure 2.12 Blocks of rows show rasters from the same target reach. Targets were ordered from bottom to top with increasing θ. The preferred direction for each neuron was calculated from hand velocity in the standard reach task. Activity from Neuron 0 is unaffected by the view change. Activity from Neuron 1 appears to have an opposite directional response during the anti-reach task.

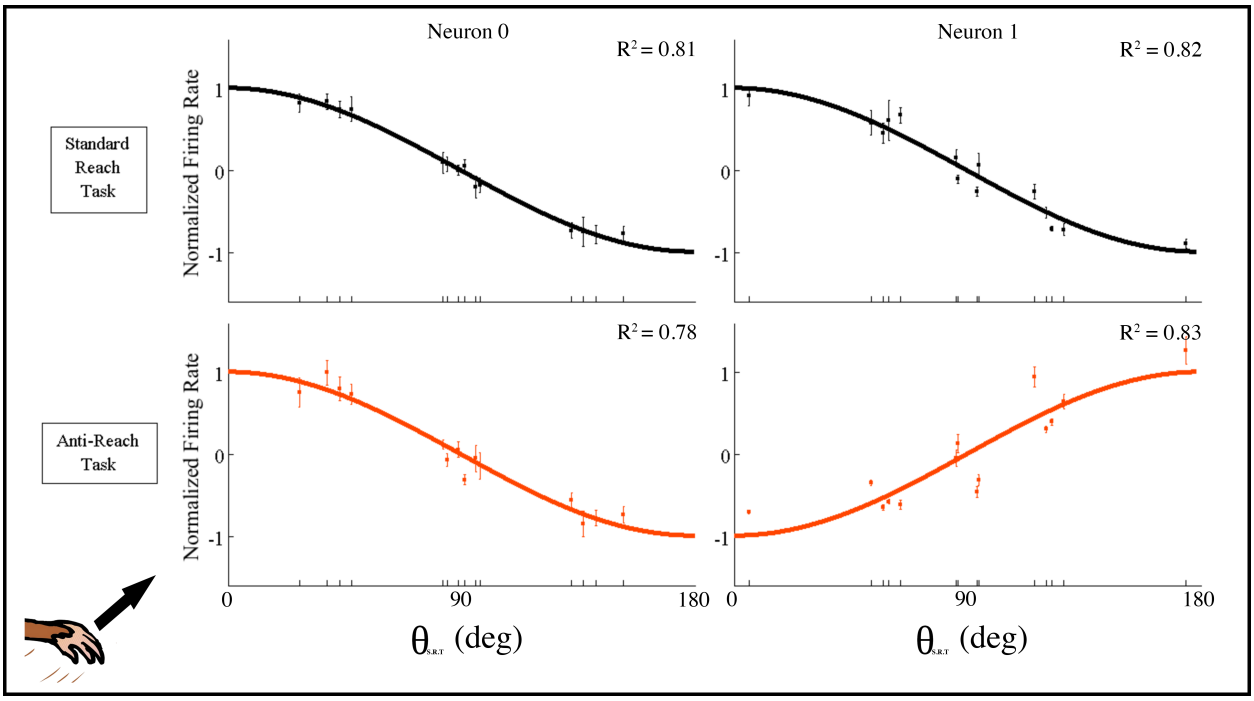

Figure 3.7: **Changes in Tuning across Tasks:** Tuning curves are explained in figure 2.12. Data points represent firing rate for the same target reach for each neuron/column. $\theta_{S.R.T}$ indicates angular difference between hand direction and the preferred direction calculated from the standard reach task. Tuning curves were generated from a linear model of response (raster plot shown in figure 3.6) for each task.

3.3.4 Results from the Stationary Cursor Task

Firing rate from 284 task-related units was modeled as a function of hand direction. Preferred directions appeared to be uniformly distributed and did not seem constrained to any subset of dimensions (see figure 3.8).

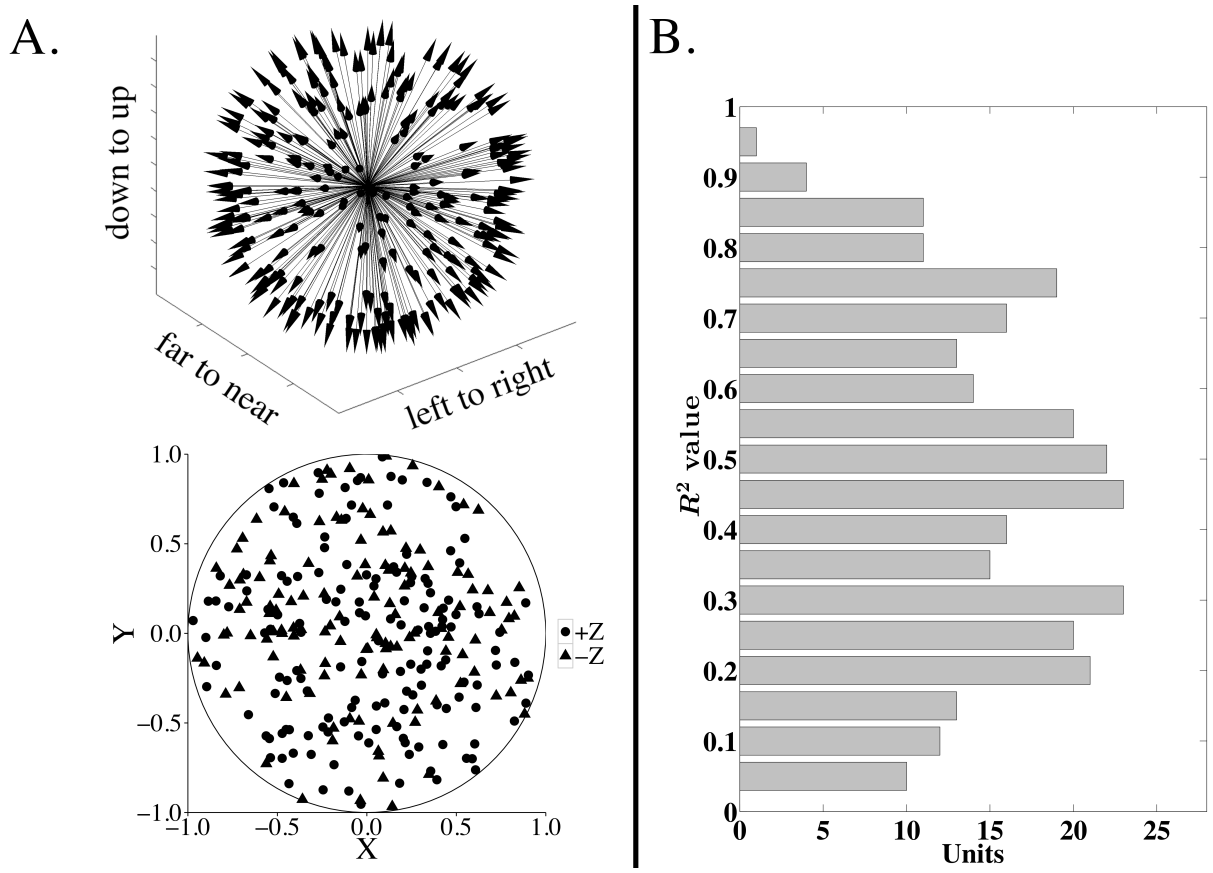

Figure 3.8: **Model Results, Stationary Cursor Task: A.** Shows distribution of 284 preferred directions. Left shows 3D arrows indicating preferred directions in cartesian coordinates. Right shows the same data on the surface of the unit sphere; an equal-area plot using cylindrical projection. **B.** Resultant R^2 values for all 284 units.

3.3.5 Changes in Neural Response Across Three Tasks

Activity from 253 units was task-related during all three tasks. Raster charts were constructed to compare their responses. Three examples (Neurons 0, 1, and 2) are shown in figure 3.9. Linear models based on hand movement reflected apparent directional tuning changes from the rasters

(see figure 3.10). Changes in preferred directions suggests sensitivity to changes in the view, since kinematics were the same across tasks. There were three notable response types. First, activity found to be insensitive to the anti-reach view change was largely insensitive to the stationary cursor view change (Neuron 0). Second, a subset of cells sensitive to the anti-reach view change were insensitive to the stationary cursor view change (Neuron 1). Third, a second subset of cells sensitive to the anti-reach view change were also sensitive to the stationary cursor view change (Neuron 2).

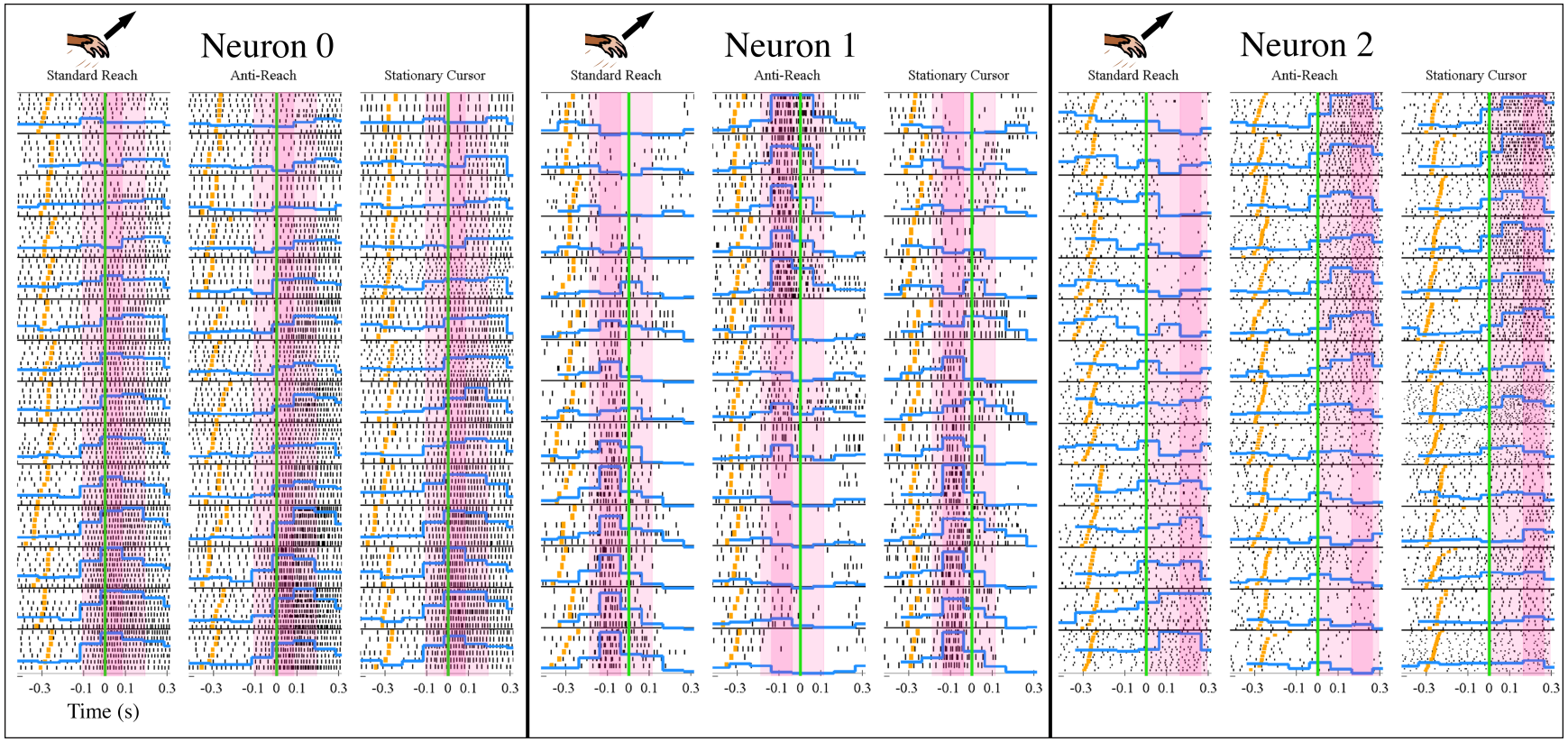

Figure 3.9: **Rasters, Three Examples Neurons, Three Tasks:** Targets are ordered according to tuning during the standard reach task for each cell (method explained in figure 2.12). Activity from Neuron 0 is unaffected by subsequent view changes. Activity from Neuron 1 appears to have an inverse directional response during the anti-reach task only. Activity from Neuron 2 shows an inverse directional response during the anti-reach and stationary cursor tasks. Neurons 0 and 1 are also in figure 3.6

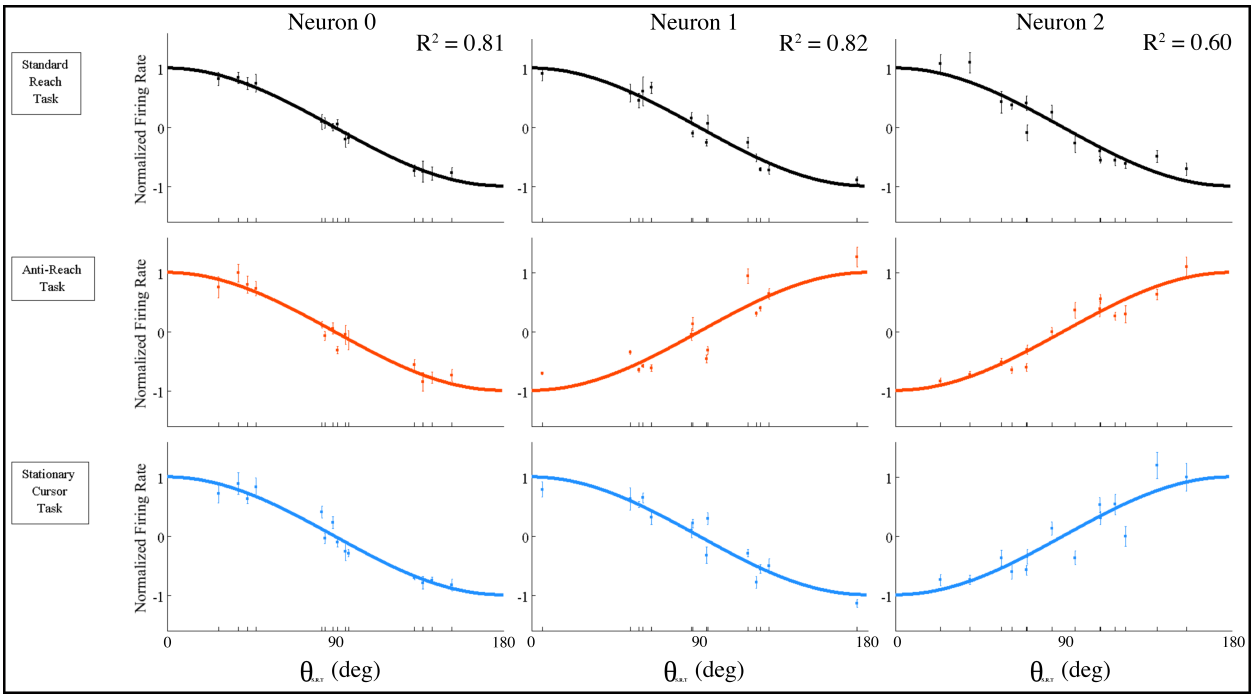

Figure 3.10: Tuning curves were previously explained in figure 2.12. Hand movement direction is the same across tasks/rows for the same neuron/column. Tuning curves fit responses from neurons 1, 2, and 3 in figure 3.9.

3.3.6 Evaluating Models with Unit Sphere Coverage

We wished to identify units that changed behavior across tasks. Significant context-induced changes in firing rate patterns suggest sensitivity to the directional variable being manipulated (i.e. cursor velocity). To compare preferred directions across different contexts, we used the tolerance interval comparison method explained in section 2.5.3 to determine if the variance in preferred direction between two conditions was overlapping. Overlapping TIs support the hypothesis that preferred directions are not changing. Non-overlapping TIs reject this, suggesting the unit is sensitive to the manipulation. A change in preferred direction would not be detected if the combined area of two elliptical tolerance intervals covered more surface area than a unit sphere. In figure 3.12, some angular differences of 180 degrees still had overlapping tolerance intervals. We used surface area as a measure of spread to determine when models were not precise enough for our purposes. Lower R^2 values corresponded to greater prediction variance, and hence greater surface area. After applying a least squares curve-fit to map surface area to R^2, we found that a value of $R^2 \geq 0.11$ generally corresponded to less than 50% coverage during all three tasks (see figure 3.11).

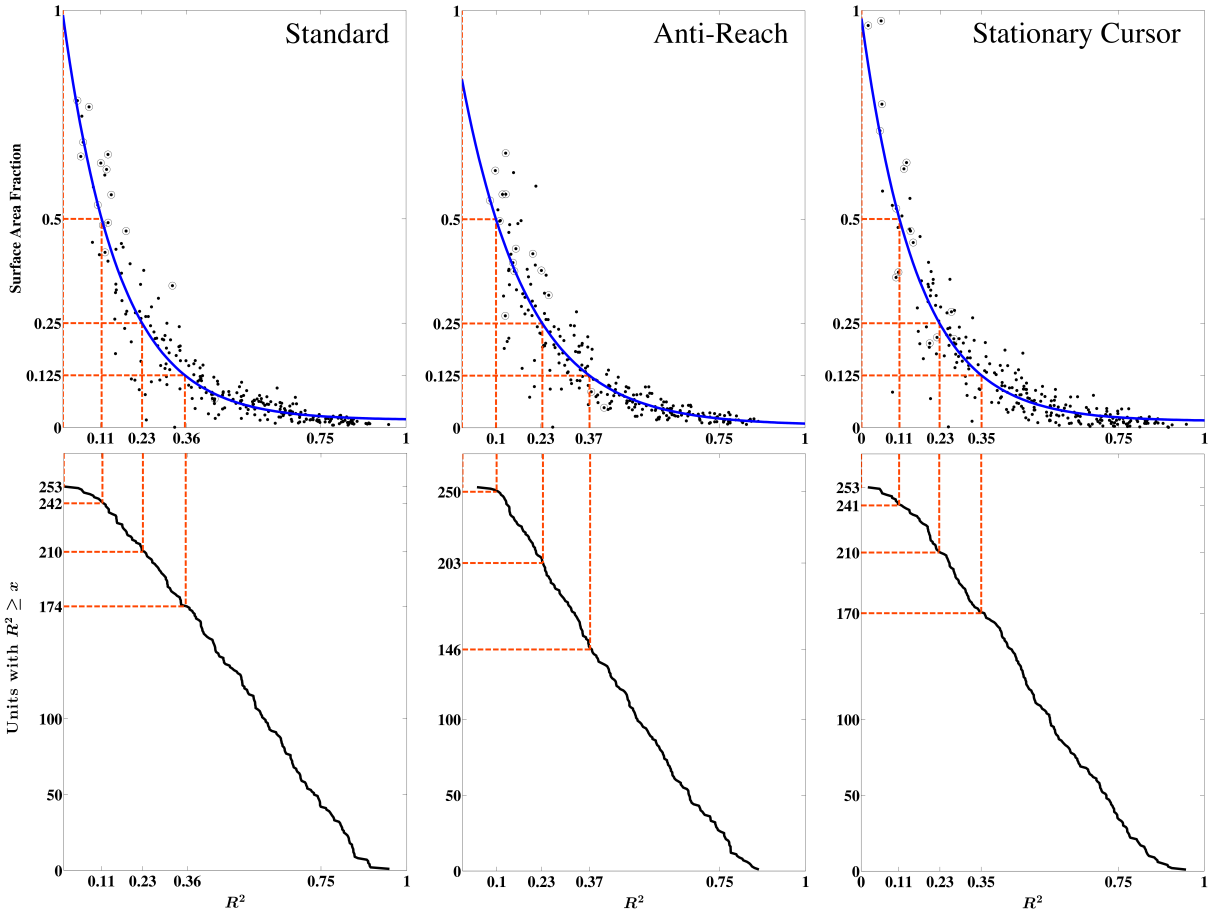

Figure 3.11: **Model Precision across Tasks** Top figure in each column shows the fractional coverage of the unit sphere, from 253 distributions of preferred direction vs. the corresponding R^2 value. Each dot represents the response of one unit. Units removed from analysis due to surface area size are circled. Fractional area values of 1, 0.5, 0.25, and 0.125 were estimated (orange dotted lines) to compare with R^2 values. Bottom plot shows a cumulative plot of resultant R^2 values for each model fit. Orange dotted lines from the top plot indicate the location of fractional area percentages from the top figure. For example, in the standard task, 210 models had coverage of 25% or less, and corresponded to an R^2 value of 0.23 or greater. In the anti-reach task, 203 models had coverage of 25% or less, and corresponded to an R^2 value of 0.23 or greater.

Units that showed activity with a summed TI area greater than a unit sphere for any two tasks were removed from further analysis. In figure 3.11, these units were indicated with a hollow circle marker. After removing 16 units based on this criteria, preferred direction comparisons with greater angular differences were more likely to have non-overlapping intervals. In figure 3.12, we show a preferred direction comparison between the preferred directions from the standard reach task and

the anti-reach task. The top plot shows the original population results, with overlapping TI's in the 160-180 range. The bottom plot shows the population after removing units with high variability, resulting in less overlapping tolerance intervals for high angular differences.

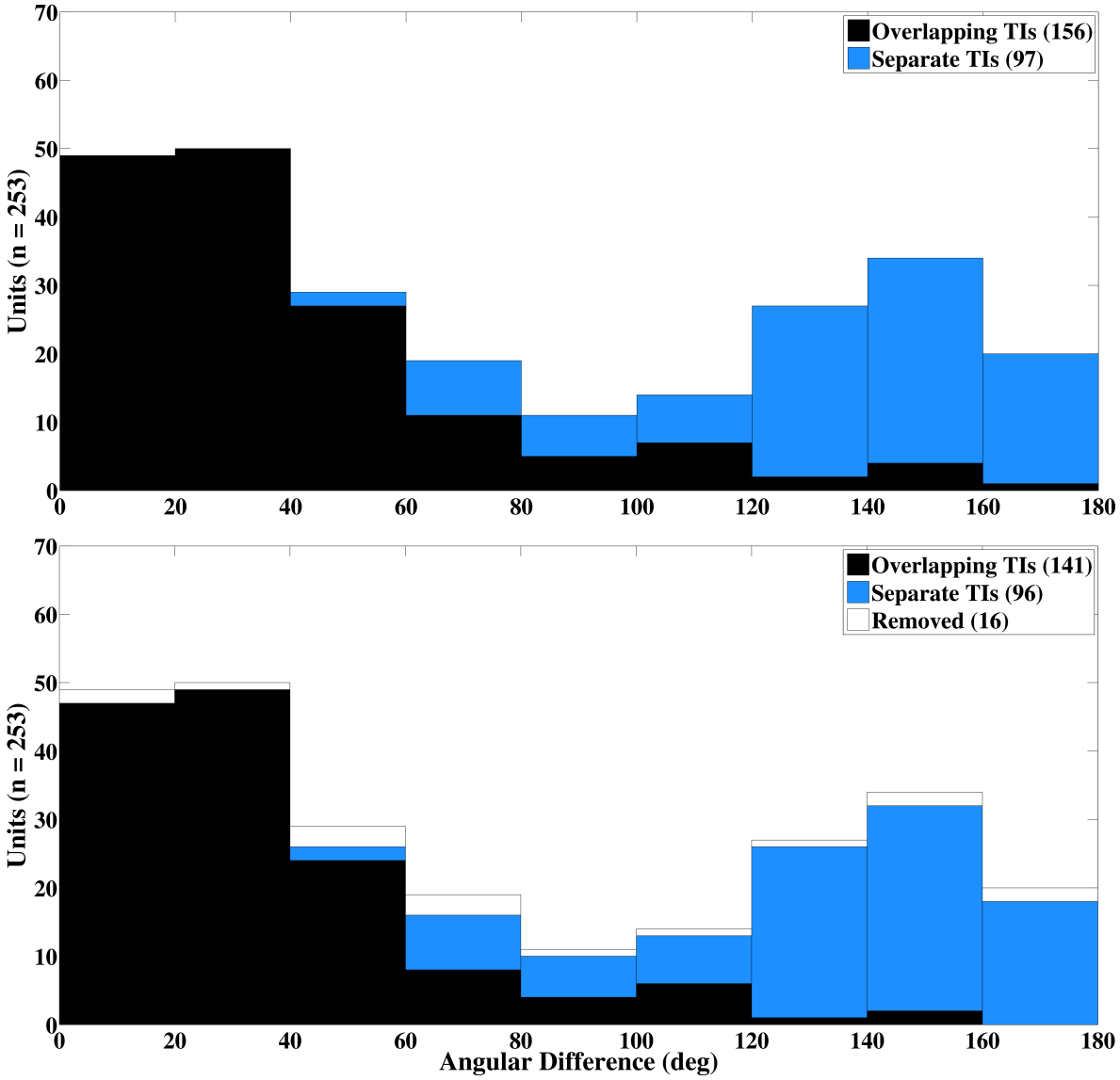

Figure 3.12: **Standard Reach vs. Anti-Reach, Change in P.D.** An example showing how removing cells from analysis based on variance of preferred direction results in less overlapping tolerance intervals for high angular differences. **TOP:** Histogram of the angular differences between preferred directions from the same cell during the standard reach and the anti-reach tasks. **BOTTOM:** Units having pairs of preferred direction tolerance intervals with a sum surface area greater than that of the unit sphere were left out (See "Removed" in legend).

Three types of neuron were labeled based on preferred direction changes compared with those from the standard reach task. Neurons were removed from analysis if they were not tested in all three tasks, or if the variance was too large (see section 3.3.6). Cells with task sensitivity similar to Neuron 0 were labeled Type 0, as there were no changes in preferred direction across tasks. Cells with task sensitivity similar to Neuron 1 were labeled Type 1, having one change in preferred direction during the anti-reach task only. Cells with task sensitivity similar to Neuron 2 were labeled Type 2, having preferred direction changes in both the anti-reach task and the stationary-cursor task (see summary in figure 3.13).

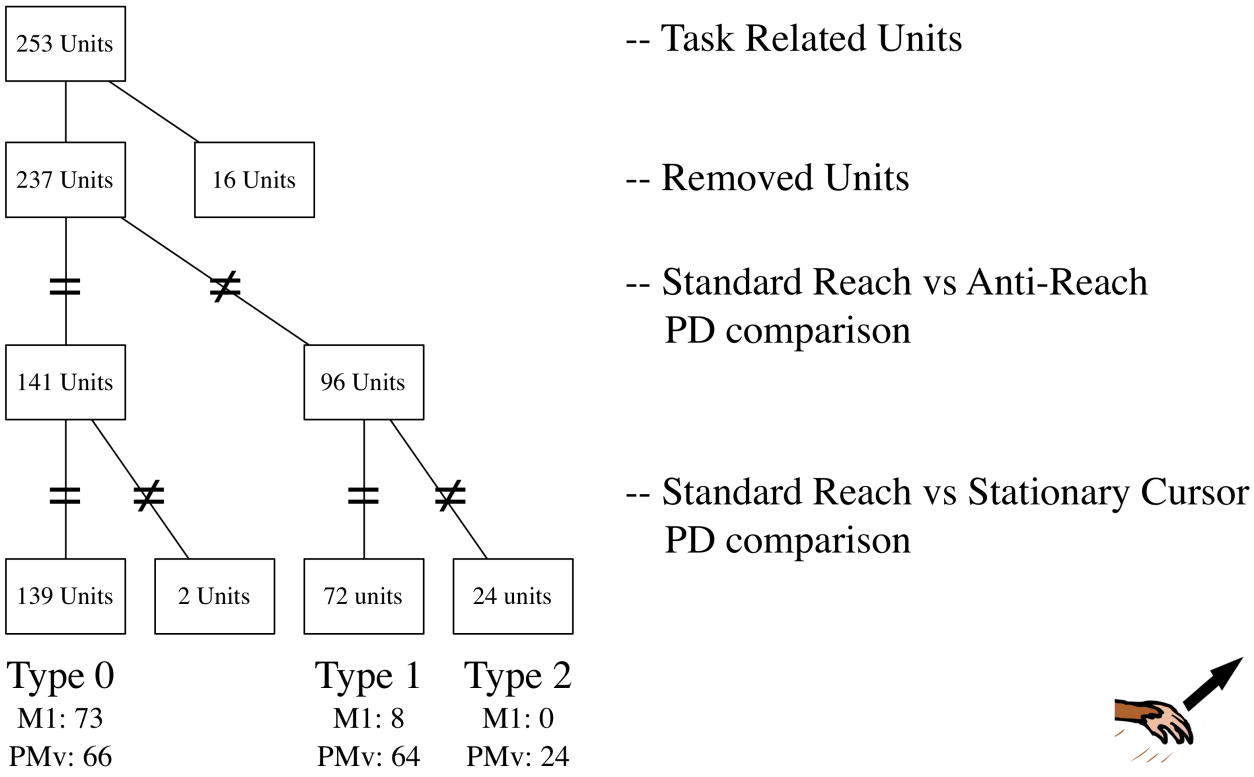

Figure 3.13: **Labels for Response Types** Types determined by preferred direction TI comparisons across tasks.

3.4 NEW COORDINATE SYSTEMS

Our analysis has revealed neuronal discharge that modulates with reach direction originating on the hand. When the view of the task changes, a subset of units show no change, implying visual insensitivity (Type 0). A second subset changes preferred direction with the view, suggesting a visually-derived construct. This group can further be subdivided into two groups, depending on if and how preferred directions change across tasks (Type 1 & 2). In this section, models were constructed that predict firing rate as a function of movement velocity in two additional coordinate systems, originating on either the cursor or the object in motion on the display (the target or cursor). The resultant preferred directions were compared across tasks to determine if view-sensitive responses were invariant in the new coordinate frames. These findings were then compared to latency and anatomical location to lend insight to the visuospatial transformation facilitating the pattern of activity.

3.4.1 A Cursor-Centered Coordinate System

96 units changed preferred direction when calculated as a function of hand movement (*hand-centered* coordinates) during the standard reach and anti-reach tasks. Although the hand motion to each target was the same in the two tasks, the direction of cursor movement to each target was reversed in the anti-reach task. Therefore, the change in preferred direction should be linked to the movement of the cursor, and not the hand. To test this hypothesis, we constructed firing rate models from the same neural activity as a function of cursor movement (*cursor-centered*) instead of that of the hand. For data from the standard reach task, where hand and cursor directions were identical, this calculation had no effect. Since the cursor was always moving in the opposite direction of the hand in the anti-reach task, the cursor-centered preferred directions were effectively rotated 180 degrees from the hand-centered preferred direction, without changing other output metrics such as R^2.

Two example units (0 and 1) are shown in figure 3.14. In row **A**, standard reach and anti-reach responses are compared. Neuron 0 shows an opposing directional response in the anti-reach task, relative to the standard reach task response, when plotted in cursor-centered coordinates. Neuron 1

shows an opposite directional response when plotted in hand-centered coordinates. In rows **B-D**, it can be seen that Neuron 0 has the same normalized response for each target in hand-centered coordinates across both tasks (B vs C). Neuron 1 has the same response for the same targets in cursor-centered coordinates (B vs D). In rows **E** and **F**, tolerance intervals from Neuron 0 overlap in hand-centered coordinates. Conversely, tolerance intervals from Neuron 1 overlap in cursor-centered coordinates.

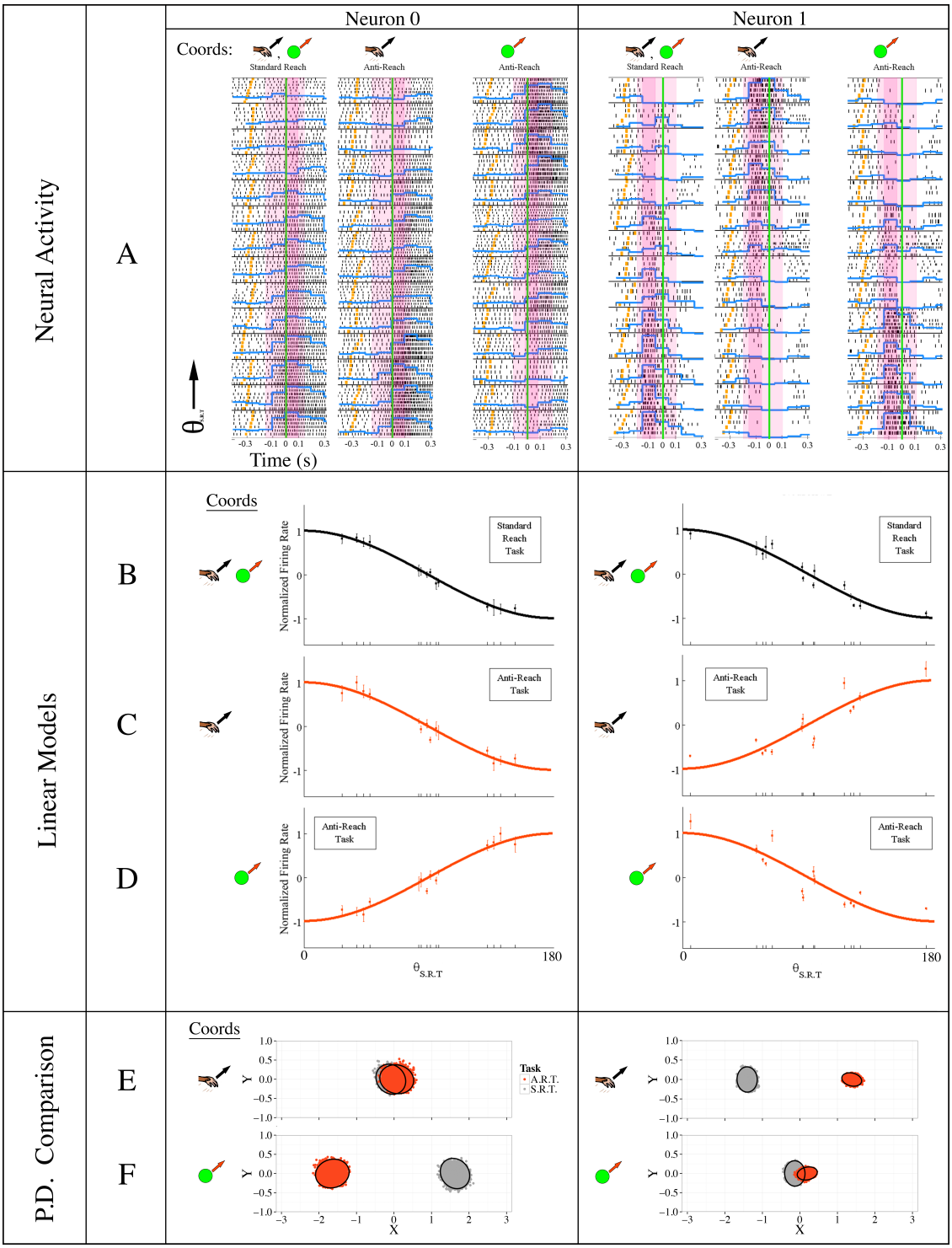

Figure 3.14: **Hand- vs. Cursor-Centered Coordinates:** Neurons 0 and 1 (also in figures 3.6, 3.7, 3.9, and 3.10) are examples of hand-centered and cursor-centered responses, respectively. Raster plots and tuning curves (A-D) are explained fully in figure 2.12). Preferred direction tolerance interval comparison (E,F) explained in section 2.5.3. Icons in each plot indicate the coordinate system used for the firing rate model. The standard reach task by default has identical preferred directions in both coordinate systems. $\theta_{S.R.T}$ indicates angular difference in hand/cursor-centered coordinates using only the standard reach data set.

3.4.2 Classification

To determine if neural activity corresponded to either a hand-centered or a cursor-centered coordinate system, we evaluated preferred direction similarities between the standard reach and the anti-reach tasks. For instance, if preferred directions tolerance intervals were overlapping in coordinate system A and separate in coordinate system B, we classified that activity as corresponding to movement in coordinate system A. Table 2 summarizes this method by showing the angular differences and number of overlaps between preferred directions calculated from each task. Neuron 0 has overlapping tolerance intervals in hand-centered coordinates, non-overlapping tolerance intervals in cursor-centered coordinates and was classified as having hand-centered activity. Neuron 1 has overlapping tolerance intervals in cursor-centered coordinates, non-overlapping tolerance intervals in hand-centered coordinates and was classified as having cursor-centered activity.

Table 2: **Classification Method for Two Coordinate Systems**

Example Unit	**Neuron 0**		**Neuron 1**	
PD Coords*	H	C	H	C
Standard Reach PD vs. Anti-Reach PD	9.6°	170.3°	159.7°	20.3°
# of TI overlaps	1	0	0	1
Coordinate Classification	**Hand**		**Cursor**	

*H = Hand-Centered, C = Cursor-Centered

3.4.3 Anatomical Localization

We compared neuronal responses from M1 and PMv. We found a slight majority (55.6%) of cursor-centered responses from neurons located in the PMv. Conversely, neurons located in the M1 had mostly hand-centered responses (90.8%). The results for the entire sample are summarized in table 3.

Table 3: **Anatomical Location of Units with Responses in One of Two Coordinate Systems**

Cortical Area	**All**	**M1**			**PMv**		
Monkey	D+J	D+J	D	J	D+J	D	J
Total Units Recorded	400	117	54	63	283	145	138
Task Related (both tasks)	281	88	51	37	193	124	69
Units with Classified Activity	209	76	46	30	133	84	49
➥ Classified, Hand-Centered	128	69	39	30	59	35	24
➥ Classified, Cursor-Centered	81	7	7	0	74	49	25

3.4.4 Latency Distribution

The response latency of each classified unit was evaluated relative to movement onset. We found significant differences when comparing the medians of the of hand-centered and cursor-centered groups in PMv, and similar distributions for subpopulations of units with hand-centered activity in PMv and M1 (see figure 3.15).

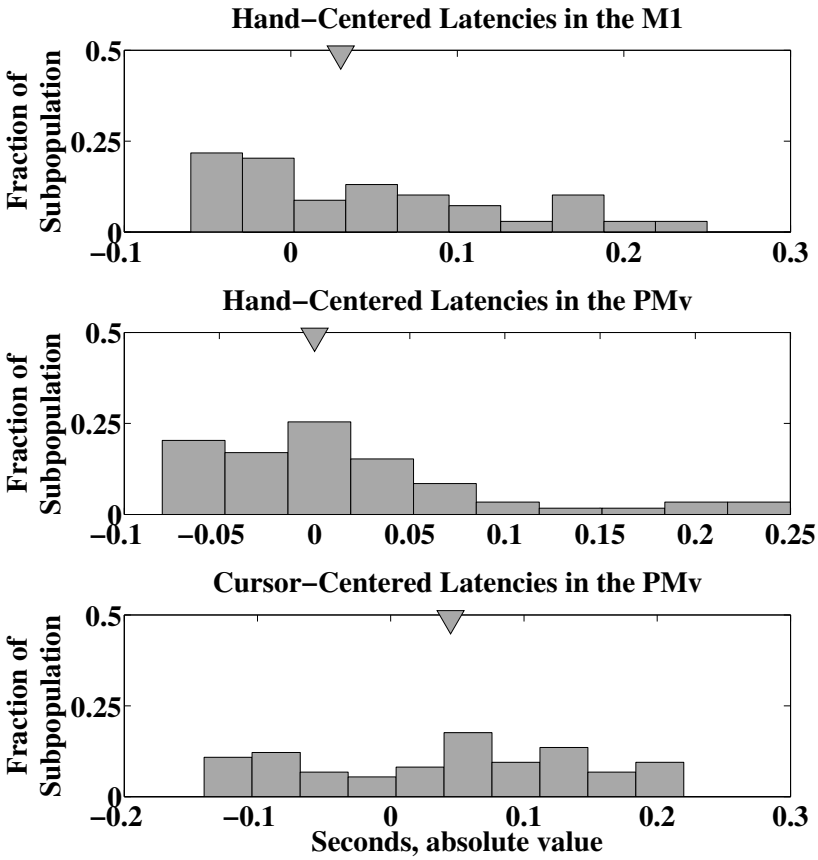

Figure 3.15: **Latency vs. Movement Onset:** Median latency of the subpopulation with cursor-centered responses in PMv was significantly different from that of the subpopulations with hand-centered responses in PMv and M1. No significant difference was found between the hand-centered subpopulations in PMv and M1 (Wilcoxon Rank Sum Test, $p<.05$).

3.4.5 Depth of Modulation Comparison

We wished to determine if visualization of the moving cursor was required for firing rate modulation from units classified with cursor-centered activity (see section 3.4.1). We compared the depth of modulation during the standard reach task, where the cursor moves with the hand, to that during the stationary cursor task, where the cursor appears stationary. Results showed that the activity during both tasks was modulated, suggesting that visualization of a moving cursor was not required. Figure 3.16 shows that the depth of modulation across tasks was similar, implying that the same directional

variable may be driving the response in each task. Since the activity from this subpopulation of cells was classified as sensitive to visual changes, it may correspond to motion in either of two previously proposed coordinate systems (see section 2.2.4). First, the difference vector was defined as the direction of target location relative to the cursor and did not require cursor motion. Second, displayed motion was defined as the direction of motion from either the target, which moves during the stationary cursor task, or the cursor, which moves during the standard reach task.

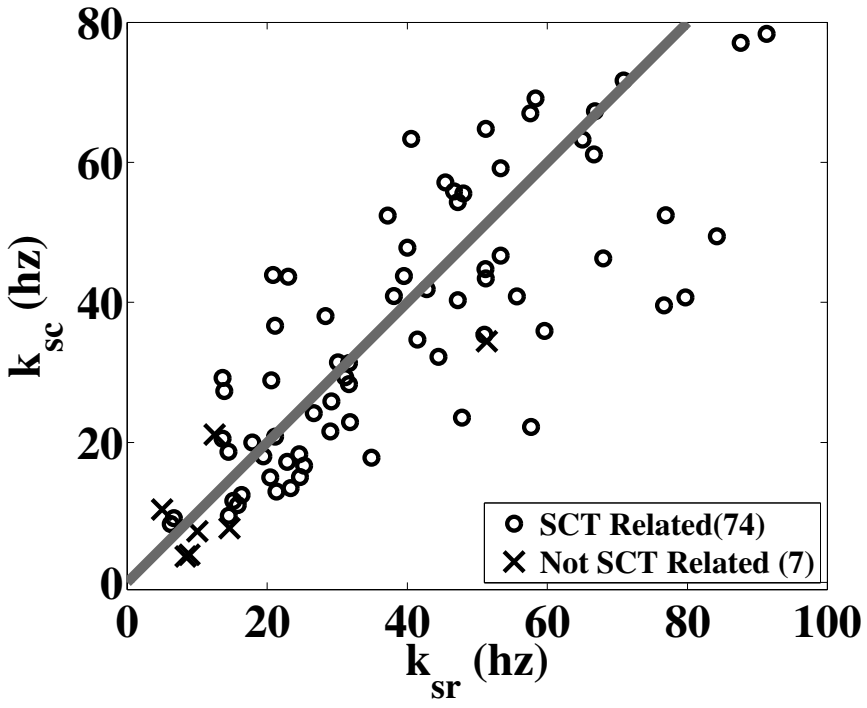

Figure 3.16: **Modulation Depth During the Stationary Cursor Task** This figure supports the conclusion that visual motion is not required for directional modulation. Modulation depth from the stationary cursor task (k_{sc}, y-axis) is compared to that from the standard reach task (k_{sr}, x-axis). Each point represents the activity response of one unit during both tasks. Most of these units (all classified as *cursor-centered*) appear to have similar modulation during both tasks (correlation follows slope of 1, $R^2 = 0.36$). Since the motion of the cursor is not present during the stationary cursor task, modulation may correspond instead to either the difference vector or displayed motion (see further explanation in the text).

3.4.6 A Coordinate System for Displayed Motion

Responses that were solely cursor-centered should have maintained similar tuning across all three tasks. Changes in preferred direction suggest that a neural response may correspond to a different

coordinate system. We examined the subpopulation of cells initially classified as having *cursor-centered* activity for changes in preferred direction during the stationary cursor task and found that 24/96 units showed changes in their tuning. One explanation for this apparent change may be that the activity corresponds to the direction of *displayed motion*, rather than the cursor-centered direction. We define displayed motion as the velocity of the moving object on the screen, whether it was the cursor or the target. To test this hypothesis, we compared firing rate models of the same neural activity as a function of displayed motion. This calculation change had no effect relative to the cursor-centered preferred directions calculated from the standard and anti-reach tasks, since in these cases displayed motion was defined by the movement of the cursor. During the stationary cursor task, since the cursor appeared stationary and the target appeared to move toward the center of the workspace, displayed motion was defined by the movement of the target. This rotated the preferred directions by 180 degrees and had no effect on other statistical metrics such as R^2.

Figure 3.17 depicts rasters, tuning curves, and preferred direction tolerance intervals generated in terms of the cursor-centered and displayed motion coordinate systems. Two example units (type 1 and type 2) are compared. In row **A**, anti-reach and stationary cursor task results are compared. Neuron 1 shows an opposing directional response in the stationary cursor task relative to the anti-reach task when plotted in displayed motion coordinates. Neuron 2 shows an opposing directional response in the stationary-cursor task relative to the anti-reach task when plotted in cursor-centered coordinates. In rows **B-D**, tuning models illustrate that Neuron 1 had the same normalized response for the same targets in cursor-centered coordinates (B vs C). Neuron 2 had the same response for the same targets in displayed motion coordinates (B vs D). In rows **E** and **F**, preferred direction tolerance intervals from Neuron 1 overlap in cursor-centered coordinates. Conversely, preferred direction tolerance intervals from Neuron 2 overlap in displayed motion coordinates. Neuron 1 shows invariance in a cursor-centered coordinate system. For Neuron 2, the motion on the screen led to a consistent pattern of modulation when it opposed the motion of the hand, whether the target or the cursor appeared to move.

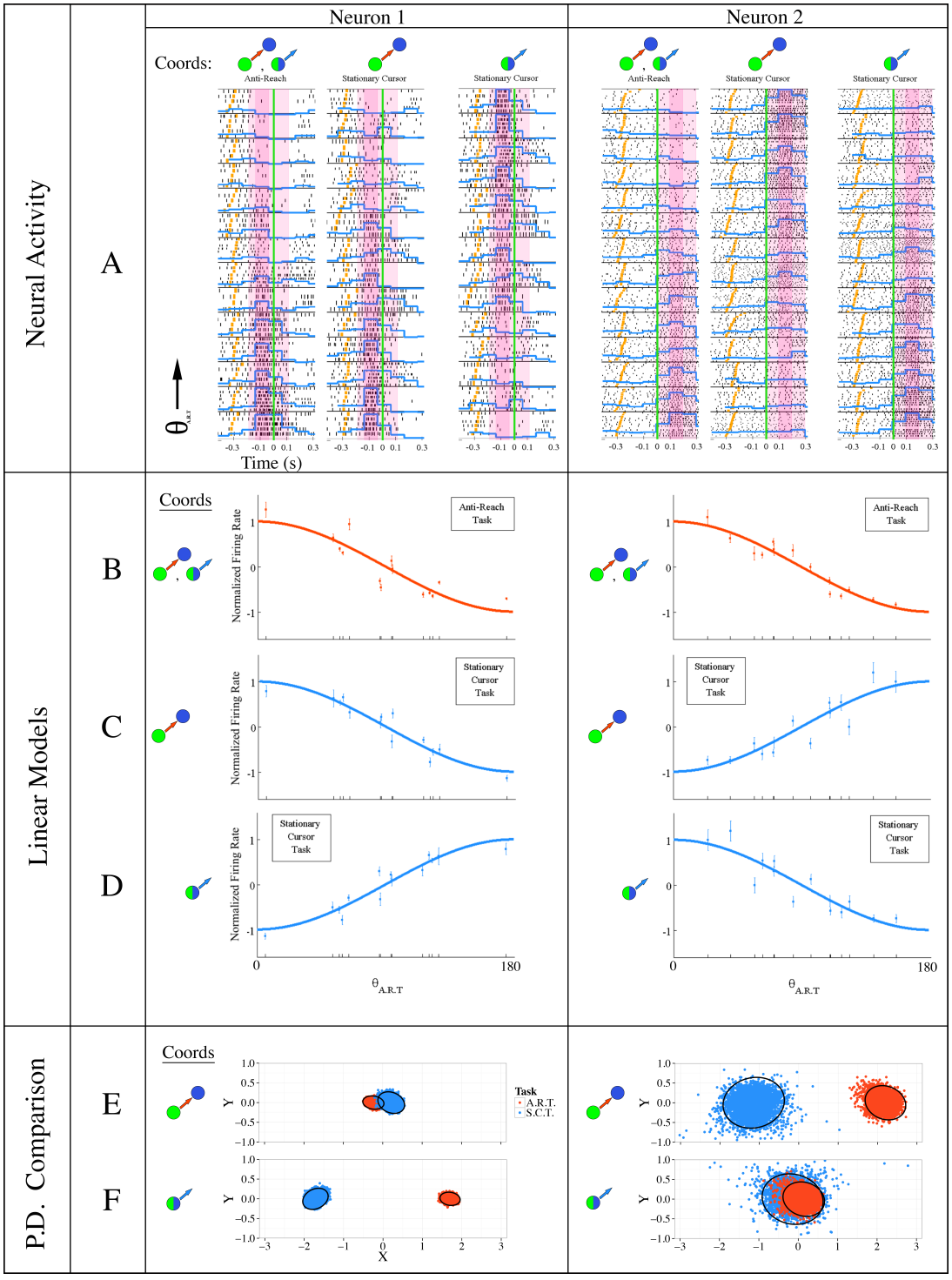

Figure 3.17: **Cursor- vs. Displayed Motion Coordinates:** Neurons 1 and 2 (also in figures 3.9, 3.10) are examples of responses in a cursor-centered and displayed motion coordinate frame, respectively. Raster plots (A) and tuning curves (B-D) were previously explained in figure 2.12. P.D. comparison (E-F) explained in section 2.5.3. Icons indicate the coordinate system used for each firing rate model. The anti-reach task has identical preferred directions in both coordinate systems. $\theta_{A.R.T}$ indicates angular difference in cursor-centered and displayed motion coordinates using only the anti-reach data set. Individual plots (A-E) are compared in the text (section 3.4.6).

We constructed cosine tuning models for all cells in each coordinate system for each task. The responses of three example units are shown in figure 3.18 to illustrate selective correspondence to each candidate coordinate system. Each of the 9 charts shows firing rate data and its corresponding model fit from each of the three reach tasks. The three columns each show firing rate as a function of the angular difference between the preferred direction and the movement direction, in either hand-centered coordinates (θ_{hand}, column 1), cursor-centered coordinates (θ_{cursor}, column 2), or displayed motion coordinates ($\theta_{d.motion}$, column 3). Similar tuning during all three tasks (shaded axes) suggests that the activity from that neuron corresponds to movement direction in the labeled coordinate system.

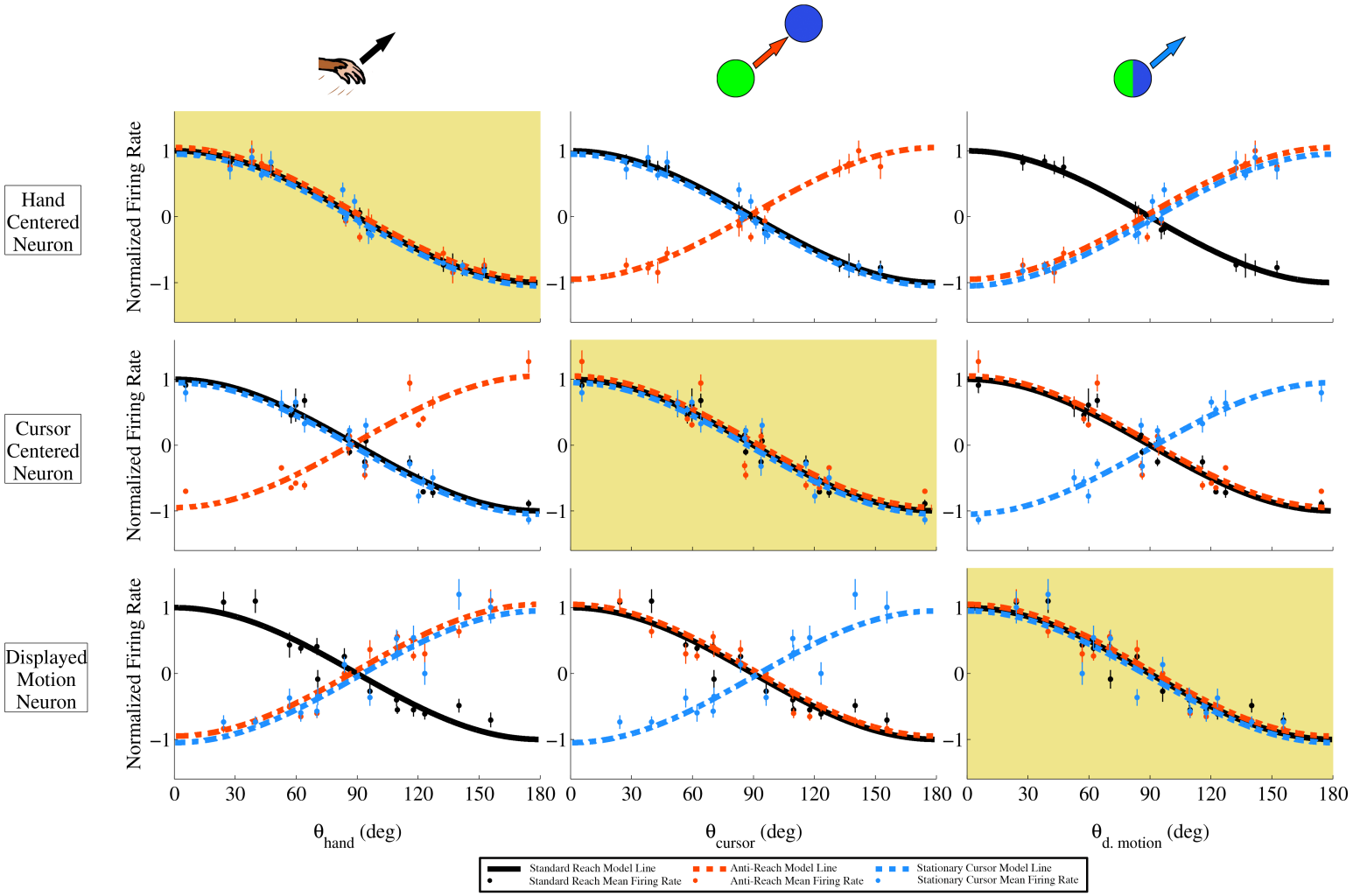

Figure 3.18: **Tuning Functions for Three Classes of Neurons:** Each of the nine charts in this figure shows model lines from each of the three tasks plotted in the same coordinate system (see legend for colors). Each column indicates the coordinate system (labeled at the top) used for the linear models. Each row indicates one example neuron, showing the same responses plotted in the coordinate frame of the column. Points illustrate mean normalized firing rate and standard error bars for each reach target. Shaded plots indicate similar directional tuning across tasks. See section 3.4.6 for further explanation.

3.4.7 Multi-task Models

We constructed firing rate models from multi-task data (all task data) to evaluate the model fit for each coordinate system. These models were constructed in the same way as those from individual tasks (see section 2.5.1). Since modulation depth varied across tasks, we normalized firing rate for each task data set before regression. Figure 3.19-left compares R^2 values from multi-task models from the same 253 task-related units in hand-centered vs. the best fit coordinate system (including hand-centered). The improvement in R^2 value suggests that using three coordinate systems improves the model fit to the data. Figure 3.19-right shows the R^2 values for each firing rate model in the three coordinate systems. The models tend to fit movement in one coordinate system better than the other two. This suggests that this population can likely be segregated based on correspondence to movement in a given coordinate system.

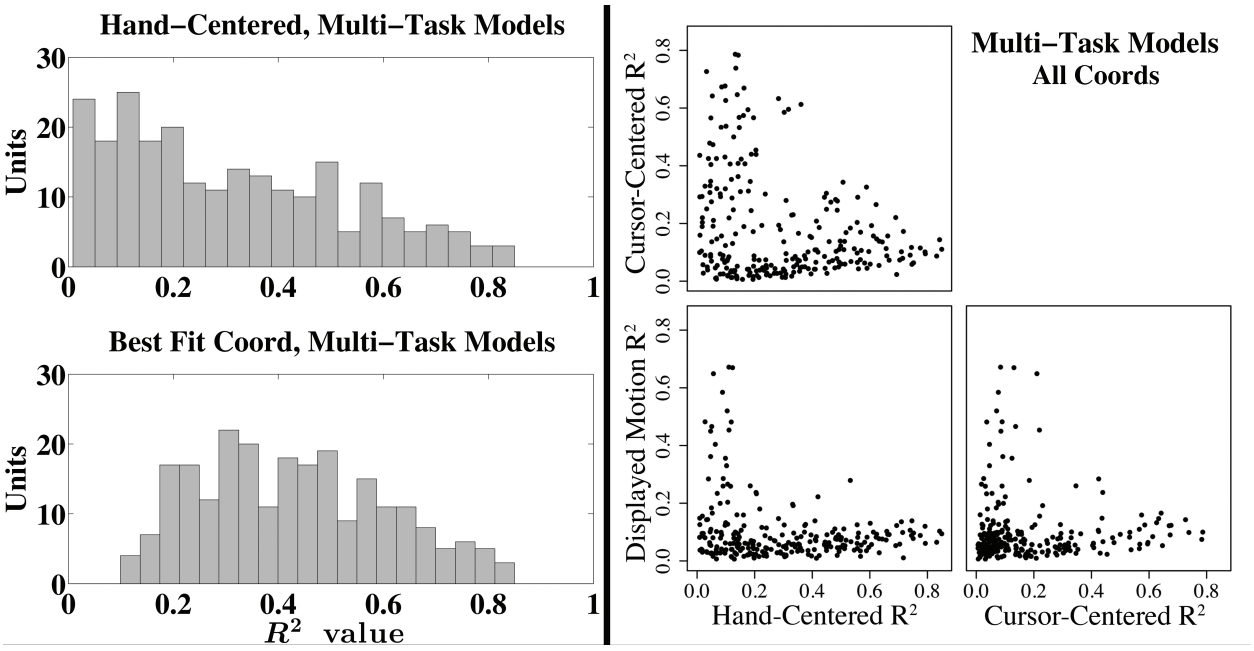

Figure 3.19: **Multi-task Model R^2 comparison:** *Left-Top:* A histogram of R^2 values from 253 task-related units fit with hand-centered models only. *Left-Bottom:* A histogram of R^2 values from the same 253 units fit with models from the best-fit coordinate system. *Right:* Three scatterplot comparisons showing R^2 values in the three coordinate systems. Each sub-plot shows 253 model results (filled circles), each representing the response from a task-related unit.

3.4.8 Classification

To determine if neural activity corresponds to a hand-centered, cursor-centered, or a displayed motion coordinate system, we evaluated whether preferred directions may be the same across the three tasks for each coordinate system. Firing rate for this analysis was calculated using the 300 mS time windows centered on the latency values found from multi-task model regression. We then calculated the TI's for the resultant preferred directions using the method described in section 2.5.3. We then labeled preferred directions as similar if they had overlapping TI's. Totaling these similarities gives a pattern unique to each coordinate system classification. Table 4 illustrates how we classified each example neuron, showing angular differences and the sum of the TI overlaps for each coordinate system. To classify activity as corresponding to movement in a coordinate system, preferred directions from all tasks must be similar in that coordinate system and also have one pair of overlapping TI's (similar preferred directions) in one of the other two coordinate systems. For example, analysis of Neuron 0 (a unit with hand-centered activity) revealed three pairs of overlapping tolerance intervals in hand-centered space, one in cursor-centered space (anti-reach task was dissociated from standard reach and stationary cursor), and one in displayed motion space (standard reach task was dissociated from the anti-reach task and the stationary cursor task). This results in 3 TI overlaps in hand-centered space and 1 in each of the other coordinate systems. The criterion for any unit classification to a particular coordinate system was that it had to fit this specific 3/1/1 overlap pattern. This pattern can also be thought of as a combination of non-overlap : 0/2/2.

Table 4: **Classification Pattern for Three Coordinate Systems**

Example Unit	**Neuron 0**			**Neuron 1**			**Neuron 2**		
P.D. Coords*:	H	C	D	H	C	D	H	C	D
SR vs AR PD**	10°	170°	170°	160°	20°	20°	172°	8°	8°
SR vs SC PD	9°	9°	171°	10°	10°	170°	160°	160°	20°
AR vs SC PD	12°	168°	12°	153°	27°	153°	17°	163°	17°
# TI Overlaps	3	1	1	1	3	1	1	1	3
Classification	**Hand**			**Cursor**			**D. Motion**		

*H = Hand-Centered, C = Cursor-Centered, D = Displayed Motion
**SR = Standard Reach Task, AR = Anti-Reach Task, SC = Stationary Cursor Task

3.4.9 R^2 values from Multi-task Models of Classified Activity

For a unit to be classified successfully, it had to be directionally tuned and have an invariant preferred direction across our battery of tasks. To determine how well classified activity was fit by multi-task models in their labeled coordinate frame vs. the other coordinate frames, we compared R^2 values in each coordinate frame for each unit. Figure 3.20 illustrates that the model fit was best when calculated in the classified coordinate system. This figure is the same as figure 3.19-right, with units labeled according to their classified coordinate systems. Rather than set a cutoff R^2 value for labeling each unit, we have evaluated each model by confirming its expected preferred direction in each task.

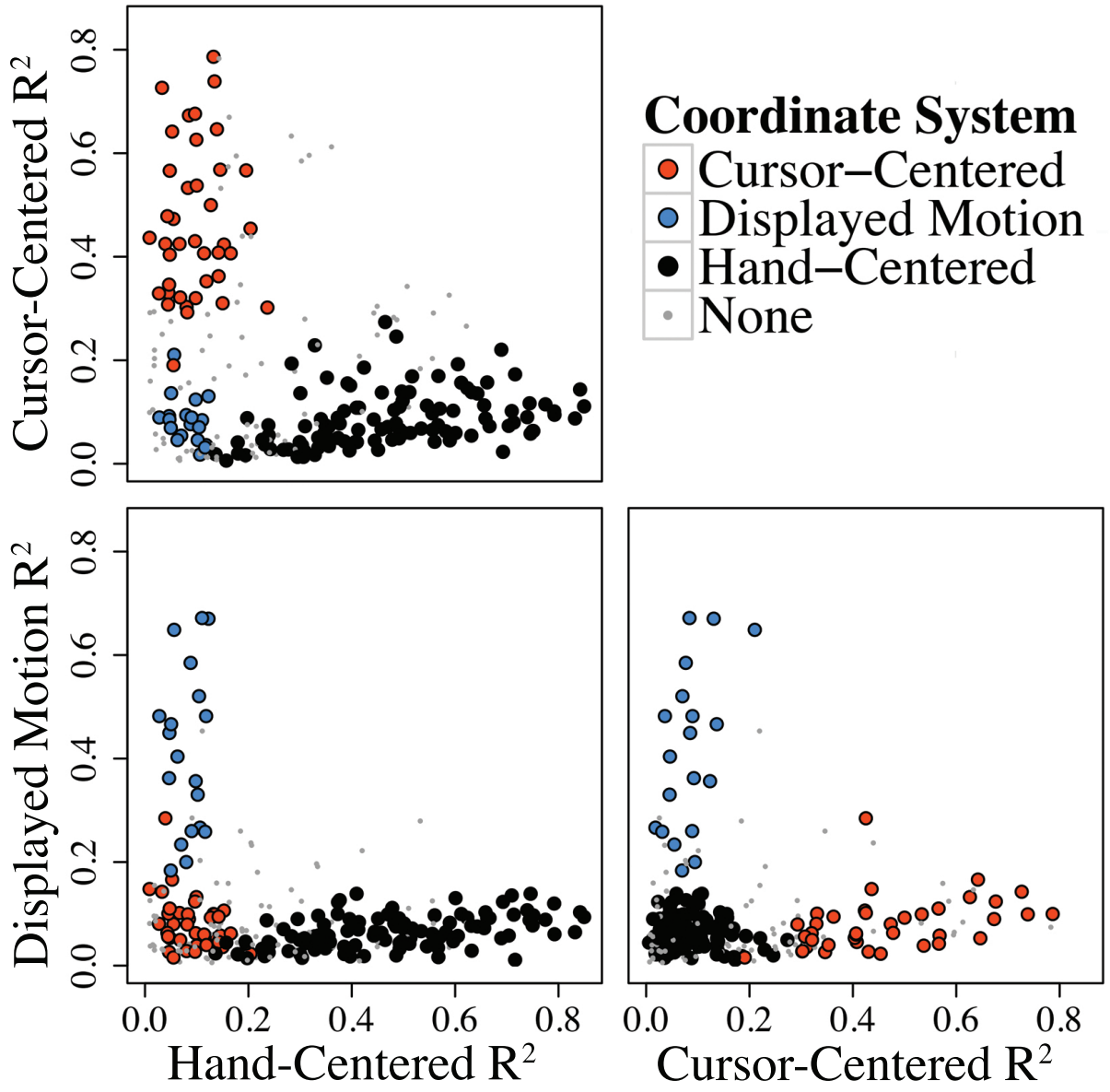

Figure 3.20: **Multi-task Models after Classification:** Classified activity was fit better in its labeled coordinate system than the other two. Three scatterplots show R^2 values for each unit in each coordinate system. Each plot shows all units' R^2 values in two coordinate systems. See legend for colors designating classified activity.

3.4.10 Anatomical Location

After classifying the units, we evaluated the anterior-posterior location of each penetration, relative to the arcuate sulcus (see figure 3.21). Units with activity corresponding to displayed motion were closer to the arcuate sulcus than neurons with cursor-centered modulation, which in turn were closer than neurons with hand-centered modulation. We calculated median locations of 6.7mm, 3.1mm, and 1.4mm for Hand-Centered, Cursor-Centered, and Displayed Motion coordinates respectively. Each subpopulation had a median distance that was significantly different from the other two (Mann-Whitney, $p<0.0001$).

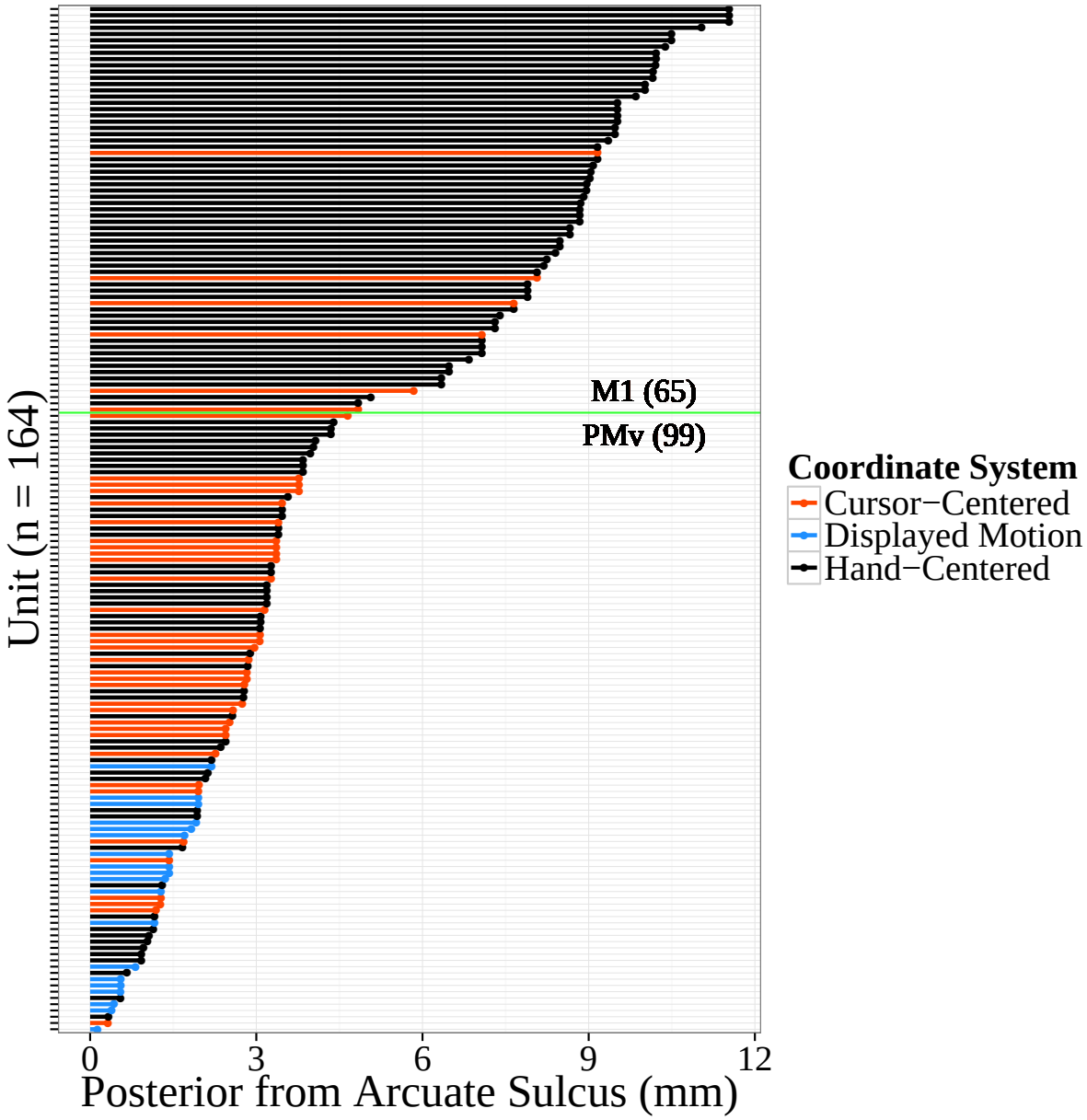

Figure 3.21: **Posterior Distance from the Arcuate Sulcus**

View-sensitive activity (classified as cursor-centered or displayed motion) was found to be generally located in the PMv. Hand-centered activity was found in M1 and PMv (90.8% of classified units in M1, 47.5% in PMv). All three coordinate systems were found in both monkeys, with monkey D having a much larger cursor-centered sample and monkey J having a much larger displayed motion sample.

Table 5: **Anatomical Location of Neuronal Activity in Three Coordinate Systems**

Cortical Area	**All**	**M1**			**PMv**		
Monkey	D+J	D+J	D	J	D+J	D	J
Total Units Recorded	400	117	54	63	283	145	138
Task Related (all 3 tasks)	253	85	51	34	168	111	57
Units with Classified Activity	164	65	42	23	99	66	33
➥ Hand-Centered	106	59	36	23	47	31	16
➥ Cursor-Centered	39	6	6	0	33	31	2
➥ Displayed Motion	19	0	0	0	19	4	15

3.4.11 Latency in Three Coordinate Systems

Figure 3.22 shows latencies for each classified unit from the multi-task models (method described in section 2.5.1.1). Hand and cursor-centered activity both had a median latency of ~0 ms and were tuned before units with activity corresponding to displayed motion. All activity corresponding to displayed motion came after movement onset, and the median was significantly different from the cursor-centered and hand-centered groups (Mann-Whitney, $p<0.0001$). Second, during the reaction-time period (before movement onset), median cursor-centered activity responded before median hand-centered activity (Mann-Whitney, $p<0.0001$).

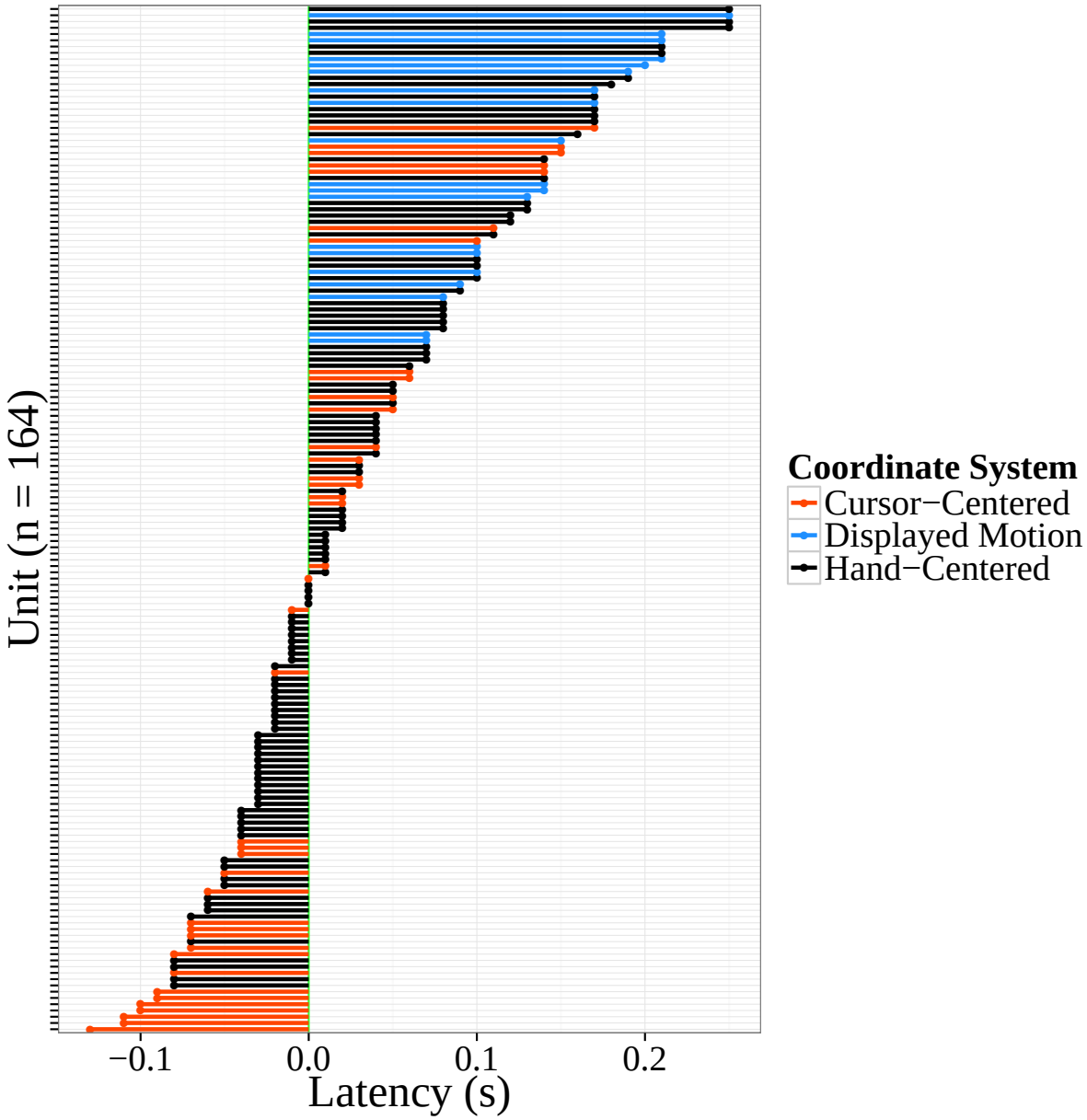

Figure 3.22: **Response Latency in Classified Coordinate Systems**

3.4.12 Preferred Direction Separation in Classified Units

It is possible that the variance of the preferred directions was so large that their tolerance intervals (TI's) overlapped in every coordinate system. The pattern we used for classification (3/1/1) required separation in two of three coordinate systems, making this case unlikely. Even so, another possibility is that the tolerance intervals TI's were large, far apart, and only barely shifted when calculated in different coordinate systems, and thus were classified at random. Ideally, preferred directions with overlapping tolerance intervals should have a low angular difference. To evaluate how close the preferred directions were across tasks, we compared the means of the distributions. The average angular difference was calculated across tasks for each classified neuron in the classified coordinate system. A perfect alignment value would have been an angular difference of 0°. The largest separation possible was 120°. Results showed a minimum value of 11.2°, a median value of 37.1°, and a maximum value of 66.0° (see figure 3.23). These results suggest that the distributions were moderately sized and shifting due to changes in the coordinate system used for the model.

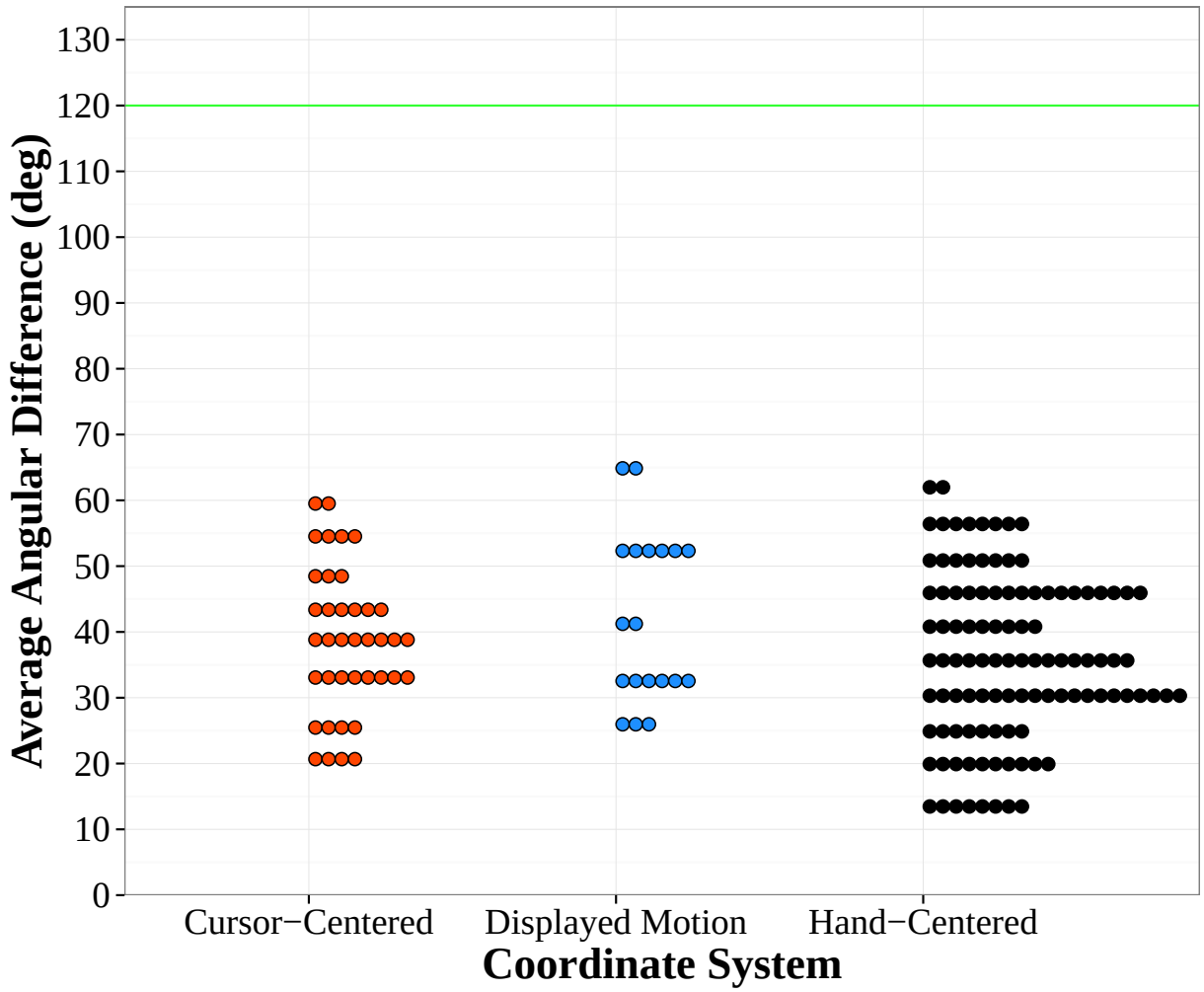

Figure 3.23: **Model Validation: Average Angular Difference** Each point represents one classified unit, colored by coordinate system. Points were arranged into rows binned in 5° increments. The green horizontal line represents the largest possible separation (120°).

3.4.13 Evaluating Possible Eye Direction Correlation

Recent evidence shows that a portion of the PMv is involved in interactions between the neck and oculomotor control systems [3]. Other premotor areas have been shown to at least partially encode eye movement variables as well. Eye direction was correlated with features of movement we were studying in the active reaching experiments. It was necessary to resolve this ambiguity using partial correlation (see section 2.5.4 for methods). Our results revealed that 2 neurons with classified activity had a stronger partial correlation with eye direction than with velocity in their respective coordinate frames. These cells were removed from our reported results. Those units were not located in one area of the cortex, nor did they have similar latency values. Figure 3.24 shows examples of both positive and negative results from this analysis.

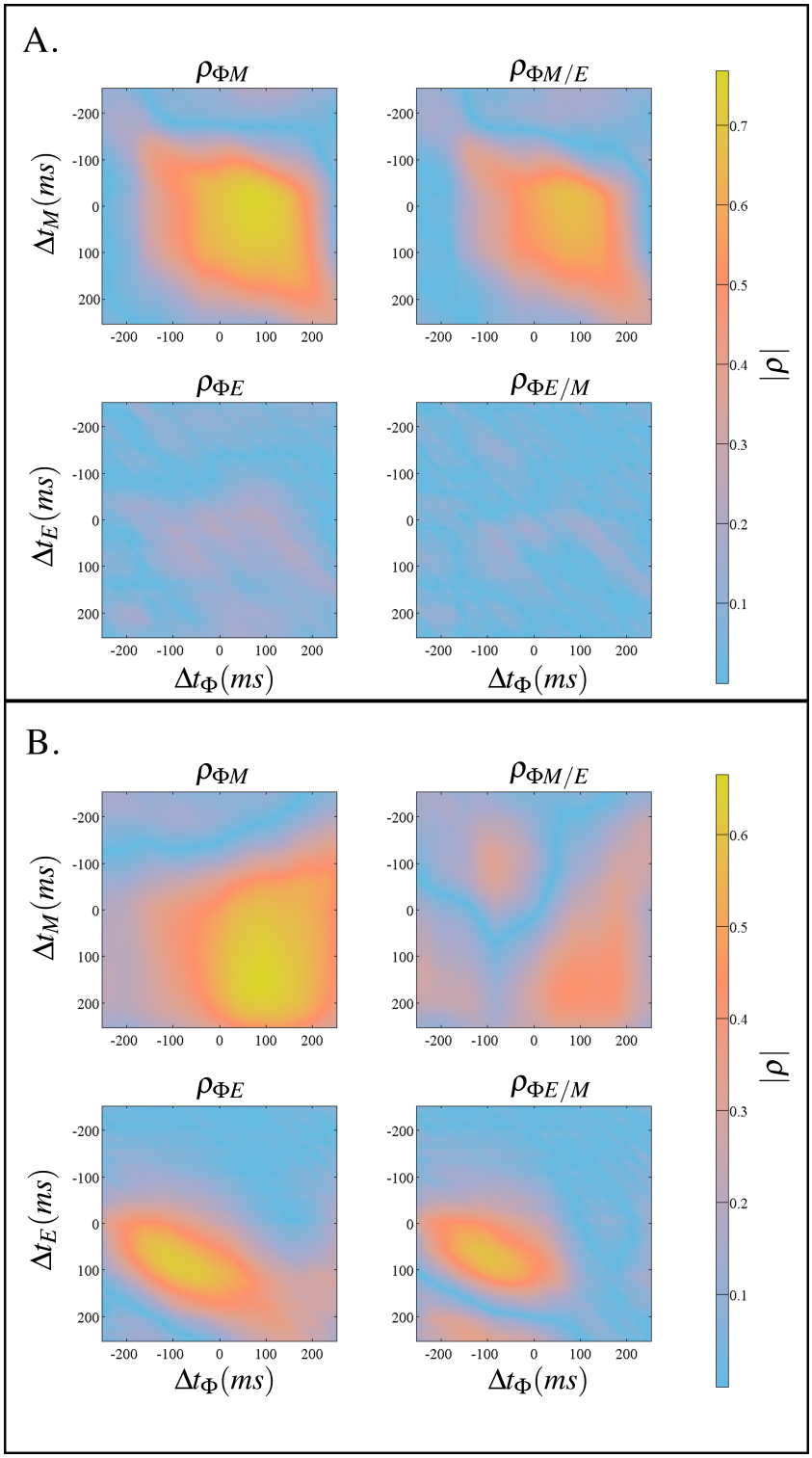

Figure 3.24: **Eye Direction Correlation Examples:** Standard correlation in the left column. Partial correlation in the right column. Φ = Discharge Rate. M = Salient Movement Feature. E = Eye Direction. Δt = time shift of labeled variable. **Top four plots:** A neuron not correlated with eye direction. The majority of the recorded cells in this experiment showed similar results. **Bottom four plots:** Activity from one unit correlated with eye direction. One other unit had similarly correlated responses with eye direction.

4.0 RESULTS FROM THE REPLAY EXPERIMENT

4.1 INTRODUCTION

Single-unit recordings are evaluated in this chapter to determine whether evidence of visuospatial transformation was present in PMv and M1 as monkeys passively watched replays of active trials they just completed. In section 4.2, kinematics of the arm and eyes in each experimental task are evaluated. In section 4.3, we model how neuronal discharge varies as the replayed movement is observed from different view conditions. In section 4.4, we compare these results to the hypothetical coordinate systems described in the previous chapter. Finally, in section 4.5 we compare results from the active reaching experiment to those collected during passive replays.

4.1.1 Task Summary:

Kinematic data the end of the Hold A period to the end of the Hold B period was buffered and replayed for the subject after each successful reach trial throughout the set of active reaching tasks. Each active reaching task was performed in a block. For example, 14 anti-reach successes were interleaved with 14 replay successes before moving on to the next task. During replay the subject was trained to hold its hand in the center of the workspace.

4.2 KINEMATIC RESULTS

4.2.1 Hand Movement

As expected, the hand did not move appreciably in this task, and stayed in the 16mm diameter hold region during the replays (see figure 4.1). Speed profiles from both monkeys start a slight decrease in speed due to braking from the center return movement and a flat profile later, during the motion of the cursor (see figure 4.2).

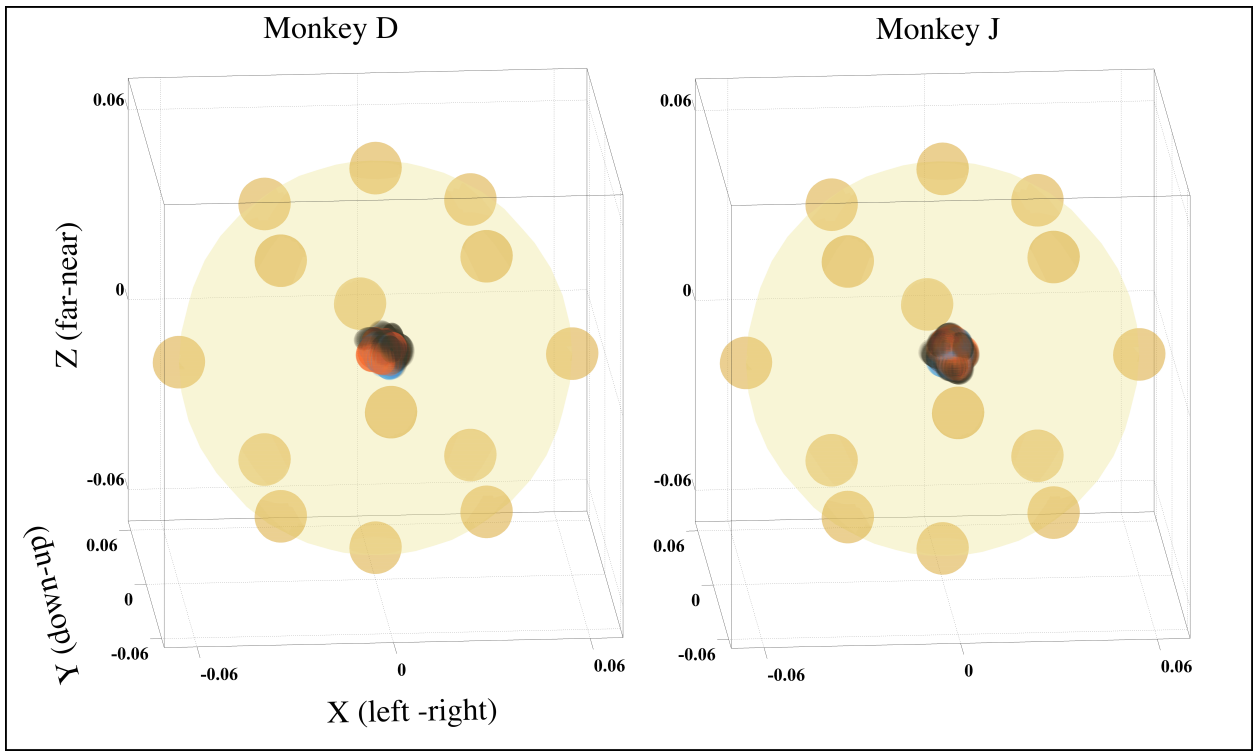

Figure 4.1: **Average Hand Position (n≈1200):** *Red:* Standard Reach Replay *Green:* Anti-Reach Replay, *Cyan:* Stationary Cursor Replay, *Transparent Blue Spheres:* Three dimensional physical target positions.

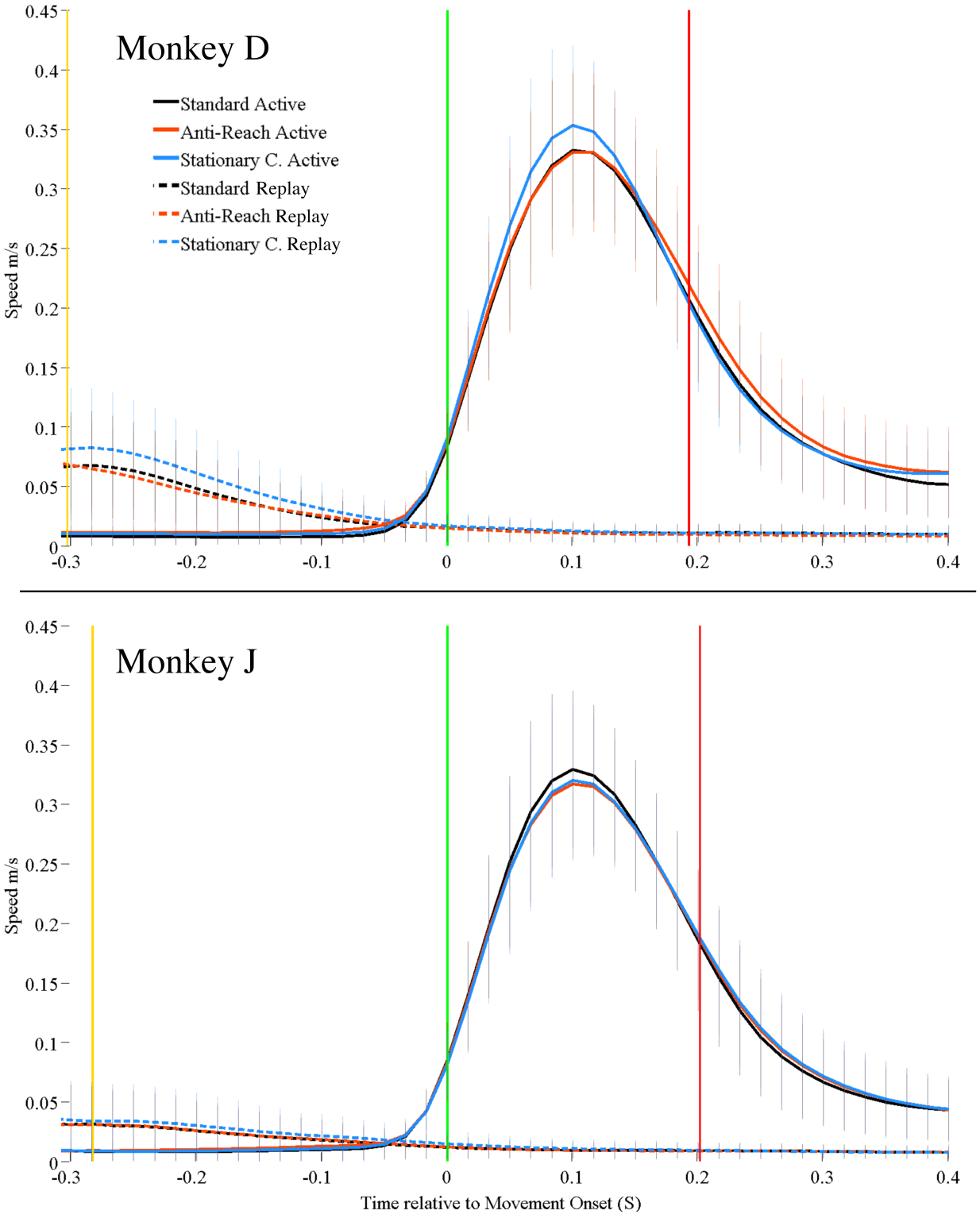

Figure 4.2: **Mean Speed Profiles from Active Reach and Task Replays:** Each curve is the average speed to all targets (n≥15400) from the go cue to ≈ 200mS after target capture for either the Standard, Anti-Reach, and the Stationary Cursor reach tasks. All trials were aligned on movement onset. *Gold Vertical:* Average Target/Go Cue Time, *Green Vertical:* Movement Onset Time, *Red Vertical:* Average Target Contact Time

4.2.2 Eye Movement

We calculated the mean value of screen coordinates from ∼1200 trials for each displayed target, in each task (see figure 4.3). Monkey J fixated on the target in the standard and anti-reach tasks, while tracking the moving target less completely in the stationary cursor task. Monkey D had less of a tendency to track the target in any of the conditions.

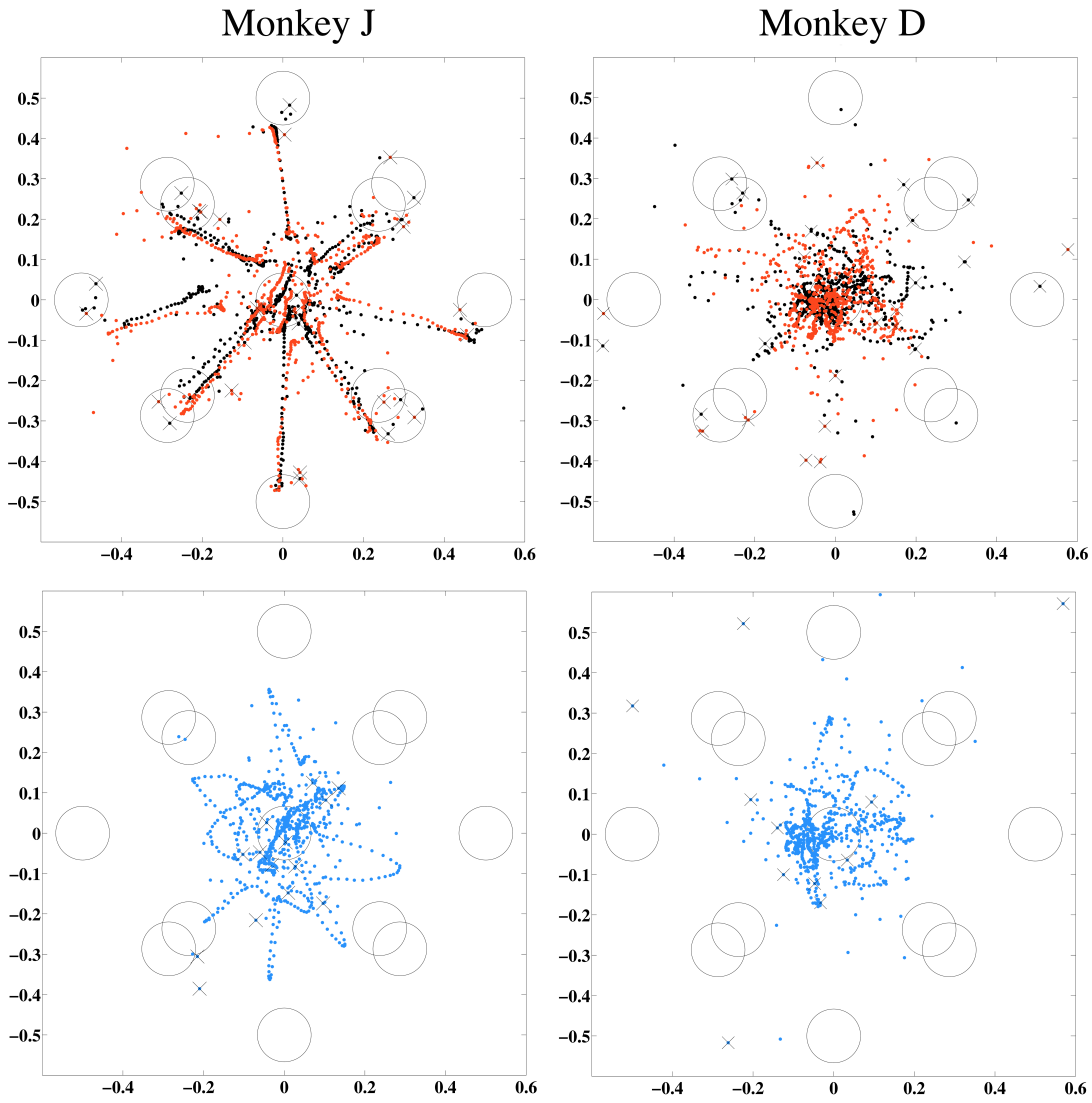

Figure 4.3: **Average Screen Coordinates of Eye Position** (n≈1200)
Screen Coordinates: Coordinates generated by the eye tracker. Center = (0,0). Right Top Corner of the screen = (1,1) *Black:* Standard Reach Task *Orange:* Anti-Reach Task *Blue:* Stationary Cursor Task *Black "X" Markers:* Eye position at the end of a successful trial, *Dark Blue Circles:* Initial screen position of the 14 targets.

4.3 NEURAL ACTIVITY RESULTS

4.3.1 Results from the Passive Replay of the Standard Reach Task

Activity from 193 task-related units was regressed against the direction of hand movement generated during the active reaching task (see section 2.5.1). Preferred directions were uniformly distributed (see figure 4.4).

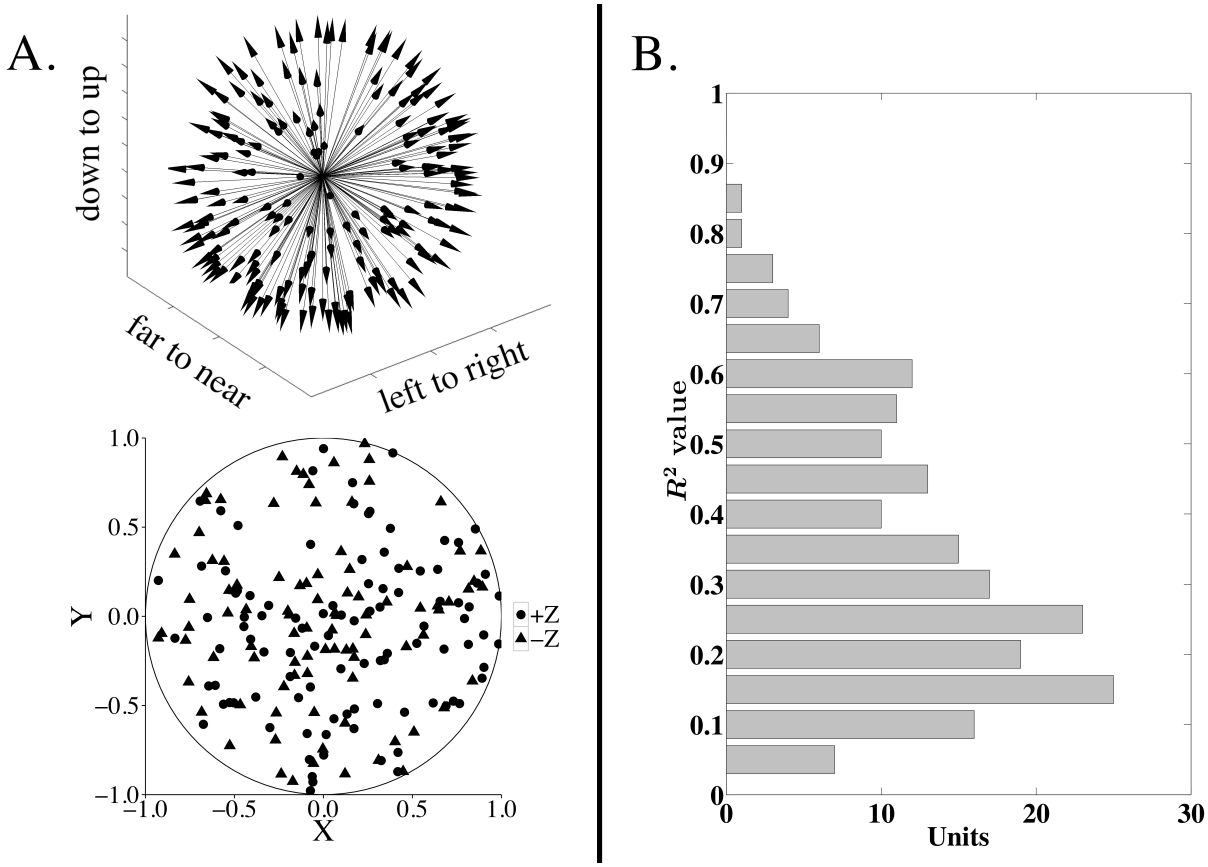

Figure 4.4: **Model Results, Standard Reach Replay A.** Shows distribution of 193 preferred directions. Top shows 3D arrows representing preferred directions in cartesian coordinates. Bottom shows the surface of the unit sphere; an equal-area plot using azimuthal projection (method: [60]). **B.** Resultant R^2 values for all 193 units.

4.3.2 Results from the Passive Replay of the Anti-Reach Task

Activity from 197 task-related units was regressed against the direction of hand movement generated during active reaching. Preferred directions were uniformly distributed (see figure 4.5).

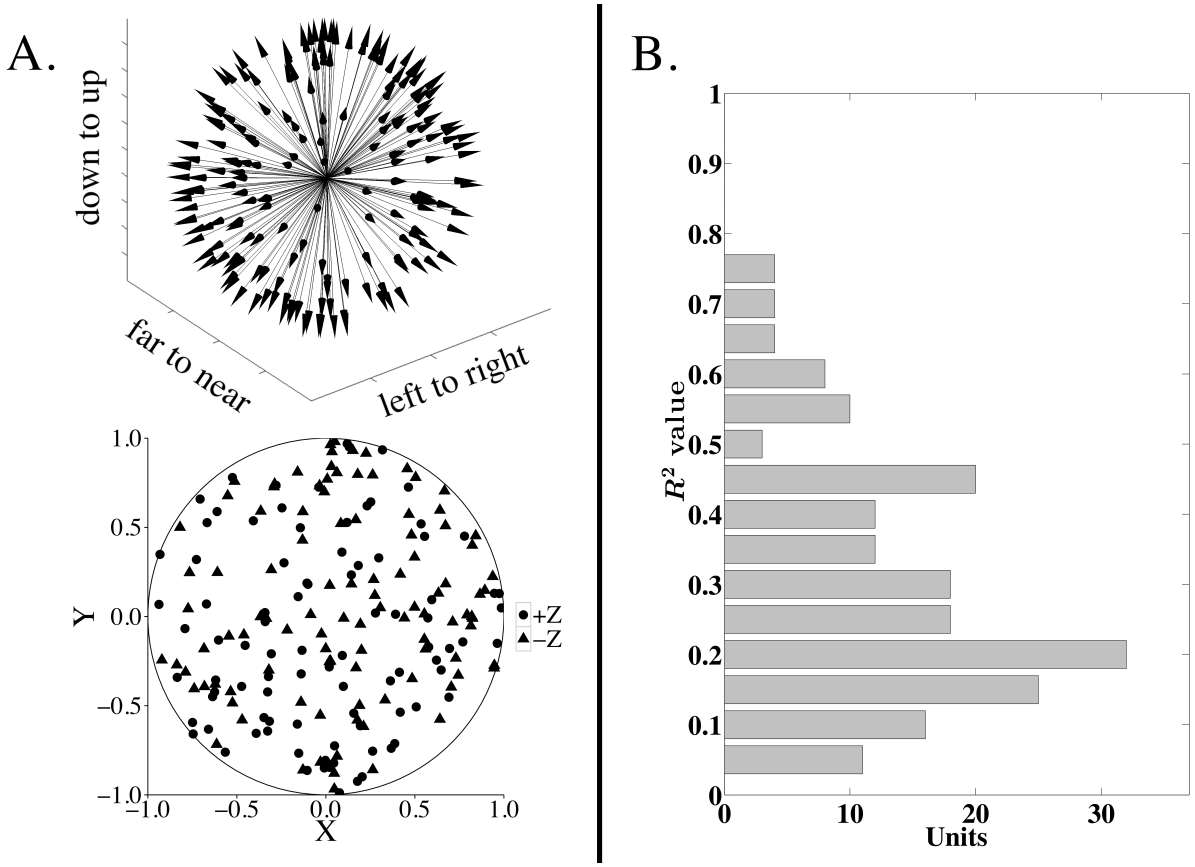

Figure 4.5: **Model Results, Anti-Reach Replay: A.** Shows distribution of 197 preferred directions. Top shows 3D arrows representing preferred directions in cartesian coordinates. Bottom shows the same data on the surface of the unit sphere; an equal-area plot using azimuthal projection. **B.** Resultant R^2 values for all 197 units.

4.3.3 Results from Passive Replays of the Stationary Cursor Task

Activity from 168 task-related units was regressed against the direction of hand movement generated during the active reaching task. Preferred directions were uniformly distributed (see figure 4.6).

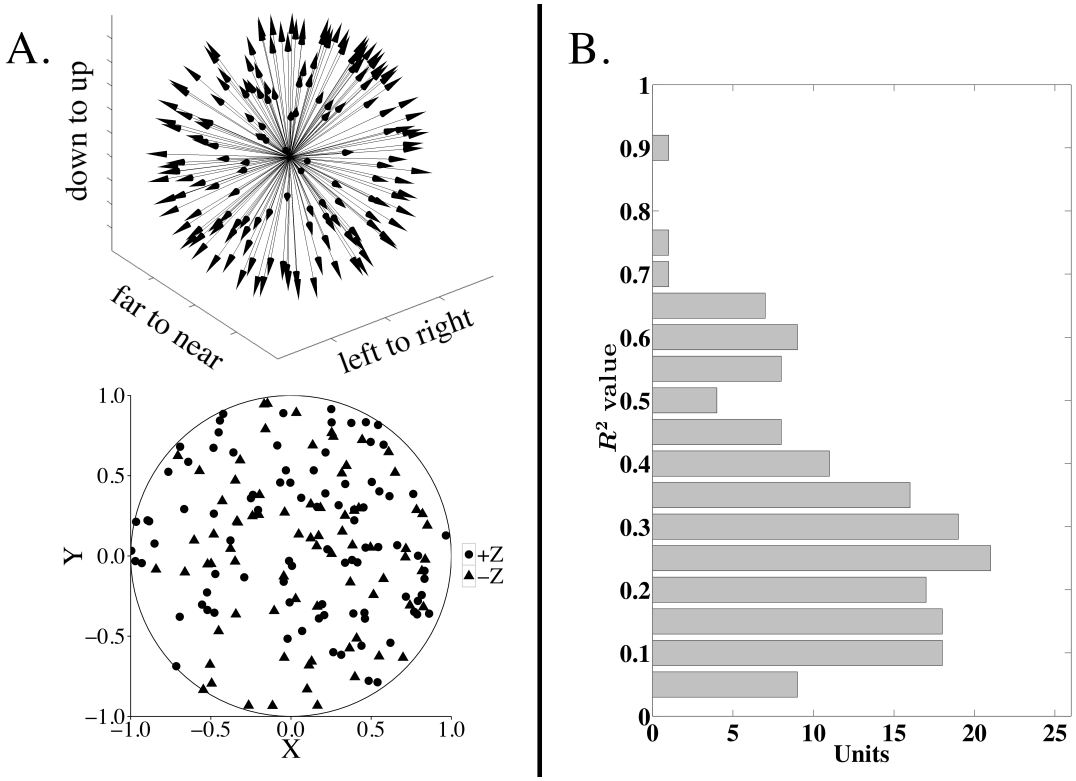

Figure 4.6: **Model Results, Stationary Cursor Replay: A.** Shows distribution of 168 preferred directions. Left shows 3D arrows indicating preferred directions in cartesian coordinates. Right shows the same data on the surface of the unit sphere; an equal-area plot using azimuthal projection. **B.** Resultant R^2 values for all 168 units.

4.3.4 Changes in Neural Response Across All Replayed Tasks

Activity from 121 units was task-related during all three task replays. We constructed raster plots to compare their responses and plotted three examples (Neurons 0, 1, and 2) in figure 4.7. Linear models reflected directional tuning changes apparent in the rasters (see figure 4.8). Changes in preferred directions suggests sensitivity to changes in the visual variables, since kinematics were stationary across all tasks. Three sets of unit response were most prevalent. One set of neurons had directional tuning that was insensitive to the changes in view (Neuron 0). Another set had the same tuning during replays of the standard and stationary cursor tasks but inverted preferred directions during the anti-reach task (Neuron 1). The last set had inverted preferred directions during replays of the anti-reach and stationary cursor tasks (Neuron 2).

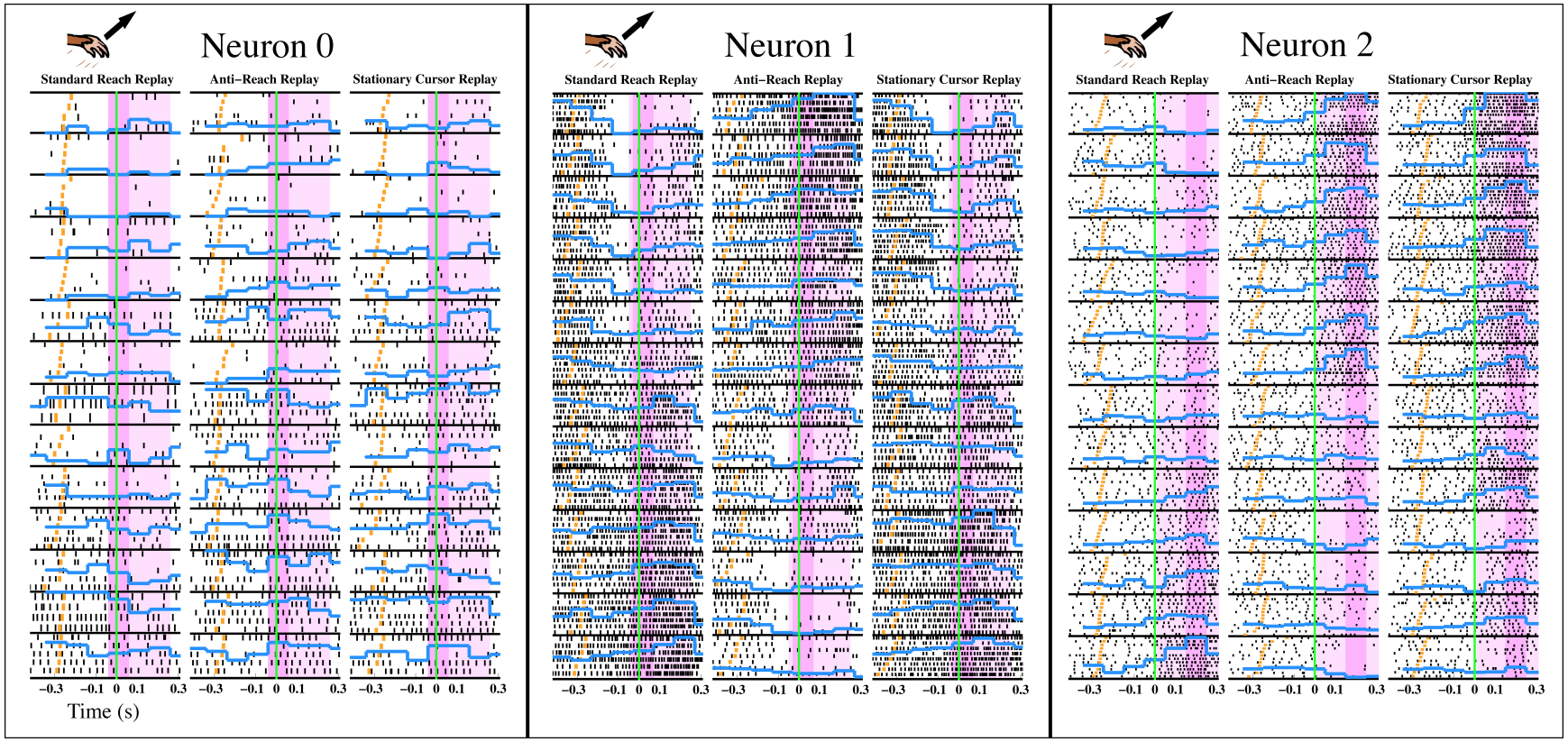

Figure 4.7: **Rasters, Three Examples Neurons, Three Replay Tasks:** Target rows are ordered according to tuning during the standard reach task replay for each cell (method explained in figure 2.12). Activity from Neuron 0 is unaffected by subsequent view changes. Activity from Neuron 1 appears to have an opposite directional response while observing the anti-reach task replay only. Activity from Neuron 2 shows an opposite directional response while observing the anti-reach and stationary cursor task replays.

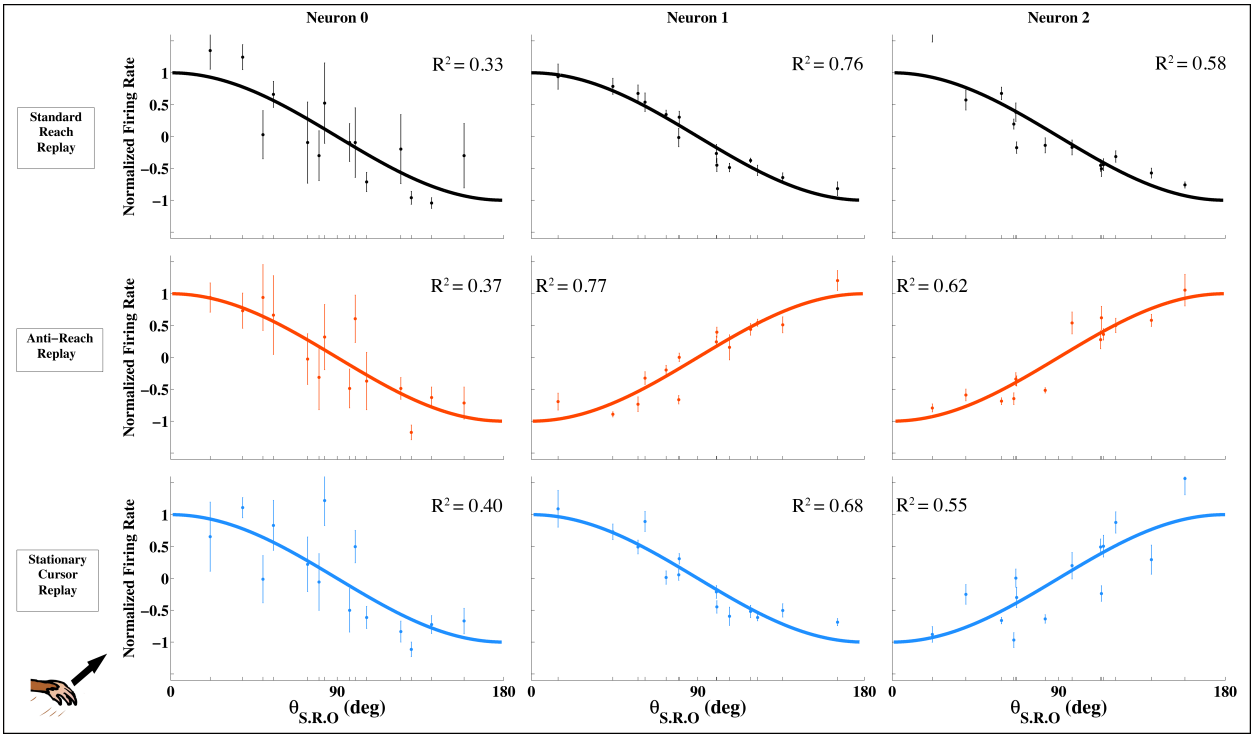

Figure 4.8: Tuning curves were previously explained in figure 2.12. Hand movement direction is stationary across tasks/rows for the same neuron/column. Models were constructed using the hand direction that was previously generated in the active version of the task. $\theta_{S.R.O}$ indicates the angular difference between hand direction and the preferred direction calculated from the standard reach task replay. 0° indicates the preferred direction from the standard task replay. Tuning curves fit responses from neurons 1, 2, and 3 in figure 4.7.

4.3.5 Evaluating Models with Unit Sphere Coverage

We wished to identify units that changed their directional tuning across tasks. Significant context-induced changes in firing rate patterns suggest sensitivity to the directional variable being manipulated (i.e. cursor velocity). To compare preferred directions across different contexts, we again used the tolerance interval (TI) comparison method explained in section 2.5.3 to determine if the variance in preferred direction between two contexts was overlapped. Overlapped TIs show that the preferred direction did not change. Non-overlapping TIs show that the unit's tuning is sensitive to the manipulation. A change in preferred direction would not be detected if the combined area of two elliptical tolerance intervals covered more surface area than the unit sphere. We used surface area as a measure of spread to determine when models were not precise enough for our purposes.

Lower R^2 values corresponded to greater prediction variance, and hence greater surface area. The least squares curve-fit between surface area and R^2 showed that a value of $R^2 \leq 0.13$ generally corresponded to less than 50% coverage in all three replay tasks (see figure 4.9).

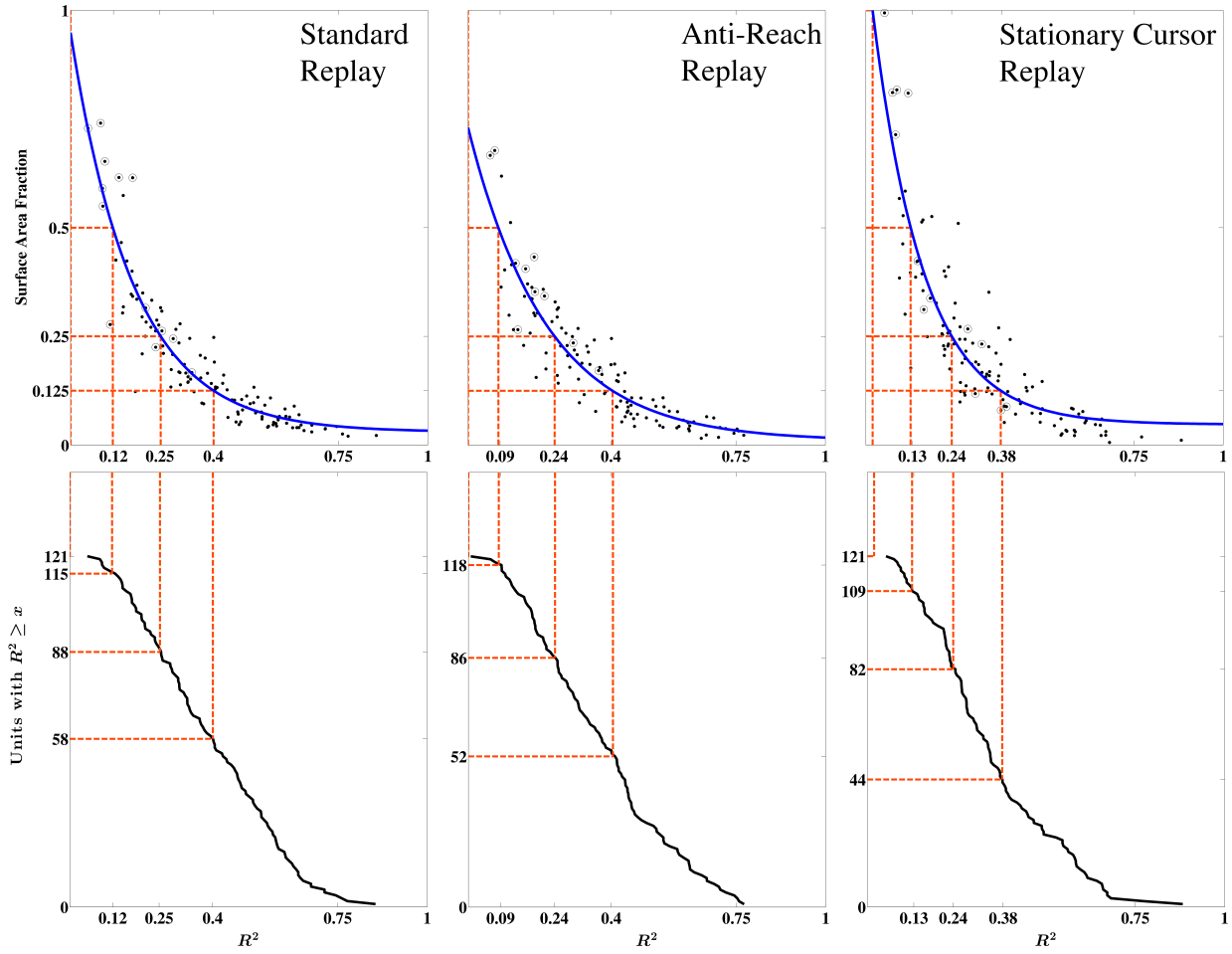

Figure 4.9: **Model Precision across Tasks** Top figure in each column shows the fractional coverage of the unit sphere, from all distributions of preferred direction vs. the corresponding R^2 value. Each point represents a model of one unit. Fractional area percentages of 1, 0.5, 0.25, and 0.125 were estimated (orange dotted lines) to compare with R^2 values. Solid blue line indicates the least squares curve fit of R^2 to Surface Area Fraction. Bottom plot shows a cumulative plot of resultant R^2 values for each model fit. Orange dotted lines from the top plot indicate the location of fractional area percentages from the top figure. For example, in the standard reach task replay, 88 models had coverage of 25% or less, and corresponded to an R^2 value of 0.25 or greater. In the anti-reach task, 86 models had coverage of 25% or less, and corresponded to an R^2 value of 0.24 or greater. Units that showed activity with a summed tolerance interval area greater than a unit sphere for any combination of two tasks (marked with circles) were omitted from further analysis.

Three types of neuron were labeled based on preferred direction compared with those from the standard reach task replay. 13 task-related units were removed from analysis due to large variance in preferred direction. Cells with task sensitivity similar to Neuron 0 were labeled Type 0, as there were no changes in preferred direction across tasks. Cells with task sensitivity similar to Neuron 1 were labeled Type 1, having one change in preferred direction during the anti-reach task replay only. Cells with task sensitivity similar to Neuron 2 were labeled Type 2, having preferred direction changes in both the anti-reach and stationary-cursor task replays (see summary in figure 4.10).

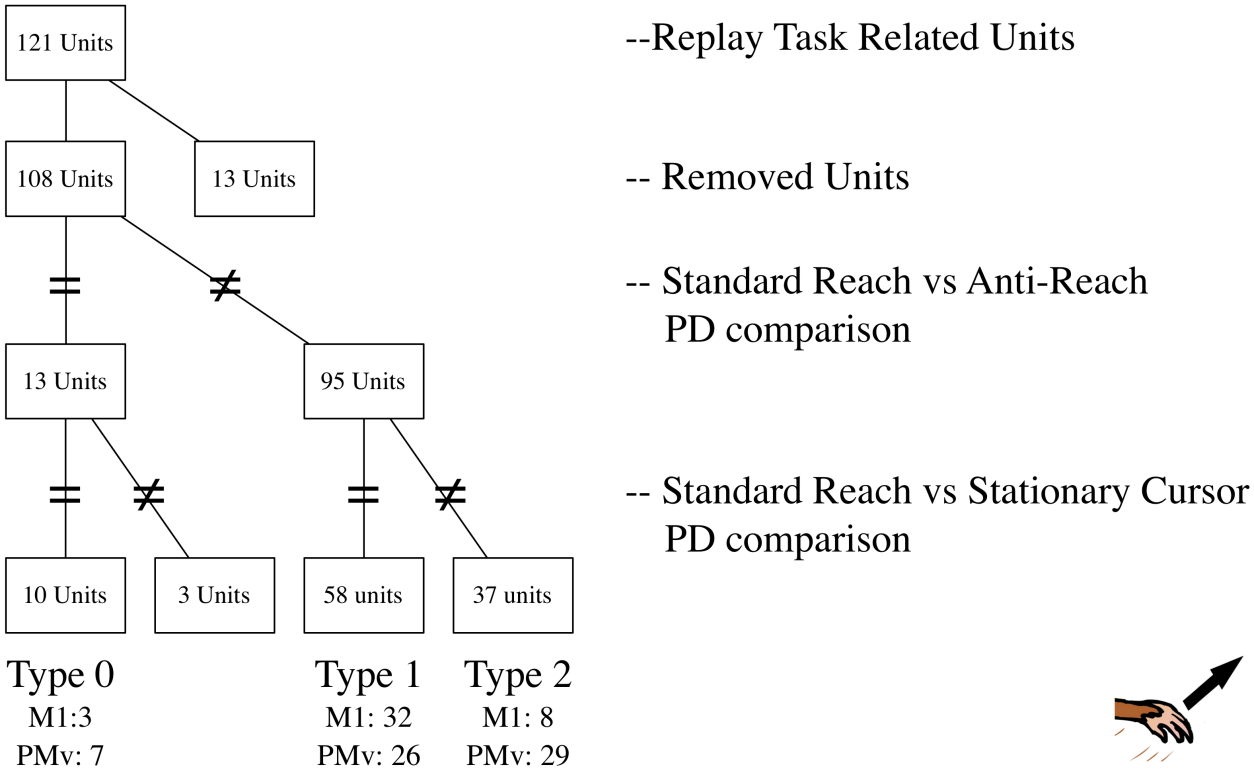

Figure 4.10: **Labels for Response Types based on PD TI comparisons across tasks**

4.4 COORDINATE SYSTEM CLASSIFICATION

4.4.1 Firing Rate Models from Multi-Task Data

Data from each set of replays of one task were combined to build a multi-task multi-task sample from each neuron to evaluate a global model fit for each coordinate system. These models were constructed in a similar manner to those from individual tasks (see section 2.5.1). Since modulation depth varied across tasks, we normalized firing rate for each task data set before regression. Figure 4.11 compares R^2 values from multi-task models of the 187 valid units in hand-centered (top) vs. the best fit coordinate system (bottom). These best fit coordinate frames included hand-centered, cursor-centered, and displayed motion. R^2 values were greatly improved when activity was fit with the selected coordinate system relative to using only the hand-centered coordinate system.

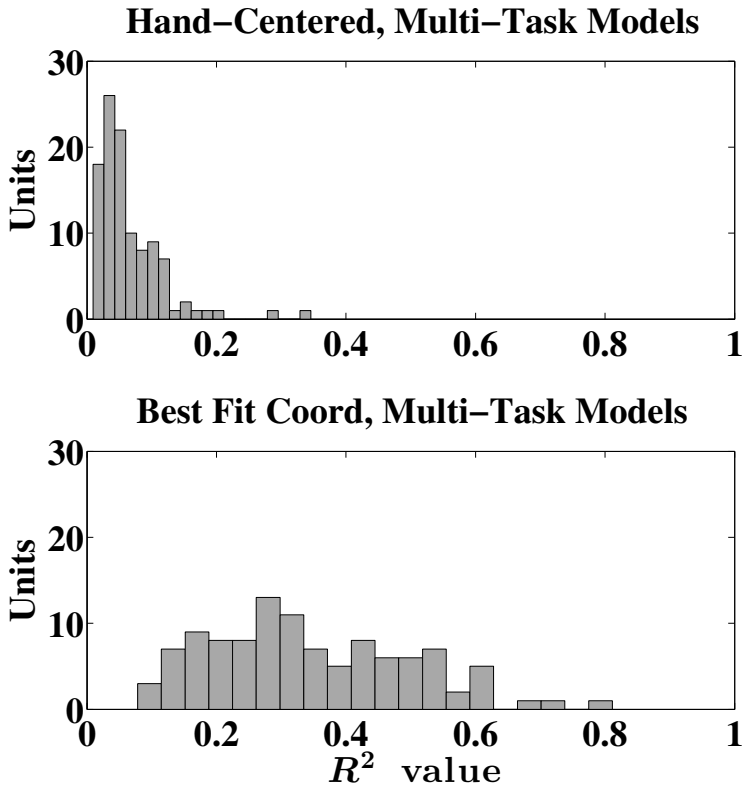

Figure 4.11: **Multi-Task Model R^2 comparison:** *Top:* A histogram of R^2 values from 187 units fit with hand-centered models only. *Bottom:* A histogram of R^2 values from the same 187 units fit with models from the best-fit coordinate system.

Table 6: **Anatomical Location of Neuronal Activity in Three Coordinate Systems**

Cortical Area	**All**	**M1**			**PMv**		
Monkey	D+J	D+J	D	J	D+J	D	J
Total Units Recorded	400	117	54	63	283	145	138
Task-Related (all 3 replay tasks)	121	27	25	2	94	58	36
Units with Classified Activity	78	17	16	1	61	40	21
➥ Hand-Centered	2	2	1	1	0	0	0
➥ Cursor-Centered	42	15	15	0	27	25	2
➥ Displayed Motion	34	0	0	0	34	15	19

4.4.2 Anatomical Location

Units were classified using the same tolerance interval overlap method (described fully in section 3.4.8), which looks for combinations of overlapping variance to determine when preferred directions are the same. A pattern of preferred direction similarity across tasks were required for classification and 92 units satisfied this constraint. View-sensitive activity (classified as cursor-centered or displayed motion) was found to be generally located in the PMv. Hand-centered activity was found mostly in M1 (4 in M1, 1 in PMv). All three coordinate systems were found in both monkeys, with monkey D having a larger cursor-centered sample and monkey J having a larger displayed motion sample (see table 6). We evaluated the anterior-posterior location of each classified unit, relative to the arcuate sulcus (see figure 4.12). Units with activity corresponding to displayed motion were closer to the arcuate sulcus than units with cursor-centered modulation (significantly different, $p<0.00001$, Mann-Whitney), which in turn appeared closer than units with hand-centered modulation.

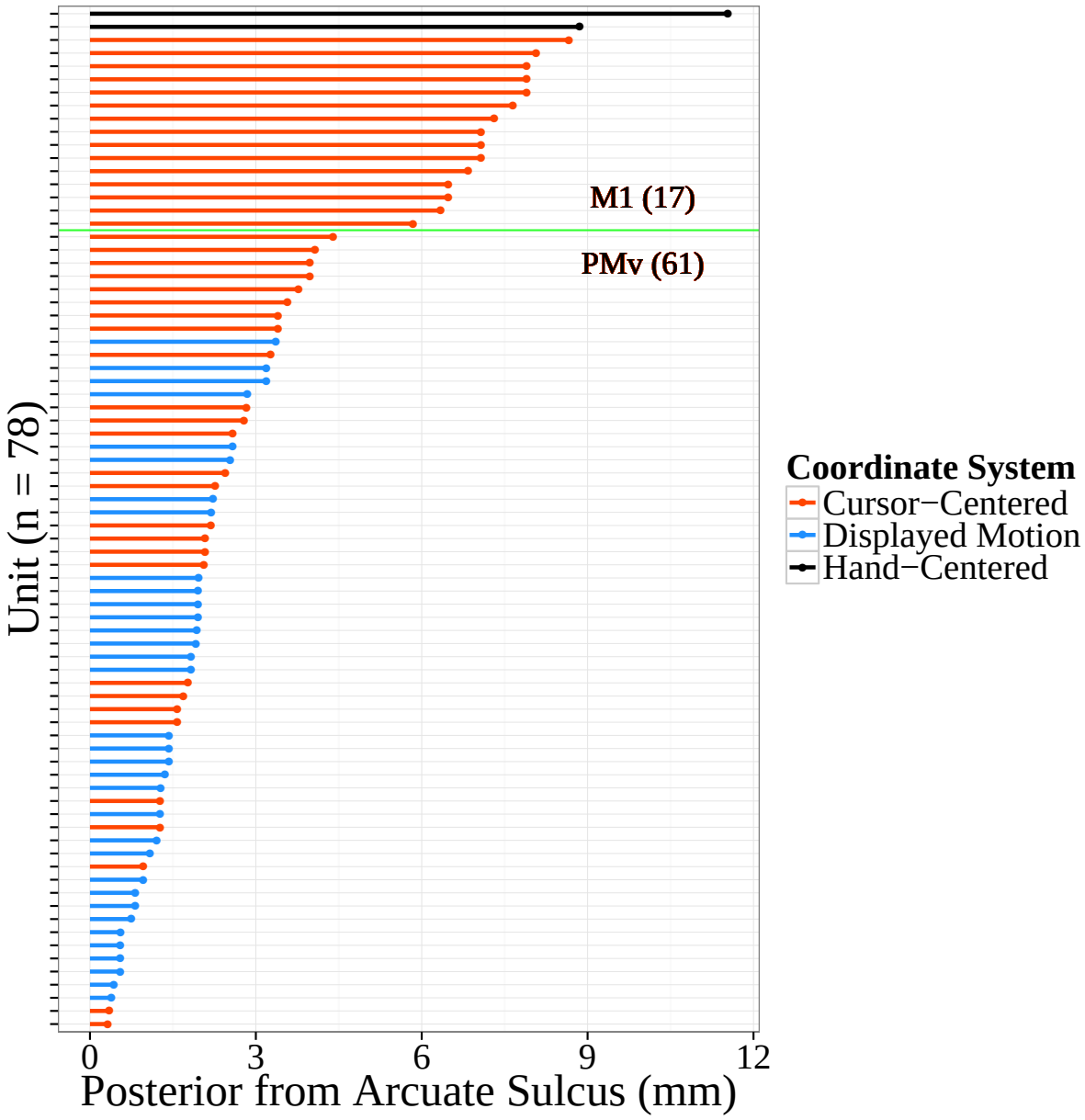

Figure 4.12: **Posterior Distance from Arcuate Sulcus:** Units with activity corresponding to displayed motion were closer to the arcuate sulcus than units with cursor-centered modulation (significantly different, $p<0.00001$, Mann-Whitney), which in turn appeared closer than units with hand-centered modulation.

4.4.3 Replay Latency

Latencies were evaluated from multi-task models constructed using the method described in section 2.5.1.1 for all classified units. Since the reach replays began with a cue presentation immediately after returning to the center of the workspace, the subjects' hands were still slightly decelerating in the returning arm movement. The first 100ms sliding window for latency calculation was increased from -200ms to -100ms (from the active reaching chapter) relative to movement onset to avoid including residual modulation from the return movement. The average reaction time from target presentation to movement onset was about 300mS. The minimum latency between stimulus and activity change was 125-150ms [12, 14]. This left 75ms of potential recorded activity omitted from analysis. Future versions of this experiment could increase the Hold A period by 100ms before target presentation to avoid this. Results showed that replay-related activity was tuned after movement onset with no clear order for the various coordinate systems (see figure 4.14).

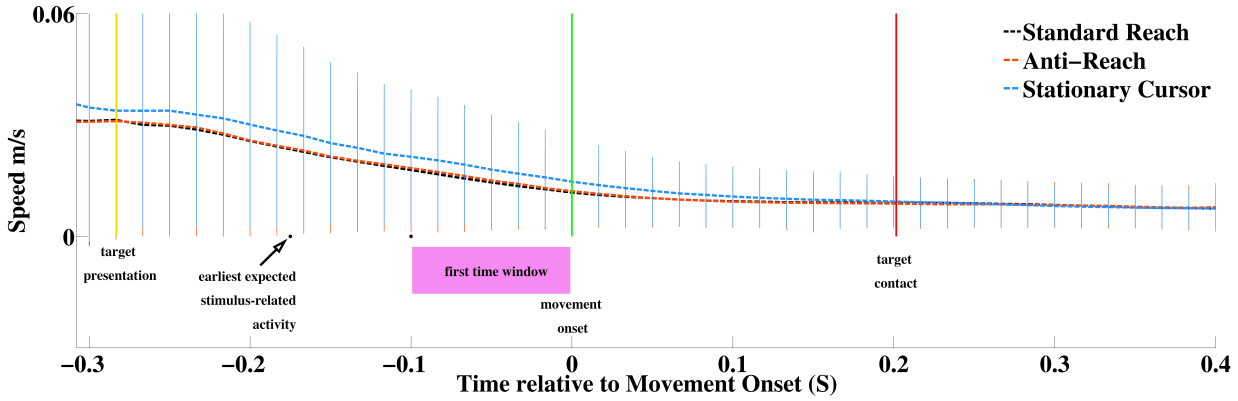

Figure 4.13: **Timeline for Replay Response Latency Calculation:** Each curve is the average speed to all targets (n≥15400) from the target presentation/go cue to ≈ 200mS after target capture for either the Standard, Anti-Reach, and the Stationary Cursor replay tasks. Time stamps related to analysis are marked. *Gold Vertical:* Average Target/Go Cue Time, *Green Vertical:* Movement Onset Time, *Red Vertical:* Average Target Contact Time

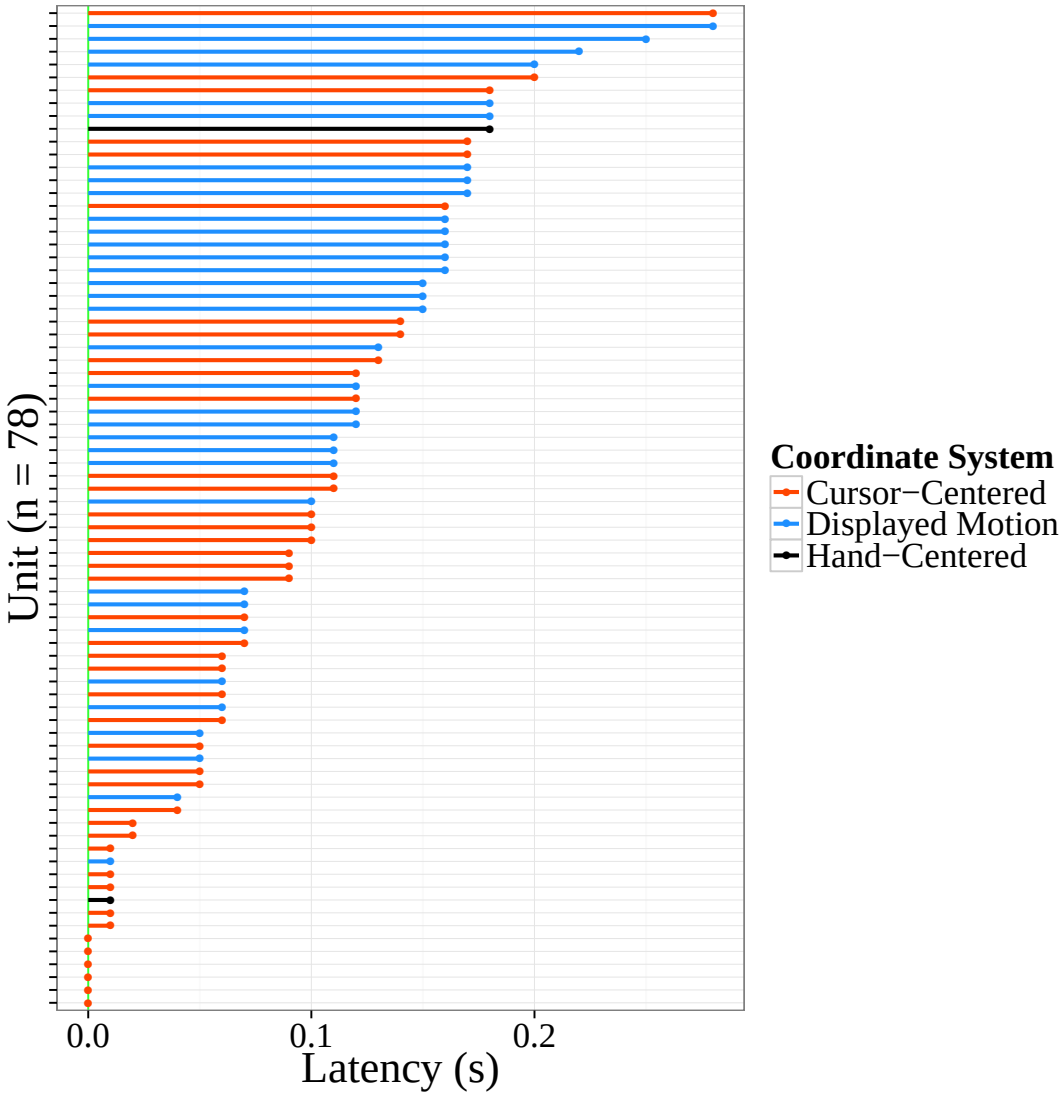

Figure 4.14: **Response Latencies in Classified Coordinate Systems**

4.4.4 Preferred Direction Separation in Classified Units

It is possible that the variance of the preferred directions was so large that their TI's overlapped in every coordinate system. The pattern we used for classification (3/1/1 - see section 3.4.8) required separation in two of three coordinate systems, making this case unlikely. Even so, another possibility is that the tolerance intervals were large, far apart, and only barely shifted when calculated

in different coordinate systems, and thus were classified based on fluctuations in variance instead of shifts in preferred direction. Ideally, preferred directions with overlapping tolerance intervals should have a low angular difference. To evaluate how close the preferred directions were across tasks, we compared the means of the distributions. The average angular difference was calculated across tasks for each classified neuron in the classified coordinate system. A perfect alignment value was an angular difference of 0°. The largest separation possible was 120°. Results showed a minimum value of 18.0°, a median value of 44.5°, and a maximum value of 66.1° (see figure 4.15).

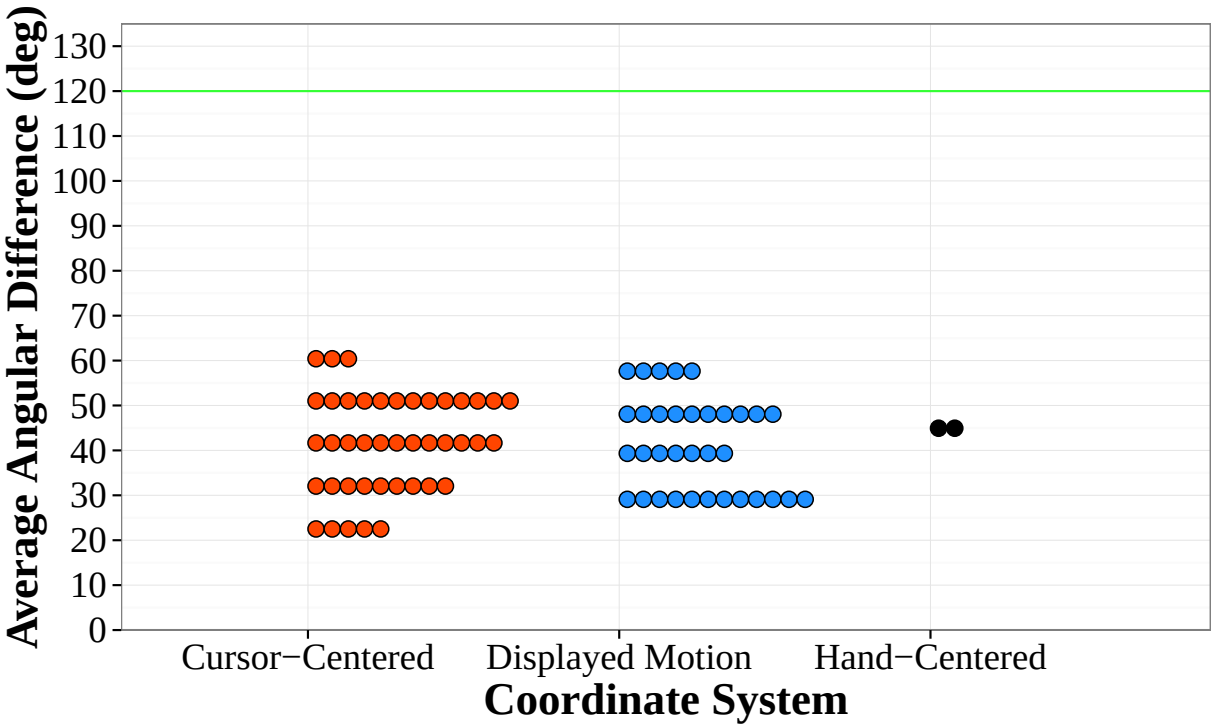

Figure 4.15: **Model Validation: Average Angular Difference** Each point represents one classified unit, colored by classified coordinate system. Points were arranged into rows binned in 9° increments. The green horizontal line represents the largest possible separation (120°).

4.4.5 Multi-Task R^2 values of Classified Activity

For a unit to be classified successfully, it had to be directionally tuned and have an invariant preferred direction across our battery of tasks. To determine how well classified activity was fit by multi-task models in their labeled coordinate frame vs. the other coordinate frames, we compared R^2 values

in each coordinate frame for each unit. Figure 4.16 illustrates that the model fit was best in the classified coordinate system. This also shows that when the classification method successfully labels activity, it is also identifying the most likely coordinate system.

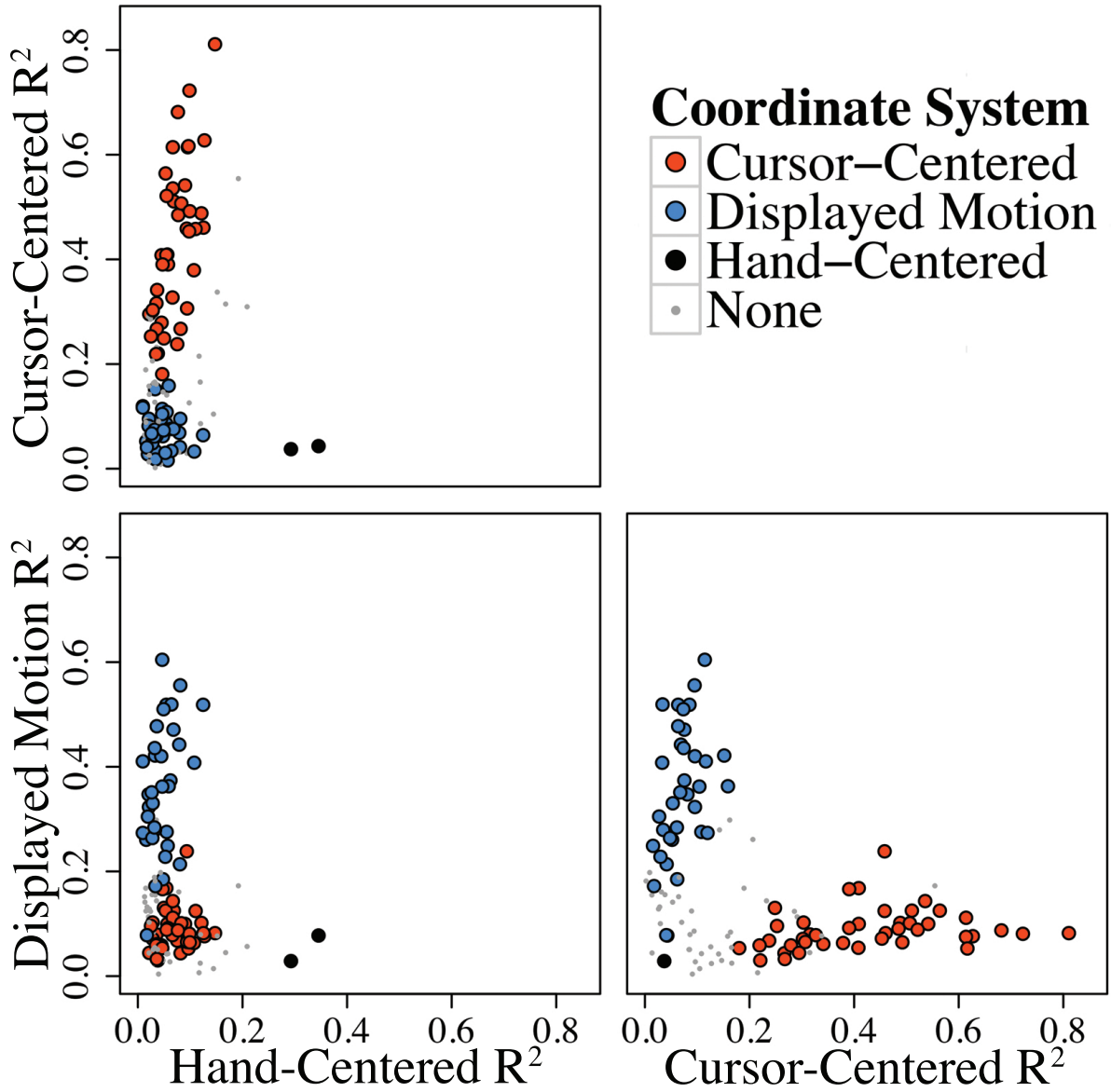

Figure 4.16: **Multi-Task Models from the Replay Tasks:** Classified activity was modeled better in its labeled coordinate system than the other two. Three scatterplots show R^2 values for each unit in each coordinate system. Each plot shows all units' R^2 values in two coordinate systems. See legend for colors designating classified activity.

4.5 ACTIVE REACHING AND REPLAY RESULTS COMPARED

A total of 203 units were classified with a coordinate frame in at least one of the two experiments. Table 9 shows the anatomical distribution of units that were classified in the Active Reach Experiment Only, the Replay Experiment Only, or Both (*A&R*). The majority of M1 units (67.2%) were classified during Active Reaching Only, with 6.0% classified during Replay Only and 26.9% classified during Both. PMv units had a flatter distribution with 48.5% Active Only, 22.0% Replay Only, and 29.4% Both. Monkey J had considerably less classified replay-related activity than Monkey D in M1. Results were similar across subjects for area PMv.

Table 7: **Anatomical Location of Classified Units in Active and Replay Experiments**

Cortical Area	**All**	**M1**			**PMv**		
Monkey	D+J	D+J	D	J	D+J	D	J
Total Units Recorded	400	117	54	63	283	145	138
Units with Classified Activity	192	68	45	23	124	83	41
➥ Active Only	114	51	29	22	63	43	20
➥ Replay Only	28	3	3	0	25	17	8
➥ Both (A&R)	50	14	13	1	36	23	13

Coordinate systems were loosely ranked by visual sensitivity. Hand-centered activity corresponded to the movement of the hand, regardless of what was moving on the display, and was deemed the *least visually sensitive*. Cursor-centered activity is derived from visual cues, but does not seem to require visual motion for a response and was deemed *moderately visually sensitive*. Activity corresponding to displayed motion seemed to respond to visual motion without requiring context, so we referred to this coordinate system as the *most visually sensitive*. Activity classified during the replay experiments generally corresponded to a more visually sensitive coordinate system. Subpopulations grouped by experiment type show a higher percentage of visually sensitive units during the task replays. Figure 4.17 illustrates this construct in M1 and PMv from active to replay: Active Only, A/R (active classification), A/R (replay classification), and Replay Only.

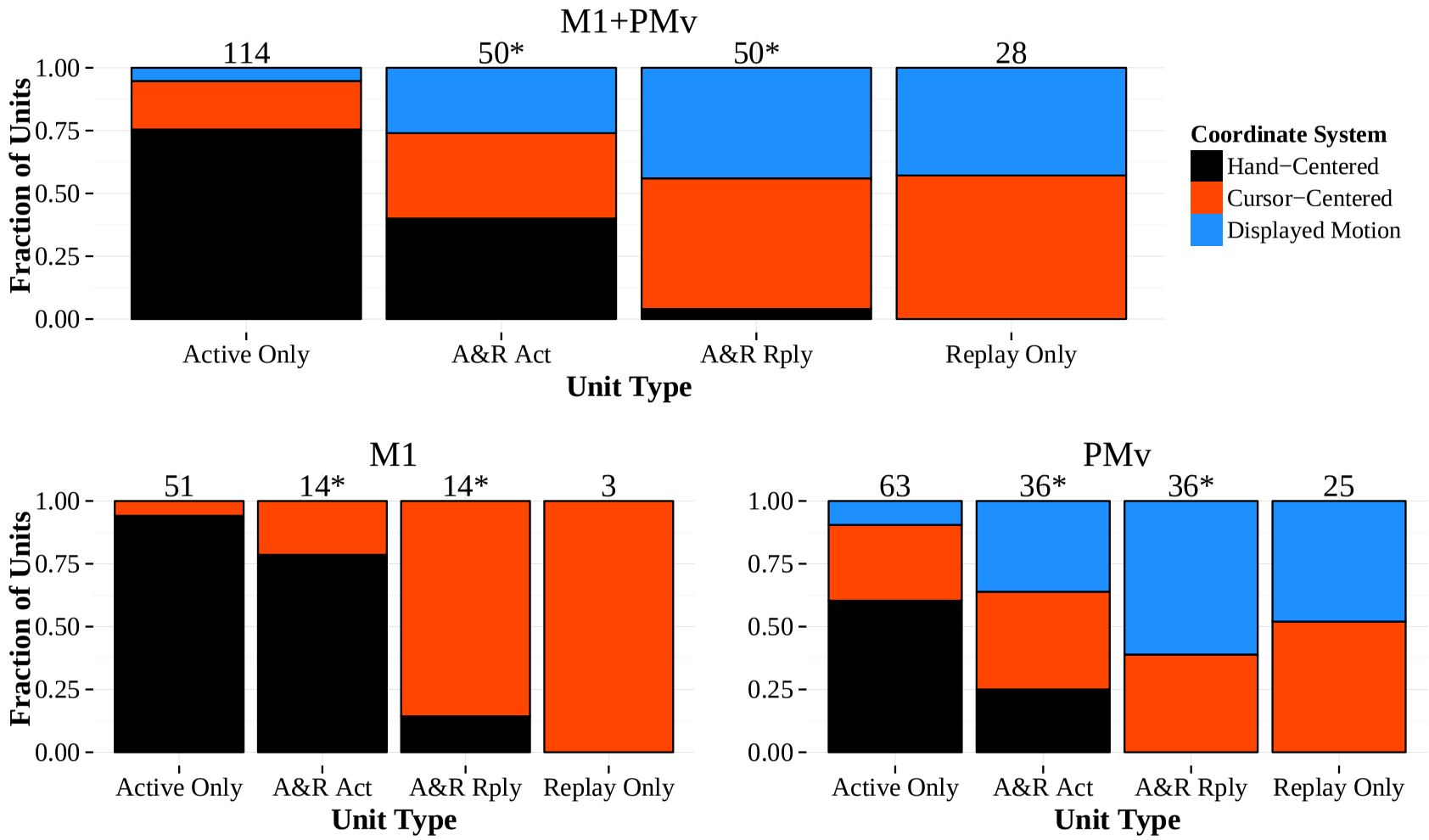

Figure 4.17: **Coordinate Systems during the Active and Replay Experiments:** Each block of 4 charts shows the distribution of coordinate systems in classified *unit types*. Unit type was determined by which experiment activity was successfully classified. Units only classified during the active reaching experiment were labeled *Active Only*. Units successfully classified during both active and replay experiments were labeled *A&R* with corresponding coordinates labeled *Act* and *Rply*, respectively. The number of units in each type is labeled at the top of each chart. Asterisks designate that the same units were used for pairs of A&R charts.

4.5.1 Units with Activity Corresponding to Coordinate Frames during Both Experiments

Units that were successfully classified in the Active Reaching and Replay experiments (A&R units) consistently corresponded to the same or a more visually sensitive coordinate system during the replay experiment (see table 8). Anatomical locations are shown in figure 4.18. The three largest sub-populations of A&R units included those with activity that corresponded to: a) active hand-centered and replay cursor-centered coordinates (25.9%), b) cursor-centered coordinates in both experiments (24.1%), and c) displayed motion coordinates in both experiments (25.9%).

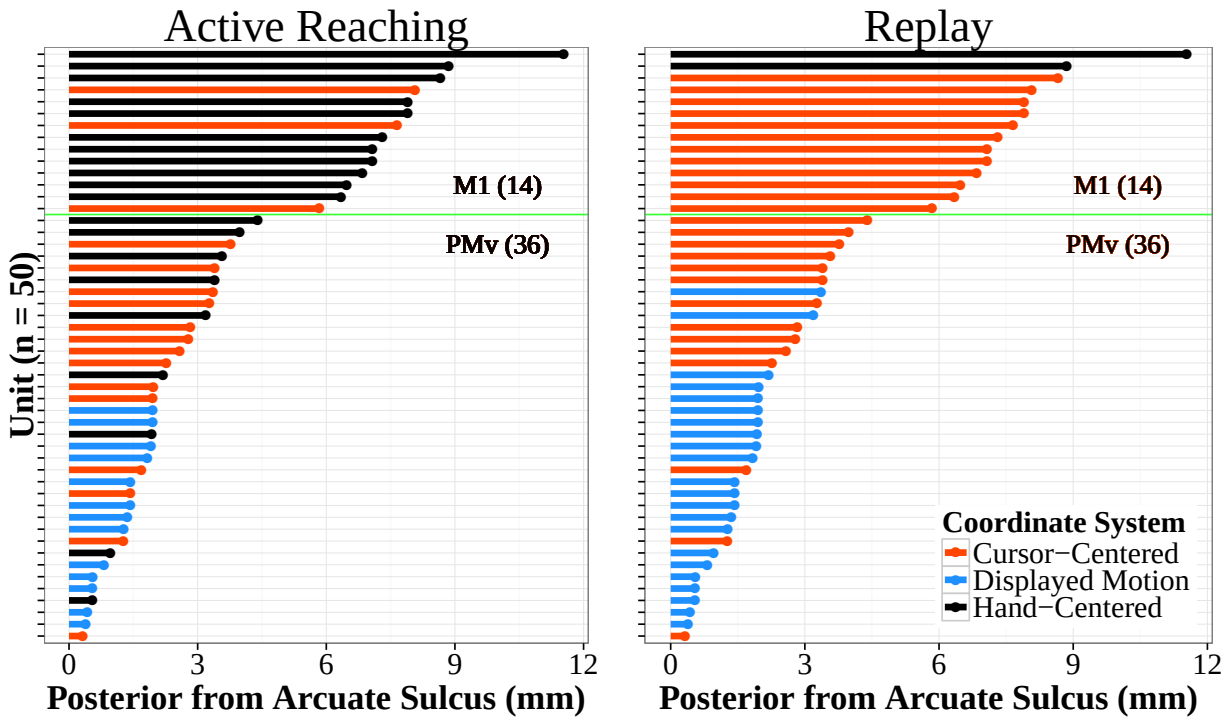

Figure 4.18: **Active vs. Replay Classification: Anatomical Location:** Each line-dot pair represents one unit's distance from the arcuate sulcus. Coordinate systems are labeled by color. The left plot shows the classified coordinate system during active reaching. The right plot shows the same units, with coordinate systems determined from the Replay Tasks.

Preferred directions from the multi-task models (see sections 3.4.7 and 4.4.1) were compared for each A&R unit. Figure 4.19 shows the angular difference between the active and replay preferred directions and are labeled by the grouping (active coords-replay coords) identified in table 8. Median angular difference for subpopulations *Cursor-Cursor* and *D.Motion-D.Motion* were small (~10°) with low variability. These were the most likely subpopulations to have unchanging coordinate

frames and preferred direction. The group with the largest angular difference was the *Hand-Hand* group, having a median of 139.2° and being the most likely group to have changing preferred directions. This suggests that these cells may be corresponding to hand-centered features with different directions across experiments.

Table 8: **A&R Classification: Unit Count**
(50 units were classified during both experiments.)

		Replay Coordinates		
		Hand-Centered	Cursor-Centered	D. Motion
Active Coords	Hand-Centered	2	13	5
	Cursor-Centered	0	13	4
	D. Motion	0	0	13

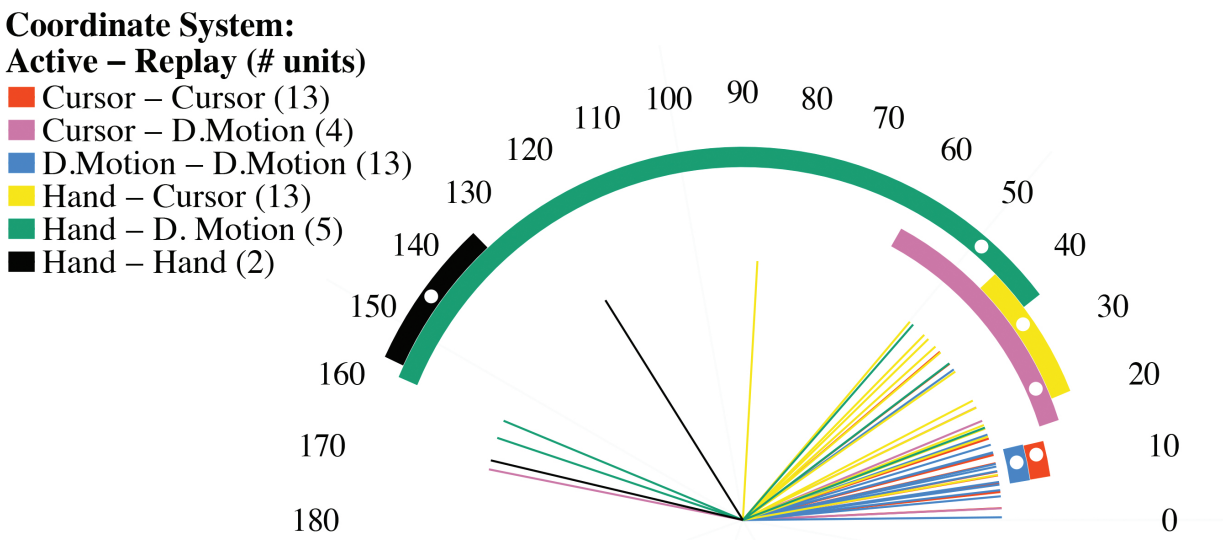

Figure 4.19: **Active vs. Replay Classification: Preferred Direction Angular Difference** Each radial line represents the angular difference of preferred direction between the active and replay experiments from one unit. Each arc shows the IQR of angular difference for subpopulations of units that were classified similarly across experiments. Filled white circles indicate the median angular difference for each subpopulation. The legend indicates the classified coordinate system of each subpopulation.

5.0 RESULTS FROM THE OBJECT MOTION TASK

5.1 INTRODUCTION

Single-unit recordings were evaluated in this chapter to determine whether evidence of evoked sensory responses were present in PMv and M1 while observing the object motion task. In section 5.2, trajectories of the arm and eyes in the experimental task were evaluated. Section 5.3 examines how neuronal discharge varied with the moving stimulus. Models that explain this variance are presented. Finally, in section 5.4, results from the previous experiments are compared to those from the passive stimulus experiment.

5.1.1 Task Summary:

We designed an experiment to determine whether activity corresponds to object motion or cursor-centered object direction in the displayed workspace used during the active reaching and replay tasks. It required the monkey to hold a central cursor position while a blue sphere translated at a constant speed from the center to the 14 reach target locations and back to center. This allowed for opposite motion directions to be sampled for each target direction. Firing rate models were evaluated as a function of either the direction of motion or direction of the object relative to the cursor for each task-related unit.

5.2 BEHAVIORAL RESULTS

Hand kinematic data showed the animal held a stationary cursor position in the middle of the workspace while the object moved out and back to each target location (see figure 5.1). Mean eye data tracked the target object as it moved, in both monkeys (see figure 5.2).

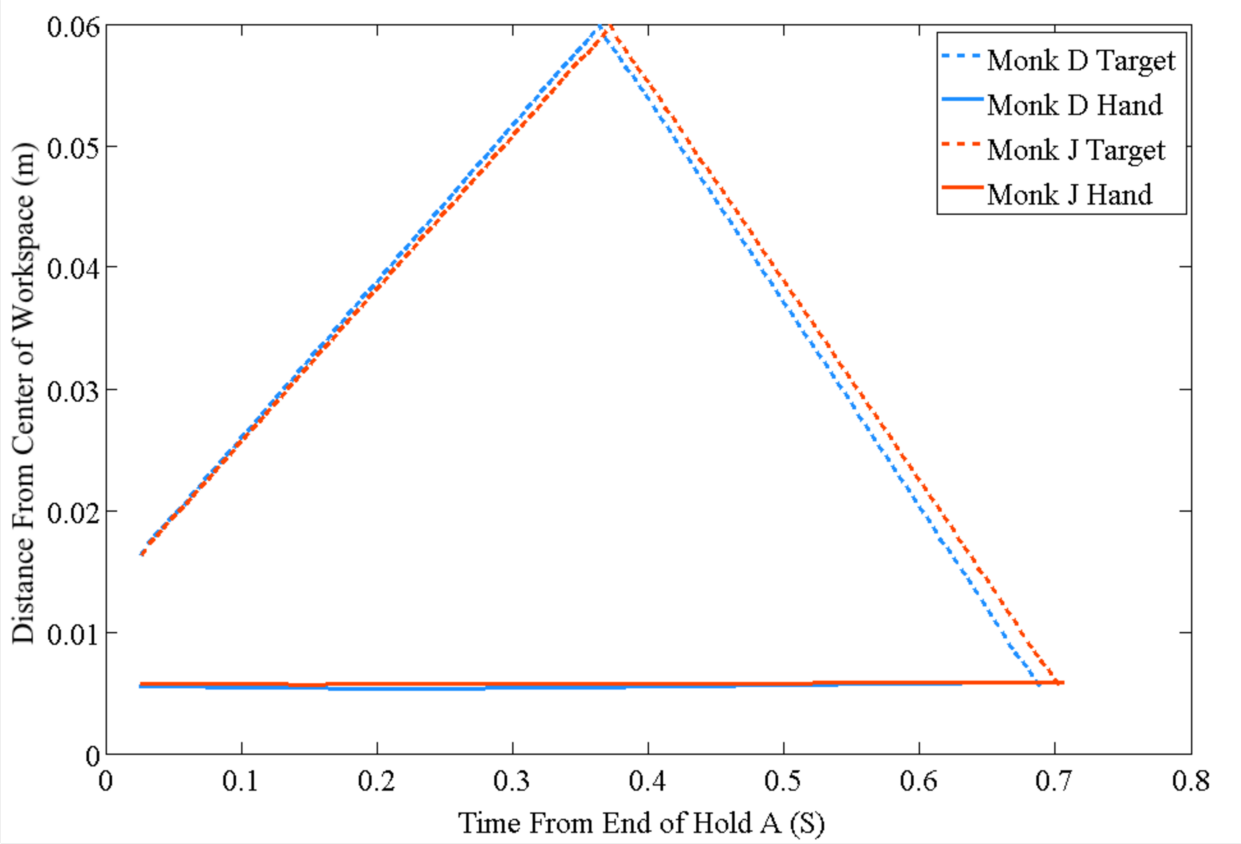

Figure 5.1: **Kinematic Profiles during Object Motion Task:** Y-axis is the average distance from the center of the workspace, across all directions, throughout the passive stimulus task.

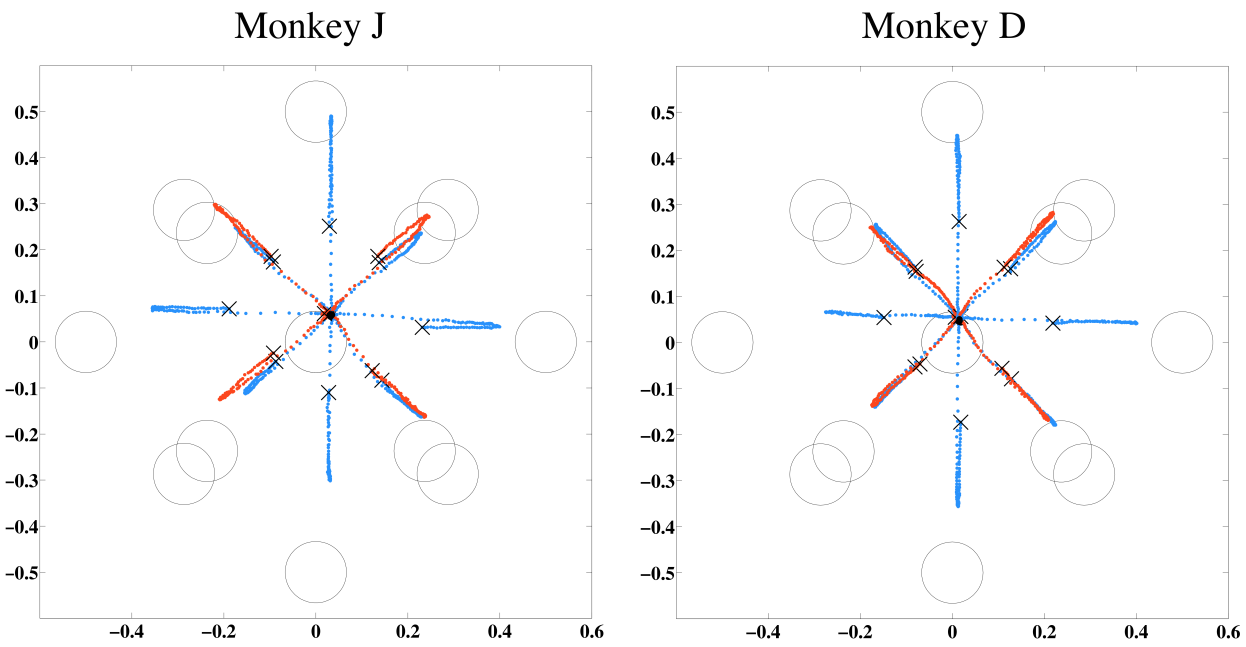

Figure 5.2: **Average Screen Coordinates of Eye Position during the Passive Stimulus Task** (n≈1200) *Screen Coordinates:* Coordinates generated by the eye tracker. Center = (0,0). Right Top Corner of the screen = (1,1) *Orange-Red:* Close Targets, *Blue:* Far Targets, *Black filled circles:* Eye position during the time of the Target/Go cue, *Black "X" Markers:* Eye position at the end of a successful trial, *Circles:* Target, mid-position, 14 targets.

5.3 NEURAL RESULTS

Models were constructed to predict firing rate as a function of cursor-centered direction or displayed motion direction. Task-related units were classified in one of these two models. R^2 values for each unit were not similar in magnitude across coordinate systems, so one classification was always a much better fit than the other. During the *center-out* phase of each trial, the cursor-centered direction of the object is in the same direction as the displayed motion. During the *out-center* phase of each trial, they are opposite. We used these phases as separate regressors. Section 2.5.5 further explains the mechanics of this analysis. Activity from 69/92 task-related units was found to be adequately tuned ($R^2 > 0.1$), with 67 units located in PMv and 2 in M1. Firing rate models corresponded more often to cursor-centered direction than displayed motion direction (see figure 5.3). The responses from 29 units corresponded to the displayed motion direction of the stimulus, with a mean R^2 value of 0.30 and maximum value of 0.66. Due to their directional motion correspondence, these units

often had high firing rate in one phase of the trial and an opposite response in the other. Firing rate models classified in cursor-centered direction with a mean R^2 value of 0.24 and a maximum value of 0.51. These responses generally had a baseline firing rate near the center hold position, and were modulated as the target translated out to each section of the displayed workspace. Two example units' responses are shown in figure 5.3. Responses to passive manipulation before the experiment did not consistently translate to directional modulation while observing the task. All classified units located in M1 were tuned for cursor-centered direction. Units located in PMv were tuned in both coordinate systems. A summary of anatomical results is shown in table 9.

Table 9: **Anatomical Location of Classified Units during the Object Motion Task**

Cortical Area	**All**	**M1**			**PMv**		
Monkey	D+J	D+J	D	J	D+J	D	J
Total Units Recorded	400	117	54	63	283	145	138
Task-Related	92	2	2	0	90	55	35
Tuned during Object Motion	69	2	2	0	67	42	25
➥ Cursor-Centered	40	2	2	0	38	24	14
➥ Displayed Motion	29	0	0	0	29	18	11

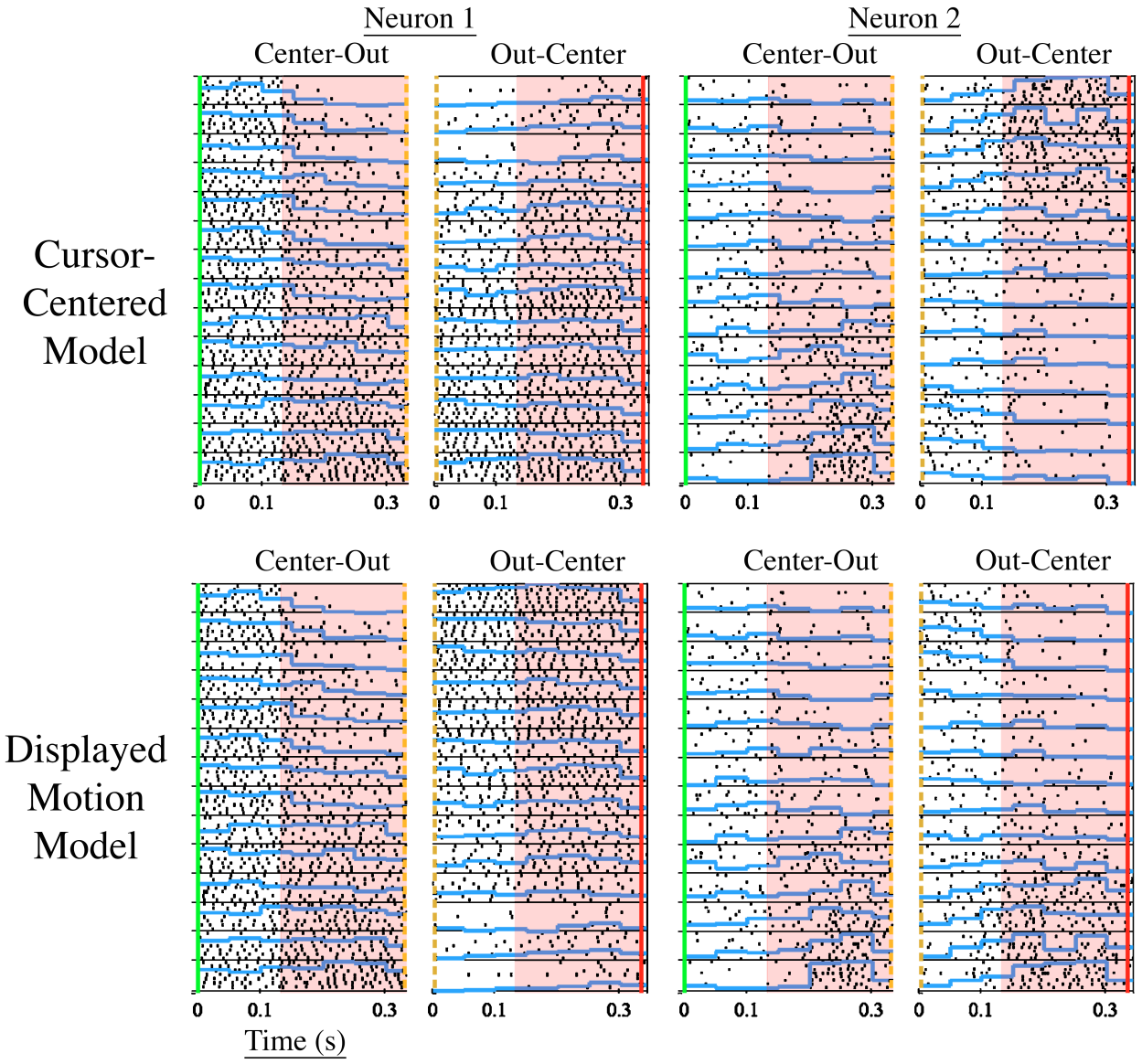

Figure 5.3: **Two classes of Object Motion Modulation:** During the *center-out* phase of each trial, the cursor-centered direction of the object is in the same direction as the displayed motion. During the *out-center* phase of each trial, they are opposite. The rows in each quadrant were ordered from bottom to top by the angular difference from the preferred direction during the *Center-Out* phase of the trial. The Out-Center rows were arranged according to angular difference in cursor-centered direction (top two quadrants) or in displayed motion (bottom two quadrants). R^2 values: 0.66, left unit, in cursor-centered coordinates, 0.47, right unit, in displayed motion coordinates. Both cells were located in the PMv of Monkey D, ~1mm and ~2mm posterior from the center of the arcuate sulcus, respectively. Passive manipulation revealed a visuo-tactle receptive field on the left cheek of the position-tuned neuron, and no receptive field for the velocity-tuned neuron. No apparent eye movement related modulation was observed outside of the behavioral task for either neuron. *Vertical Green Solid Line:* Beginning Stimulus Moving Period, *Vertical Red Solid Line:* End of Stimulus Moving Period, *Vertical Yellow Dotted Lines:* Trial split time, Stimulus reverses direction of motion (see section 2.5.5). *Blue Line:* Average normalized firing rate, 100 mS bins. *Pink Shaded Area:* Time window used for regression model fit.

5.4 COMPARISON WITH RESULTS FROM THE PREVIOUS EXPERIMENTS

Figures 5.4 and 5.5 show object motion results from units classified during the both active reaching and replay experiments (**A&R units**) and those classified during replay only. A&R unit types were abbreviated "<Active Coordinate System>- <Replay Coordinate System>". Coordinate systems and angular differences between preferred directions were compared. 10/13 Hand-Cursor and 10/13 Cursor-Cursor A&R units were not tuned during the object motion task. 11/13 D.Motion-D.Motion A&R units were tuned during the object motion task in both cursor-centered and displayed motion coordinates. Both Hand-Hand A&R units were not tuned during the object motion task. 18/28 units that were classified during replay only were not tuned during the object motion task.

	M1	M1	M1	M1	PMv	M1	PMv	PMv	M1	M1	M1	M1	M1	M1	PMv	PMv	PMv	PMv	PMv	PMv
Active Reaching	0°	0°	0°	0°	0°	0°	0°	0°	0°	0°	0°	0°	0°	0°	0°	0°	0°	0°	0°	0°
Replay	122°	167°	10°	21°	21°	26°	27°	35°	42°	44°	50°	87°	19°	40°	46°	37°	49°	162°	21°	157°
Object Motion													43°	34°	54°				76°	165°

	M1	M1	PMv	PMv	PMv	PMv	PMv	PMv	M1	PMv	PMv	PMv	PMv	PMv	PMv	PMv	PMv
Active Reaching	0°	0°	0°	0°	0°	0°	0°	0°	0°	0°	0°	0°	0°	0°	0°	0°	0°
Replay	6°	8°	10°	11°	13°	13°	15°	18°	37°	40°	3°	6°	15°	3°	22°	169°	26°
Object Motion											92°	9°	23°		136°	173°	2°

	PMv	PMv	PMv	PMv	PMv	PMv	PMv	PMv	PMv	PMv	PMv	PMv	PMv
Active Reaching	0°	0°	0°	0°	0°	0°	0°	0°	0°	0°	0°	0°	0°
Replay	7°	12°	8°	8°	11°	15°	35°	1°	5°	12°	15°	17°	19°
Object Motion			164°	177°	151°	174°	129°	17°	38°	15°	21°	37°	39°

Coordinate System: Hand-Centered | Cursor-Centered | D. Motion

Figure 5.4: **Units classified during Active Reaching and Replay**
Each row displays results from one set of experiments, labeled on the left. Each column shows the responses of one unit with the anatomical area labeled at the top. White numeric values indicate the angular difference from the active reaching experiment. Empty squares indicate a lack of tuning during an experiment. Coordinate system classifications are indicated with color (see legend).

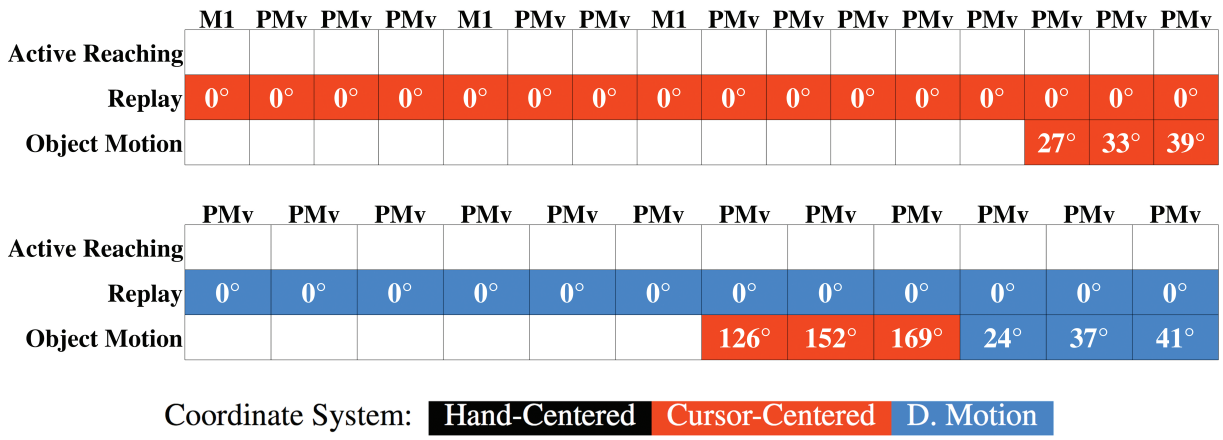

Figure 5.5: **Units classified during Replay Only**
Each row displays results from one set of experiments. Each column shows the responses of one unit with the anatomical area labeled at the top. White numeric values indicate the angular difference from the replay experiment. Empty squares indicate a lack of tuning during an experiment. Coordinate system classifications are indicated with color (see legend).

The Cursor-Centered Subpopulation: These units had previous classifications in all three coordinate systems during the active reaching experiment. 11 units were not classified in previous experiments. Angular differences between preferred directions was highest when the classified coordinate system was displayed motion during active reaching or replay. Visual motion in the previous experiments approached the same region of the display for each target. A possible explanation for this would be a receptive field encompassing one or more of these regions.

The Displayed Motion Subpopulation: These units also had previous classifications in all three coordinate systems during the active reaching experiment. 8 units had not been classified in previous experiments. Angular differences between preferred directions was lowest when the classified coordinate system was displayed motion during the replay experiment.

6.0 DISCUSSION

This final chapter is divided into sections that discuss the specific aims presented in the second chapter. Each specific aim is addressed using the following steps: 1) reiterate the specific aim, 2) examine summaries of previous work and the questions still unanswered, 3) summarize the experimental methods used to address each question, 4) summarize the results for each question, 5) interpret what was found, and 6) conclude the specific aim.

6.1 SPECIFIC AIM 1

Does neural activity in M1 and PMv show evidence of visuospatial transformation?

In chapter 2, we presented the example of a pilot using the same hand movements to control an airplane from two different views: in the cockpit and remotely from the ground. In each condition, the brain must interpret the visual scene and generate identical control signals to the muscles of the arm. The process by which visual information is incorporated for control is not well understood, but there is evidence of neural activity corresponding to various stages of a visuospatial transformation.

Neuronal activity from the primary motor cortex (M1) is correlated with the hand-centered direction of movement. Individual neurons fire maximally for one direction of movement, called the *preferred direction*. As movement direction changes, firing rate can be linearly modeled as a function of the cosine of angular difference with the preferred direction. If this signal is generated in the brain, it represents an extrinsic construct built upon a network relaying various forms of sensory, memory, and decision-making information. A key element of this network is thought to

operate through various parallel coordinate transformations from the areas of the brain associated with vision to provide relevant visually-derived information. Results from previous studies support the idea that visual precursors to this M1 signal may be located in the ventral premotor cortex (PMv). Kakei et al. have shown that a higher percentage of neurons are correlated with the extrinsic direction of hand movement in PMv than M1 [48]. This suggests that PMv may be more involved in transforming the visual coordinates of target location into the direction of hand movement, while M1 may be more involved in intrinsic control (i.e., muscles of the arm and/or joint angles). Schwartz et al. evaluated population activity while subjects performed an illusion task that dissociated the movement of a virtual cursor from the movement of the hand [74]. They found that the summed directional activity from PMv matched the trajectory of the cursor, while those from M1 matched the trajectory of the hand. This suggests that activity in PMv is not only extrinsic, but also corresponds to the displayed movement of the effector. Assuming that the units found in the Kakei study are similar in function to those in the the Schwartz study, we have learned four things:

1. Activity that corresponds to intrinsic coordinates of reaching is located primarily in M1.
2. Activity that corresponds to extrinsic coordinates of reaching is more prevalent in PMv.
3. Population activity in M1 corresponds to the direction of movement centered on the hand.
4. Population activity in PMv corresponds to the direction of movement centered on a displayed effector.

The Kakei experiment was not designed to dissociate several extrinsic factors, such as the movement direction of the arm, the movement direction of the cursor, and target location. Another possibility that still remains is that neurons in PMv are encoding an evoked sensory signal. Two studies have reported activity in PMv that is tuned to position and directional motion of a visible stimulus greater than a meter away from the body during passive behavior [27, 38]. Iriki et al. have found similar neurons in parietal cortex that correspond to similar stimuli on a video monitor [42].

The Schwartz et al. experiment results regarding extrinsic parameters in PMv can currently be explained by activity corresponding to cursor-centered movement or to the motion of the displayed stimulus. In addition, the Schwartz experiment was not designed to determine what the activity from individual units corresponded to. Therefore the connection from PMv extrinsic-related activity to a cortical control signal for arm movement is still unclear.

6.1.1 Question 1

> Are there multiple discrete extrinsic coordinate systems represented in neural activity during active movement? We will search for these as the subject is required to perform different transformations to complete a task.

The purpose of this dissertation was to further define the role of activity related to extrinsic parameters in M1 and PMv. This experiment used multiple view changes during the same set of arm movements to segregate activity into three coordinate systems. Each of these coordinate systems represented a different visual context based on previous studies.

1. **Hand-Centered Coordinates**: An extrinsic vector with *motor* context, in that it originates on the hand and points in the direction of movement. It is unaffected by view changes.
2. **Cursor-Centered Coordinates**: An extrinsic vector with *visuomotor* context, in that it originates on the cursor and points in the direction of the target. It is sensitive to view changes.
3. **Displayed Motion Coordinates**: An extrinsic vector with *visual* context that originates on any object moving on the display and points in the direction of motion. It is sensitive to view changes.

The following tasks were designed for a 3D interactive display with a spherical cursor representing the position of the hand and a spherical target representing the goal position of the reach. Coordinate systems were dissociated using a different view in each task:

1. **Standard Reach Task**: Cursor direction matched the hand direction. Displayed motion was defined as the motion of the cursor. All three vector types were parallel as the subject reached to 14 different targets locations. No coordinate systems were dissociated.

2. **Anti-Reach Task**: The hand moved to the same 14 locations as in the standard reach task as the cursor moved in the opposite direction. Displayed motion was that of the cursor, so hand-centered coordinates were dissociated.
3. **Stationary Cursor Task**: The hand moved to the same 14 locations as in the anti-reach and the standard reach tasks. The target appeared to move in the opposite direction of the hand, towards the cursor, while the cursor appeared stationary in the center of the display. The cursor-centered vector pointed to the target. Displayed motion was that of the target, which was dissociated by pointing in the opposite direction of both the hand- and cursor-centered vectors.

Two statistical methods were used to classify task-related units into one of the three coordinate systems. Using the combined data from all three tasks, linear models of firing rate were regressed as a function of movement in each coordinate system. Resultant R^2 values showed that each coordinate system was well fit within separate subpopulations of units. We then calculated tolerance intervals surrounding the preferred directions from each task to determine when the distributions were overlapping in the same coordinate system. Activity with three overlapping distributions in one coordinate system was defined as belonging to that coordinate system.

The sampled population of units was subdivided into all three coordinate systems based on this definition,: 106 hand-centered units, 39 cursor-centered units, and 19 displayed motion units. By comparing the depth of modulation from the cursor-centered units during the standard reach and the stationary-cursor tasks, we were able to test whether the motion of the cursor was required for a response. We found very similar modulation, suggesting that cursor motion was not required. This supports the idea of a cursor-centered *difference vector* constructed solely from the location of the target relative to the effector (see figure 6.1).

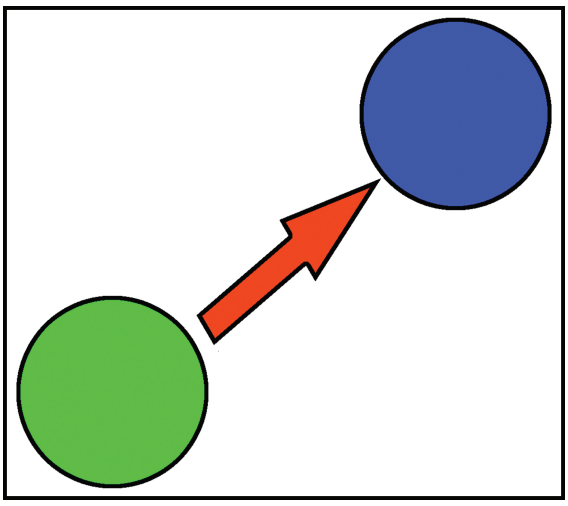

Figure 6.1: **The Difference Vector:** A visually-derived vector pointing from the displayed effector to the goal position. In the case of this experiment, it points from the cursor to the target. This association may be the output of a learned forward model

6.1.2 Question 2

> Can these coordinate frames be differentiated in the anatomical and temporal domains, suggesting a systematic substrate for visuospatial transformation?

We used linear regression over a range of time epochs across all trials to determine when each model best fit the classified coordinate system. We found two significant results. First, all activity corresponding to displayed motion came after movement onset, and the median was significantly different from the cursor-centered and hand-centered groups . Second, during the reaction-time period (before movement onset), median cursor-centered activity was tuned before median hand-centered activity.

We compared the locations of the classified units on the posterior-anterior axis, relative to the arcuate sulcus. We calculated median locations of 6.7mm, 3.1mm, and 1.4mm for Hand-Centered, Cursor-Centered, and Displayed Motion coordinates respectively. Each subpopulation had a median distance that was significantly different from the other two. Result summaries in each cortical area were as follows:

- M1: 90.8% Hand-Centered, 9.2% Cursor-Centered, 0.0% Displayed Motion
- PMv: 47.5% Hand-Centered, 33.3% Cursor-Centered, 19.2% Displayed Motion

Most of the cursor-centered activity was found in Monkey D and most of the displayed motion activity was found in Monkey J. There were three possible reasons for this disparity. First, dura growth constrained the regions for electrode penetration which increased sampling bias. Monkey J had 111/201 of possible electrode penetration locations within the recording chamber within 2mm of the arcuate sulcus, versus 33/199 in monkey D. This region has been hypothesized to have isolated functional characteristics [31, 63, 59]. Second, Monkey D had a different intermediate kinematic path during the anti-reach task, suggesting that a different combination of muscle contractions was used to reach each target. This may have reversed activity related to intrinsic muscle activation. Previous research, however, shows that the pattern of activity in PMv greatly favors an extrinsic representation [48]. Third, Monkey D was better trained on the anti-reach task, as observed during reaches to untrained targets, so the large cursor-centered population may have corresponded to a well-developed internal model. We believe the first explanation was most likely.

6.1.3 Conclusion

Identifying coordinate systems in the brain activity is analogous to the "black box" approach used to identify an unknown electrical circuit. A collection of known input signals are connected to a device and corresponding outputs are monitored and analyzed to determine how the input signals were transformed. Before this experiment, we knew that PMv had an "output" during active reaching that was correlated with an extrinsic parameter related to visuospatial transformation. The results of this dissertation suggest that this ostensibly uniform population corresponds to multiple outputs that may represent multiple extrinsic phases of visuomotor transformation. To conceptualize these phases,

we refer to a framework of forward and inverse models in the context of visuospatial transformation. *Forward models* are built from experience and transform sensory information into a visualized trajectory. *Inverse models* transform the visualized trajectory into a command signal. Based on our results, we propose the following functions for each coordinate system:

6.1.3.1 Hand-Centered Coordinates This activity was found throughout PMv and in ~90% of the cells in M1. During the reaction time period, these units responded later than units corresponding to cursor-centered coordinates. This activity may encode a control signal in a purely motor context, as it was insensitive to view-changes and centered on the effector. Intrinsic activity would be directionally tuned and view-insensitive, and could have been classified in this coordinate system. Results from previous studies suggest that this representation would be more evident in M1. In any case, this activity type is more related to the output of inverse models that transform high-order visual planning into lower-order control signals, in contrast to the other two coordinate systems discussed in this dissertation.

6.1.3.2 Cursor-Centered Coordinates This view-sensitive coordinate system was well represented in PMv and modestly represented in M1. During the reaction time period, activity corresponding to this coordinate system was tuned before hand-centered activity. Cursor motion was not required for a response, which supports the idea of a *difference vector* constructed from the cursor-centered target location. This visually-derived vector is consistent with inverse models for movement generation.

6.1.3.3 Displayed Motion Coordinates This coordinate system is based on the vector between two consecutive positions of either a moving cursor or a moving target in a 3D virtual space. It was only represented in the anterior portion of the PMv. Activity corresponding to this coordinate system was tuned after movement onset. This coordinate frame may represent a visual facet of sensory feedback used by forward models to construct and update a high-order visual planning signal.

This set of experiments has successfully dissociated discrete extrinsic coordinate systems with distinct latencies and anatomical locations. This suggests that a systematic substrate for visuospatial transformation exists in PMv and M1.

6.2 SPECIFIC AIM 2

> We hypothesized in Aim 1 that cortical neurons in motor regions have discharge rates that are sensitive to different visuomotor transformations. If this is true, is there an inherent component of this process driven by visual input in the absence of movement?

Our results support the idea that activity in the PMv translates the visual features of the workspace into a potential motor action. Neuronal responses are evoked in the visual areas of the brain and respond to simple visual stimuli. The putative network originating in these areas and projecting to the motor regions provides a stream of processed, visually-derived information. Previous work suggests that observing a learned action elicits a response from neurons in PMv that is also active while performing the action. This could possibly reflect processing related to learning and understanding that action. There are also neurons that respond to moving objects near the body without the subject having any intention to move. We wished to evaluate how PMv activity differs in correspondence between these contexts during active reaching, observing replays of active reaching, and observing object motion.

6.2.1 Question 1

> Which coordinate systems (found in the first set of experiments) are neurally represented during reach replays? For each neuron, we will compare the most likely corresponding coordinate frame from active movement to that from visually congruent passive replays.

Many different types of activity related to the observation of action have been reported. Mental rehearsal has been studied in the PMd [13], and M1 [19, 82] and may represent the intended trajectory of an effector (or surrogate effector) whether or not the action is generated. This signal is most active before movement onset (in a delay period task) and is speculatively related to anticipated visualized action[13]. Lemon and colleagues have shown that pyramidal tract neurons in M1 also have observation-related activity [87]. Action recognition has been studied extensively by Rizzolatti and colleagues in a subgroup of cells located primarily in the F5 subregion of PMv known as *mirror*

neurons [70]. No previous study has evaluated firing rate models as a function of the direction of replayed movement in the PMv. In addition, emphasis on multiple coordinate systems during observation-related activity in PMv and M1 has been minimal.

We wished to evaluate whether replay-related activity is driven by sensory information, a visualized version of action, or a true rehearsal of hand kinematics by classifying responses into coordinate frames. Kinematic data from the end of the Hold A period to the end of the Hold B period was buffered and replayed for the animal after each successful reach trial throughout the set of active reaching tasks. Each active reaching task was performed in a block. For example, 14 anti-reach successes were interleaved with 14 replay successes before moving on to the next task. During replay, the animal was trained to hold its hand in the center of the workspace. We classified activity using the same methods from the active reaching experiment. Previous hand movements from the active reaching task were used as regressors for the hand-centered models.

6.2.1.1 Hand-Centered Coordinates without Hand Movement: Hand-centered coordinates were dissociated from cursor-centered coordinates during the active reaching experiment with the anti-reach task. In this task, the hand and the cursor were moving in opposite directions. During the replay task, the hand wasn't moving, which created similar task conditions for both the standard and anti-reach replays. We accounted for this conundrum in several ways. First, we incorporated a change in virtual lighting direction that differentiated the appearance of the tasks. Sometimes when the task switched from standard to anti-reach, the animal missed this lighting change and reached in the opposite direction of the target. After this failure, the animal adapted to the task change and never made this type of error for that block of anti-reach trials. Here we assumed that the animal had a new association to the visual display and it updated a learned internal model of the task. Second, the replays were interleaved 1-1 throughout these active reaching blocks, and the animal responded with the correct hand direction for the presented target before and after the replay. Here we further assume that the animal had a different learned association between standard and anti-reach replay trials, setting a construct for coordinate dissociation. If these replay trials were being mentally rehearsed, the associated direction of action could have been neurally represented in hand-centered coordinates.

Activity from 64% of units with replay-related activity was classified into a coordinate system. 54% of these units had activity that corresponded to cursor-centered coordinates, with about a third of these in M1. 44% corresponded to displayed motion coordinates and were all located in the PMv. 2 units (3%) had activity that corresponded to hand-centered coordinates and they were both located in M1. Latency analysis revealed that all of these responses began during or after the replayed movement onset with no significant difference when grouped by coordinate frame. Results from the active reaching experiment were compared to those from the replay experiment and several notable results were found. First, 50/78 units classified during the replay experiments were also classified during the active reaching experiment (**A&R units**). A&R unit types were abbreviated "<Active Coordinate System>- <Replay Coordinate System>". When comparing preferred directions between the active and replay contexts, a value of $<60°$ was used to label preferred directions as similar. A value of $120°$ to $180°$ was used to label preferred directions as opposite. Second, all of the A&R units had replay-related activity that corresponded to the coordinate frame classified during active reaching or a less motor-related coordinate frame. Third, the Cursor-Cursor and D.Motion-D.Motion subpopulations of A&R units (both 13 units) both had similar preferred directions in the same coordinate system. Fourth, a Hand-Cursor A&R subpopulation (13 units) also had mostly similar preferred directions (12 units) and with a large portion located in M1 (7 units). Lastly, 2 Hand-Hand A&R units were located in M1 and had opposite preferred directions in the two contexts.

In summary, replay-related activity mostly corresponded to the cursor-centered and displayed motion coordinate systems. Three key subpopulations of A&R units corresponded to the same coordinate systems during active reaching. The fourth (Hand-Cursor) was found to change its correspondence. We analyze each subpopulation further in the conclusion of this specific aim.

6.2.2 Question 2

> Neuronal activity is modulated during passive behavior as objects move around the cursor in the virtual environment. Can this modulation be modeled as a function of cursor-centered or displayed motion coordinates? If so, do these sensory representations persist during observation and active reaching?

Two different studies have shown that activity in the PMv corresponds to object position near the body [27, 37]. This activity is also correlated with stimulus motion direction, and more dynamic parameters may be encoded [27, 38]. These neurons have gaze-independent visual receptive fields extending outward sometimes greater than 1 meter away. We have observed directional tuning in several neurons while moving a probe in a circular trajectory in front of the subject at this distance. Iriki et al. have found activity from neurons in parietal cortex that corresponds to similar stimuli on a video monitor [42]. There are two interpretations of this work. These responses may correspond to a multipurpose sensory map for proximal interactions (i.e. to serve defensive behavior) [79, 36], or they may participate in generating an *effector-centered* coordinate frame for target location [27].

We designed an experiment to determine whether activity corresponds to object motion or cursor-centered direction in the displayed workspace used during the active reaching and replay tasks. The animal was required to hold a central cursor position while a virtual object was translated at a constant speed from the center to the 14 reach target locations and then back to center. Opposite motion directions were sampled for each cursor-centered direction. The cursor did not move in this task, which effectively made cursor-centered direction a measure of position. This allowed responses tuned for object position in a section of the workspace to be dissociated from those tuned for direction of object motion. Both types of tuned activity were considered sensory responses, since each animal was never required to move its arm for this task.

Firing rate models were evaluated as a function of either coordinate system and compared for each task-related unit. 69/92 task-related units were classified in either coordinate system, with 40 (58%) corresponding to cursor-centered coordinates and 29 (42%) corresponding to displayed motion. Although this was a limited sample, this indicates that there is a comparable number of units with tuning properties that match each of the putative coordinate systems. All but two classified

units were located in PMv. These results were compared to those from the active reaching and replay experiments. Several notable results were found. First, 10/13 Hand-Cursor and 10/13 Cursor-Cursor A&R units were not tuned during the object motion task. Second, 11/13 D.Motion-D.Motion A&R units were tuned during the object motion task in both cursor-centered and displayed motion coordinates. Third, both Hand-Hand A&R units were not tuned during the object motion task. Fourth, 18/28 units that were classified during replay only were not tuned during the object motion task.

In summation, we found a modest amount of cells that were tuned in one of two types of sensory coordinate systems. 97% of these were located in the PMv. Subpopulations based on previous results from the active reaching and replay experiments had differing correspondence to these coordinate systems. We analyze each of these subpopulations further in the conclusion of this specific aim.

6.2.3 Conclusion

This dissertation evaluated activity thought to be related to visuomotor transformation in three different contexts:

- **Action:** The active reaching set of experiments evaluated how visuomotor activity responded in a context in which the animal intended to generate a reach. This process is thought to incorporate a forward model to generate a visually derived difference vector constructed from sensory information. This signal may feed into an inverse model for lower order command signals.
- **Action Observation:** The replay set of experiments were designed to examine a context that was visually congruent to the active reaching tasks without the subjects having the intention to move. Since the animal was presented with the same visual input as in a task for which it was well-trained, forward models may have generated a difference vector representing the associated goal. Since no movement was generated, however, there was no need to transform this vector into a command signal. Thus, an inverse model was not necessary.

- **Motion Observation:** The object motion set of experiments were designed to examine neural responses to a dynamic visual display without learned action-related context or the intention to move. In this case, visuomotor coordinate transformations were not needed.

6.2.3.1 Visuomotor Transformation: Due to the many permutations of results in this dissertation, subpopulations of units with a consistent interpretable role through all three contexts were selected for further discussion. Since our goal was to identify evidence of visuomotor transformation, activity related to action was specifically emphasized. Tuning during the object motion task was used to identify activity not consistently related to action.

6.2.3.2 Hand-Hand A&R units: These units were classified in the hand-centered coordinate system during active reaching and during the replay tasks. Lemon and colleagues found pyramidal tract neurons in M1 that responded during a grasping task. The same neurons reversed this response while observing the same grasp task, presumably to suppress movement [87]. Since their grasp paradigm was not designed to evaluate directional tuning, we wish to extend these findings to our own. Two similar units were located in posterior M1. Firing rate was correlated with the angular difference of the replayed reach direction from the original active reaching preferred direction. We speculate that these neurons reversed their preferred directions during observation to suppress descending command signals. Considering this and the low number of units classified as "Hand-Hand", we suggest that mental rehearsal was not taking place in hand-centered coordinates.

6.2.3.3 The Hand-Cursor A&R units: These units were classified in the hand-centered coordinate system during active reaching and in the cursor-centered coordinate system during the replay tasks. 9/13 were not tuned during the object motion task and had similar preferred directions during replay and active reaching. 6 of these were located in M1, and 3 in posterior PMv. During action, when an inverse model was active, we suggest this activity corresponded to a motor command signal. During the replay tasks, we suggest that this activity represented the output of a forward model, or the visualized goal of the task. Since the majority of these units were located in M1, this

suggests that M1 may be a *receiver* of visually-derived information. Its ability to encode a different coordinate frame during observation implies that area M1 interprets high-order information and transmits processed command signals during active reaching.

6.2.3.4 Cursor-Cursor A&R units: These units were classified in the cursor-centered coordinate system during active reaching and during the replay tasks. 10/13 were not tuned during the object motion task and had similar preferred directions during replay and active reaching. 3 of these were located in M1 and 7 were located in PMv. We suggest that these units were part of a neural circuit that consistently represented the output of a forward model for possible action.

6.2.3.5 Sensory Representations: Units with activity that corresponded to displayed motion during active reaching had very predictable responses during the replay and object motion tasks. Preferred directions from the D.Motion-D.Motion A&R subpopulation were all similar during the replay tasks, and 11/13 were tuned during the object motion task. Cursor-centered tuning from these units observed during the object motion task was the opposite of tuning in the active reaching and replay tasks. One possible explanation for this is the presence of a receptive field extending outward from the body. Displayed motion in all tasks approached the same region of the display for each target. Neurons with these receptive fields would simply respond whenever a stimulus approached the visual boundary. D.Motion-D.Motion A&R units tuned for displayed motion in the object motion task all had similar preferred directions during the object motion task. We suggest here that representations of displayed position and motion are represented in the PMv and maintain a sensory-like correspondence during action context.

These results support the idea of a complex inherent component of the visuospatial transformation process, driven by visual input in the absence of movement. One aspect of this is the sensory representation of displayed motion and position. These seem to persist in all contexts. Another aspect is the visuomotor representation of the difference vector, which may be the output of a learned forward model (see figure 6.2). It is represented in neural activity during action and action observation, but rarely during object motion observation. This suggests that it is not the intention to move that triggers the difference vector signal, but an action-related context. Furthermore, the difference vector was also represented during action observation in activity from M1 neurons that correspond to hand-centered coordinates during active reaching. This suggests that the difference vector and hand-centered coordinates may have overlapping neural substrates. Visuomotor transformation may associate a learned task with a stored internal model to generate the correct action. Our results suggest that the difference vector may be a representation of this process in action-related contexts.

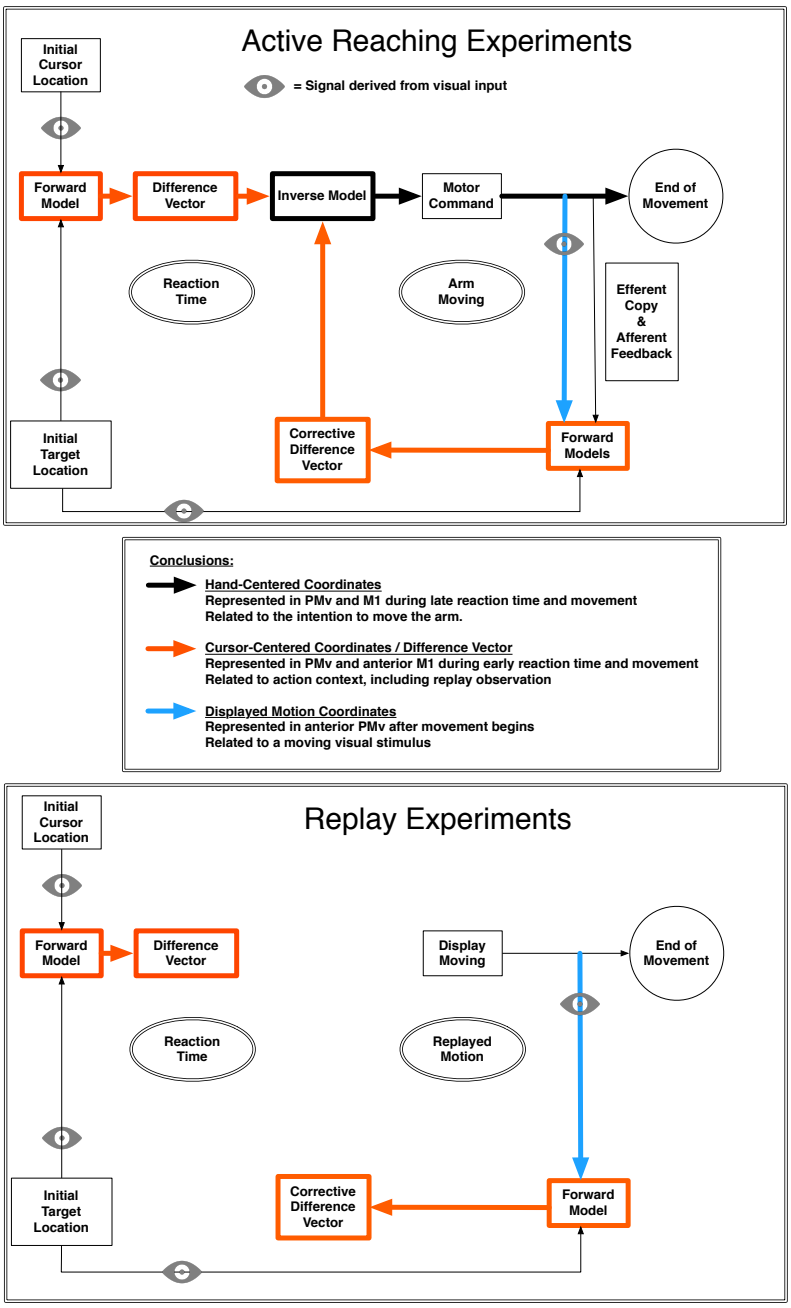

Figure 6.2: **A Proposed Internal Model:** These diagrams show a general summary of the conclusions we made in this dissertation. *Forward models* are built from experience and transform visual sensory information into a visualized goal vector, or in this case, desired cursor trajectory. *Inverse models* transform the visualized goal trajectory into a command signal, or in this case, a desired hand trajectory or intrinsic motor command. **Top:** An internal model during active reaching. Initial positions of the cursor and the target are visually recognized and used to build a difference vector using a forward model. The difference vector feeds into an inverse model and is transformed into a motor command. The arm begins to move and the resulting displayed motion is registered and transmitted to a forward model. Afferent and efferent inputs are also transmitted to evaluate the position of the hand. A new corrective difference vector is calculated and sent to the inverse model for corrections to the motor command. **Bottom:** Forward models are active but an inverse model is not needed. The feedback cycle is broken, yet difference vectors are still generated from visual input. Refer to the conclusions box for latency and anatomical conclusions made for each coordinate system.

BIBLIOGRAPHY

[1] R A Andersen, L H Snyder, A P Batista, C A Buneo, and Y E Cohen. Posterior parietal areas specialized for eye movements (LIP) and reach (PRR) using a common coordinate frame. In *Novartis foundation symposium*, volume 218, page 109, 1998.

[2] A Berti and F Frassinetti. When far becomes near: remapping of space by tool use. *Journal of cognitive neuroscience*, 2000.

[3] I Billig and P L Strick. Anatomical evidence for overlap of neck and oculomotor control systems in the ventral premotor cortex. In *2012 Neuroscience Meeting Planner*, 2012.

[4] R Breveglieri, C Galletti, M Gamberini, L Passarelli, and P Fattori. Somatosensory cells in area PEc of macaque posterior parietal cortex. *Journal of Neuroscience*, 2006.

[5] K Brodmann. Beitrage zur histologischen lokalisation der grosshirnrinde iii. die rindenfelder der niederen. *J Psychol Neurol*, 4:177–226, 1905.

[6] K Brodmann. Vergleichende lokalisationslehre der grobhirnrinde. *Barth, Leipzig*, 1909.

[7] A Browne. *Neural network perspectives on cognition and adaptive robotics*. Taylor & Francis, 1997.

[8] C A Buneo, M R Jarvis, A P Batista, and R A Andersen. Direct visuomotor transformations for reaching. *Nature*, 2002.

[9] R. Caminiti, P. B. Johnson, and A. Urbano. Making Arm Movements Within Different Parts of Space: Dynamic Aspects in the Primate Motor Cortex. *The Journal of neuroscience : the official journal of the Society for Neuroscience*, 1990.

[10] A W Campbell. *Histological studies on the localisation of cerebral function*. University Press, 1905.

[11] ST Carmichael and Joseph L Price. Sensory and premotor connections of the orbital and medial prefrontal cortex of macaque monkeys. *Journal of Comparative Neurology*, 363(4): 642–664, 1995.

[12] Mark M Churchland, Gopal Santhanam, and Krishna V Shenoy. Preparatory activity in premotor and motor cortex reflects the speed of the upcoming reach. *Journal of neurophysiology*, 96 (6):3130–3146, 2006.

[13] Paul Cisek and John F Kalaska. Neural correlates of mental rehearsal in dorsal premotor cortex. *Nature*, 2004.

[14] Paul Cisek, Donald J Crammond, and John F Kalaska. Neural activity in primary motor and dorsal premotor cortex in reaching tasks with the contralateral versus ipsilateral arm. *Journal of neurophysiology*, 89(2):922–942, 2003.

[15] C L Colby, J Duhamel, and M E Goldberg. Ventral intraparietal area of the macaque: anatomic location and visual response properties. *Journal of neurophysiology*, 69(3):902–914, 1993.

[16] M Desmurget and S Grafton. Forward modeling allows feedback control for fast reaching movements. *Trends in cognitive sciences*, 4(11):423–431, 2000.

[17] R P Dum and P L Strick. Motor areas in the frontal lobe of the primate. *Physiology & behavior*, 77(4):677–682, 2002.

[18] R P Dum and P L Strick. *Motor Areas in the Frontal Lobe*. CRC Press, 2004. ISBN 978-0-8493-1287-8. doi: 10.1201/9780203503584.sec1.

[19] Juliana Dushanova and John Donoghue. Neurons in primary motor cortex engaged during action observation. *European Journal of Neuroscience*, 31(2):386–398, 2010.

[20] E V Evarts. Motor cortex reflexes associated with learned movement. *Science; Science*, 1973.

[21] E V Evarts and J Tanji. Reflex and intended responses in motor cortex pyramidal tract neurons of monkey. *Journal of neurophysiology*, 39(5):1069–1080, 1976.

[22] E V Evarts et al. Pyramidal tract activity associated with a conditioned hand movement in the monkey. *J Neurophysiol*, 29(6):1011–27, 1966.

[23] E V Evarts et al. Relation of pyramidal tract activity to force exerted during voluntary movement. *J Neurophysiol*, 31(1):14–27, 1968.

[24] Peter Filzmoser, Ricardo Maronna, and Mark Werner. Outlier identification in high dimensions. *Computational Statistics & Data Analysis*, 2008.

[25] Martha Flanders, Stephen I Helms Tillery, and John F Soechting. Early stages in a sensorimotor transformation. *Behavioral and Brain Sciences*, 15(02):309–320, 1992.

[26] Tamar Flash and Neville Hogan. The coordination of arm movements: an experimentally confirmed mathematical model. *The journal of Neuroscience*, 5(7):1688–1703, 1985.

[27] L Fogassi, V Gallese, L Fadiga, G Luppino, M Matelli, and G Rizzolatti. Coding of peripersonal space in inferior premotor cortex (area F4). *Journal of Neurophysiology*, 1996.

[28] Leonardo Fogassi and Luciano Simone. The mirror system in monkeys and humans and its possible motor-based functions. In *Progress in Motor Control*, pages 87–110. Springer, 2013.

[29] G Fritsch and E Hitzig. Über die elektrische erregbarkeit des grosshirns. *Arch Anat Physiol Wiss Med*, 37:300–332, 1870.

[30] J F Fulton. A note on the definition of the "motor" and "premotor" areas. *Brain*, 58(2): 311–316, 1935.

[31] Vittorio Gallese, Luciano Fadiga, Leonardo Fogassi, and Giacomo Rizzolatti. Action recognition in the premotor cortex. *Brain*, 119(2):593–609, 1996.

[32] M S Gazzaniga. *The cognitive neurosciences III*. MIT press, 2004.

[33] M Gentilucci, L Fogassi, G Luppino, M Matelli, R Camarda, and G Rizzolatti. Functional organization of inferior area 6 in the macaque monkey. *Experimental Brain Research*, 71(3): 475–490, 1988.

[34] A P Georgopoulos, J F Kalaska, R Caminiti, and J T Massey. On the relations between the direction of two-dimensional arm movements and cell discharge in primate motor cortex. *The Journal of Neuroscience*, 2(11):1527–1537, 1982.

[35] S Geyer, M Matelli, G Luppino, and K Zilles. Functional neuroanatomy of the primate isocortical motor system. *Anatomy and embryology*, 202(6):443–474, 2000.

[36] M S Graziano and D F Cooke. Parieto-frontal interactions, personal space, and defensive behavior. *Neuropsychologia*, 2006.

[37] M S Graziano, X T Hu, and C G Gross. Visuospatial properties of ventral premotor cortex. *Journal of Neurophysiology*, 1997.

[38] M S Graziano, X T Hu, and C G Gross. Coding the locations of objects in the dark. *Science*, 1997.

[39] M S Graziano, L A Reiss, and C G Gross. A neuronal representation of the location of nearby sounds. *Nature*, 1999.

[40] P W Halligan, J C Marshall, et al. Left neglect for near but not far space in man. *Nature*, 350 (6318):498–500, 1991.

[41] Gary B Hughes and Mohcine Chraibi. Calculating ellipse overlap areas. 2011.

[42] A Iriki, M Tanaka, S Obayashi, Y Iwamura, et al. Self-images in the video monitor coded by monkey intraparietal neurons. *Neuroscience research*, 40(2):163–174, 2001.

[43] J H Jackson. On the anatomical and physiological localisation of movements in the brain. *The Lancet*, 101(2581):232–235, 2 1873.

[44] J H Jackson. On some implications of dissolution of the nervous system. *Med Press Circ*, 2: 411–426, 1882.

[45] M Jeannerod and B Biguer. *Visuomotor mechanisms in reaching within extrapersonal space*. Advances in the Analysis of Visual Behaviour, Ingle, D., Goodale, M. and Mansfield, R.(editors), MIT Press, 1982.

[46] M I Jordan and D E Rumelhart. Forward Models: Supervised Learning with a Distal Teacher. *Cogn Sci*, 1992.

[47] S Kakei, D S Hoffman, and P L Strick. Muscle and movement representations in the primary motor cortex. *Science*, 285(5436):2136–2139, 1999.

[48] S Kakei, D S Hoffman, and P L Strick. Direction of action is represented in the ventral premotor cortex. *Nature neuroscience*, 2001.

[49] J F Kalaska, D Cohen, M Prud'Homme, and M L Hyde. Parietal area 5 neuronal activity encodes movement kinematics, not movement dynamics. *Experimental Brain Research*, 1990.

[50] JF Kalaska and DJ Crammond. Deciding not to go: neuronal correlates of response selection in a go/nogo task in primate premotor and parietal cortex. *Cerebral Cortex*, 5(5):410–428, 1995.

[51] John F Kalaska, Stephen H Scott, Paul Cisek, and Lauren E Sergio. Cortical control of reaching movements. *Current opinion in neurobiology*, 7(6):849–859, 1997.

[52] M Kawato. Internal models for motor control and trajectory planning. *Current Opinion in Neurobiology*, 1999.

[53] Evelyne Kohler, Christian Keysers, M Alessandra Umilta, Leonardo Fogassi, Vittorio Gallese, and Giacomo Rizzolatti. Hearing sounds, understanding actions: action representation in mirror neurons. *Science*, 297(5582):846–848, 2002.

[54] K Krishnamoorthy and Sumona Mondal. Improved tolerance factors for multivariate normal distributions. *Communications in Statistics—Simulation and Computation®*, 35(2):461–478, 2006.

[55] K Kurata and D S Hoffman. Differential effects of muscimol microinjection into dorsal and ventral aspects of the premotor cortex of monkeys. *Journal of neurophysiology*, 71(3): 1151–1164, 1994.

[56] K Kurata and E Hoshi. Reacquisition deficits in prism adaptation after muscimol microinjection into the ventral premotor cortex of monkeys. *Journal of neurophysiology*, 81(4):1927–1938, 1999.

[57] A S F Leyton and C S Sherrington. Observations on the excitable cortex of the chimpanzee, orang-utan, and gorilla. *Experimental Physiology*, 11(2):135–222, 1917.

[58] Ming-Teh Lu, James B Preston, and Peter L Strick. Interconnections between the prefrontal cortex and the premotor areas in the frontal lobe. *Journal of Comparative Neurology*, 341(3): 375–392, 1994.

[59] Giuseppe Luppino, Akira Murata, Paolo Govoni, and Massimo Matelli. Largely segregated parietofrontal connections linking rostral intraparietal cortex (areas aip and vip) and the ventral premotor cortex (areas f5 and f4). *Experimental Brain Research*, 128(1-2):181–187, 1999.

[60] Kantilal Varichand Mardia and Kanti V Mardia. *Statistics of directional data*, volume 5. Academic Press London, 1972.

[61] M Matelli, V Gallese, and G Rizzolatti. Neurological deficit following a lesion in the parietal area 7b in the monkey. *Bollettino della Società italiana di biologia sperimentale*, 1984.

[62] VB Mountcastle, JC Lynch, A. Georgopoulos, H. Sakata, and C. Acuna. Posterior parietal association cortex of the monkey: command functions for operations within extrapersonal space. *Journal of Neurophysiology*, 38(4):871, 1975.

[63] Akira Murata, Luciano Fadiga, Leonardo Fogassi, Vittorio Gallese, Vassilis Raos, and Giacomo Rizzolatti. Object representation in the ventral premotor cortex (area f5) of the monkey. *Journal of neurophysiology*, 78(4):2226–2230, 1997.

[64] T Ochiai, H Mushiake, and J Tanji. Involvement of the ventral premotor cortex in controlling image motion of the hand during performance of a target-capturing task. *Cereb Cortex*, 2005.

[65] J Paillard. Fast and slow feedback loops for the visual correction of spatial errors in a pointing task: a reappraisal. *Canadian journal of physiology and pharmacology*, 1996.

[66] W Penfield and T Rasmussen. The cerebral cortex of man; a clinical study of localization of function. 1950.

[67] A Riehle and E Vaadia. *Motor cortex in voluntary movements*. CRC Press, 2004.

[68] G Rizzolatti, M Matelli, and G Pavesi. Deficits in attention and movement following the removal of postarcuate (area 6) and prearcuate (area 8) cortex in macaque monkeys. *Brain*, 106(3):655–673, 1983.

[69] G Rizzolatti, G Luppino, and M Matelli. The organization of the cortical motor system: new concepts. *Electroencephalography and clinical neurophysiology*, 1998.

[70] G Rizzolatti, L Fogassi, and V Gallese. Motor and cognitive functions of the ventral premotor cortex. *Current Opinion in Neurobiology*, 2002.

[71] H Sakata, Y Takaoka, A Kawarasaki, and H Shibutani. Somatosensory properties of neurons in the superior parietal cortex (area 5) of the rhesus monkey. *Brain Research*, 1973.

[72] H Sakata, M Taira, M Kusunoki, A Murata, Y Tanaka, and K Tsutsui. Neural coding of 3D features of objects for hand action in the parietal cortex of the monkey. *Philosophical transactions of the Royal Society of London. Series B, Biological sciences*, 1998.

[73] A B Schwartz, R E Kettner, and A P Georgopoulos. Primate motor cortex and free arm movements to visual targets in three-dimensional space. I. Relations between single cell discharge and direction of movement. *The Journal of neuroscience : the official journal of the Society for Neuroscience*, 1988.

[74] A B Schwartz, D W Moran, and G A Reina. Differential representation of perception and action in the frontal cortex. *Science*, 2004.

[75] R Shadmehr and F A Mussa-Ivaldi. Adaptive representation of dynamics during learning of a motor task. *The Journal of Neuroscience*, 14(5):3208–3224, 1994.

[76] R Shadmehr and S P Wise. *The computational neurobiology of reaching and pointing: a foundation for motor learning*. MIT press, 2005.

[77] J P Snyder. Map projections–A working manual. 2011.

[78] John F Soechting and Martha Flanders. Sensorimotor representations for pointing to targets in three-dimensional space. *Journal of Neurophysiology*, 62(2):582–594, 1989.

[79] J F Stein. Representation of egocentric space in the posterior parietal cortex. *Quarterly journal of experimental physiology (Cambridge, England)*, 1989.

[80] J Tanné-Gariépy, E M Rouiller, and D Boussaoud. Parietal inputs to dorsal versus ventral premotor areas in the macaque monkey: evidence for largely segregated visuomotor pathways. *Experimental Brain Research*, 2002.

[81] C S R Taylor and C G Gross. Twitches versus movements: a story of motor cortex. *The Neuroscientist*, 2003.

[82] D Tkach, J Reimer, and N G Hatsopoulos. Congruent Activity during Action and Action Observation in Motor Cortex. *Journal of Neuroscience*, 2007.

[83] Dennis Tkach, Jake Reimer, and Nicholas G Hatsopoulos. Observation-based learning for brain-machine interfaces. *Current Opinion in Neurobiology*, 2008.

[84] A M Travis. Neurological deficiencies following supplementary motor area lesions in macaca mulatta. *Brain*, 78(2):174–175, 1955.

[85] Yoji Uno, Mitsuo Kawato, and Rika Suzuki. Formation and control of optimal trajectory in human multijoint arm movement. *Biological cybernetics*, 61(2):89–101, 1989.

[86] Meel Velliste, Sagi Perel, M Chance Spalding, Andrew S Whitford, and Andrew B Schwartz. Cortical control of a prosthetic arm for self-feeding. *Nature*, 453(7198):1098–1101, 2008.

[87] Ganesh Vigneswaran, Roland Philipp, Roger N Lemon, and Alexander Kraskov. M1 Corticospinal Mirror Neurons and Their Role in Movement Suppression during Action Observation. *Current Biology*, 2013.

[88] S P Wise. The primate premotor cortex: past, present, and preparatory. *Annual Review of Neuroscience*, 1985.

[89] D M Wolpert, Z Ghahramani, and M I Jordan. Are arm trajectories planned in kinematic or dynamic coordinates? an adaptation study. *Experimental brain research*, 103(3):460–470, 1995.

[90] R S Woodworth. *The Accuracy of Voluntary Movement*. Columbia University contributions to philosophy, psychology and education. Columbia University., 1899.

[91] C N Woolsey, P H Settlage, D R Meyer, W Sencer, H T Pinto, A M Travis, et al. Patterns of localization in precentral and" supplementary" motor areas and their relation to the concept of a premotor area. *Research publications-Association for Research in Nervous and Mental Disease*, 30:238, 1952.